Applied Catalysis B: Environmental 343 (2024) 123584

Contents lists available at ScienceDirect

Applied Catalysis B: Environmental

journal homepage: www.elsevier.com/locate/apcatb

Recent advances in Ru/Ir-based electrocatalysts for acidic oxygen evolution reaction

Guoliang Gao [a,f,1], Zixu Sun [b,*,1], Xueli Chen [a], Guang Zhu [a,*], Bowen Sun [b], Yusuke Yamauchi [d,e,**], Shude Liu [c,*]

[a] Key Laboratory of Spin Electron and Nanomaterials of Anhui Higher Education Institutes, Suzhou University, Suzhou 234000, China
[b] Key Lab for Special Functional Materials of Ministry of Education, School of Materials Science and Engineering, Henan University, Kaifeng 475004, People's Republic of China
[c] College of Textiles, Donghua University, Shanghai 201620, China
[d] School of Chemical Engineering and Australian Institute for Bioengineering and Nanotechnology, University of Queensland, Brisbane, QLD 4072, Australia
[e] Department of Materials Process Engineering, Graduate School of Engineering, Nagoya University, Nagoya 464–8603, Japan
[f] i-lab, Suzhou Institute of Nano-Tech and Nano-Bionics, Chinese Academy of Sciences, Suzhou 215123, China

ARTICLE INFO

Keywords:
Ru/Ir
Acidic OER
Electrocatalysts
Modification strategy
Mechanisms

ABSTRACT

The electrocatalytic process of water splitting offers a promising approach to produce sustainable hydrogen. However, the slow kinetics of the oxygen evolution reaction (OER) presents a notable challenge, especially in the acidic environment of proton exchange membrane systems. Despite the extensive progress made in catalyst development for hydrogen production through electrolysis in the last century, significant advancements have been accomplished. However, the quest for acidic OER catalysts that possess both high activity and stability, while also being affordable, continues to be challenging. Currently, Ru/Ir-based electrocatalysts are the only practical anode catalysts available. Therefore, it is crucial to explore feasible strategies to enhance the electrocatalytic performance and longevity of acidic OER catalysts. This review offers a comprehensive assessment of the obstacles and prospective advancements in acidic OER catalysts. Additionally, it underscores the areas of research concentration, providing valuable perspectives for future endeavors in catalyst research and development.

1. Introduction

The sustainable development of human society is heavily reliant on addressing the crucial concerns of energy and environment. The current global energy demand is predominantly met by fossil fuels, which constitute approximately 80% of the energy sources. However, this heavy reliance on fossil fuels is bound to lead to their eventual depletion and exacerbate the issue of severe environmental pollution [1–4]. Consequently, the gradual transition from fossil fuels to sustainable non-fossil energy sources, devoid of pollution, is an imperative trajectory for development. Hydrogen has emerged as a prominent alternative to fossil fuels and other non-renewable energy sources due to its diverse range of applications, encompassing hydrogen fuel cells, hydrogen metallurgy, and methanol production [5–7]. Additionally, hydrogen offers environmental benefits and possesses a noteworthy energy density. Consequently, hydrogen plays a crucial role in facilitating the sustainable advancement of human society [8–10]. Presently, the predominant techniques for hydrogen production encompass high-temperature pyrolysis of fossil fuels (gray hydrogen) and natural gas reforming (blue hydrogen) [11,12]. Despite the inherent cleanliness of hydrogen, the aforementioned approach yields significant carbon emissions during the hydrogen production process, thereby impeding sustainable development. Water splitting, a method employed to produce hydrogen, involves the division of water into hydrogen and oxygen through the utilization of externally supplied energy [13–15]. Hydrogen production can be accomplished with minimal energy consumption or

* Corresponding authors.
** Corresponding author at: School of Chemical Engineering and Australian Institute for Bioengineering and Nanotechnology, University of Queensland, Brisbane, QLD 4072, Australia.
E-mail addresses: sunzixu@henu.edu.cn (Z. Sun), guangzhu@ahszu.edu.cn (G. Zhu), y.yamauchi@uq.edu.au (Y. Yamauchi), sdliu@dhu.edu.cn (S. Liu).
[1] G. Gao and Z. Sun contributed equally to this work.

https://doi.org/10.1016/j.apcatb.2023.123584
Received 29 October 2023; Accepted 24 November 2023
Available online 1 December 2023

without dependence on external power sources by utilizing renewable energy sources such as wind, heat, solar, or tidal power to facilitate the water-splitting process [16,17].

Alkaline water electrolysis (AWE), the prevailing technology currently, has undergone extensive development over time and has been successfully implemented in commercial settings [18–20]. However, it encounters certain challenges, including impurities in the gas due to gas crossover and low working current density resulting from high ohmic resistance. In contrast, the proton exchange membrane water electrolysis (PEMWE) operates in acidic environments and exhibits superior conductivity, higher working current, and reduced gas exchange likelihood compared to alkaline electrolyzers. This enables the PEMWE to effectively address the aforementioned challenges and significantly enhance its performance.[21–23] The process of electrocatalytic water splitting involves two half-reactions: cathodic hydrogen reduction reaction (HER) and anodic oxygen evolution reaction (OER) [24,25]. In contrast to the two-electron HER, the four-electron transfer OER necessitates a series of consecutive intermediate state changes, resulting in intricate kinetics within the catalytic cycle and a sluggish overall catalytic kinetics. Consequently, the OER, characterized by a higher energy barrier, significantly influences the rates of cathodic hydrogen production, thereby imposing more stringent requirements on the intrinsic activity of the OER catalyst [26,27]. Despite the proliferation of numerous alkaline OER electrocatalysts that exhibit high efficiency and stability [28–31], the lack of affordable, stable, and highly active acidic OER electrocatalysts remains a significant obstacle in the advancement of PEM [32–34]. Currently, Ru/Ir-based electrocatalysts have been widely recognized as the most promising catalysts for acidic OER [35,36]. Various studies have demonstrated that Ru-based materials exhibit high catalytic activity in acidic environments, but their stability is compromised because of the generation of soluble high-valence oxide species. The catalytic activity of Ir-based materials exhibits a slight deficiency, yet it demonstrates remarkable stability in acidic electrolyte conditions [37–41]. In comparison to the pursuit of cost-effective substitutes for noble metal catalysts [42–45], the modification of Ru/Ir-based catalysts holds greater potential for attaining a significant advancement in acidic OER efficiency. In comparison to catalysts based on noble metals, non-noble metal-based catalysts exhibit a significant disparity in both stability and efficiency when employed in acidic OER. Furthermore, a prompt resolution to this disparity remains elusive. Additionally, for enterprises engaged in product manufacturing, the catalyst's performance holds greater significance than its cost, thus mitigating concerns regarding the affordability of noble metal materials. Moreover, the elevated cost of Ir metals, for instance, primarily stems from their limited annual mining output rather than a scarcity within the crust of the Earth.

In recent years, there has been a proliferation of noteworthy literature reviews on the synthesis and modification strategies of acidic OER catalysts [16,44–48]. These reviews predominantly concentrate on noble metal-based, transition metal-based, and carbon materials, or adopt a nanoparticle-to-single atom perspective. However, the extensive breadth of these reviews dilutes their focus on a specific catalyst type. An in-depth understanding of catalyst modification is still lacking. Ru/Ir-based materials exhibit superior catalytic activity and stability, rendering them the most optimal choice for PEM anode catalysts. The modification of Ru/Ir-based catalysts represents a direct and efficient approach to address the inherent tradeoff between activity, stability, and cost associated with acidic OER catalysts. To the best of our knowledge, a comprehensive and organized review specifically addressing Ru/Ir-based catalysts remains absent in the literature. Given the swift advancement of Ru/Ir-based catalysts, it becomes imperative to promptly consolidate the most recent advancements, obstacles, and prospects in this cutting-edge domain. This paper undertakes a comprehensive review of the latest advancements in Ru/Ir-based catalysts for acidic OER, commencing with an introduction to the classical OER mechanisms. Subsequently, the recent literature on Ru/Ir-based catalysts, encompassing pure metals, oxides, alloys, and other variations, is critically examined. Simultaneously, the strategies for modifying catalytic activity and stability (Scheme 1), are also summarized. Ultimately, the challenges and areas of future research about acidic OER are deliberated upon.

2. Working mechanism of OER

Researchers have identified two potential four-electron transfer mechanisms, namely the adsorbed evolution mechanism (AEM) and the lattice oxygen participation mechanism (LOM) for the acidic OER mechanism, as depicted in Fig. 1**a**, **b** [49]. When the electronic state of the catalyst close to the Fermi level exhibits metallic properties, the metal functions as a redox center, consequently leading to the conventional AEM mechanism during the OER [50,51]. This mechanism is commonly observed in current catalyst OER processes. In the AEM, water molecules initially adsorb onto the surface of the catalysts, initiating a sequence of events involving charge-proton transfer, chemical bond cleavage/formation, and adsorption/desorption of surface oxygen intermediates, ultimately resulting in the generation of oxygen molecular [52–54]. Fig. 1**a** and Eqs. (1)–(5) illustrate the sequential steps involved in the OER process. Initially, water undergoes dissociation, yielding a proton (H^+) and the adsorption of OH on surface metal cations. Subsequently, the OH species dissociates further, leading to the adsorption of O in the second step. In the third step, the adsorbed O species reacts with another water molecule, resulting in the generation of an adsorbed OOH species. This reaction ultimately leads to the release of O_2(g). It is important to note that the OER process involves the conversion of two H_2O molecules into four protons (H^+), four electrons, and one O_2 molecule.

$$H_2O(l) + M \rightarrow HO\text{-}M + H^+ + e^- \quad (1)$$

$$HO\text{-}M \rightarrow O\text{-}M + H^+ + e^- \quad (2)$$

$$O\text{-}M + H_2O(l) \rightarrow HOO\text{-}M + H^+ + e^- \quad (3)$$

$$HOO\text{-}M \rightarrow O_2(g) + M + H^+ + e^- \quad (4)$$

$$\text{Overall } 2\,H_2O(l) \rightarrow O_2(g) + 4\,H^+ + 4e^- \quad (5)$$

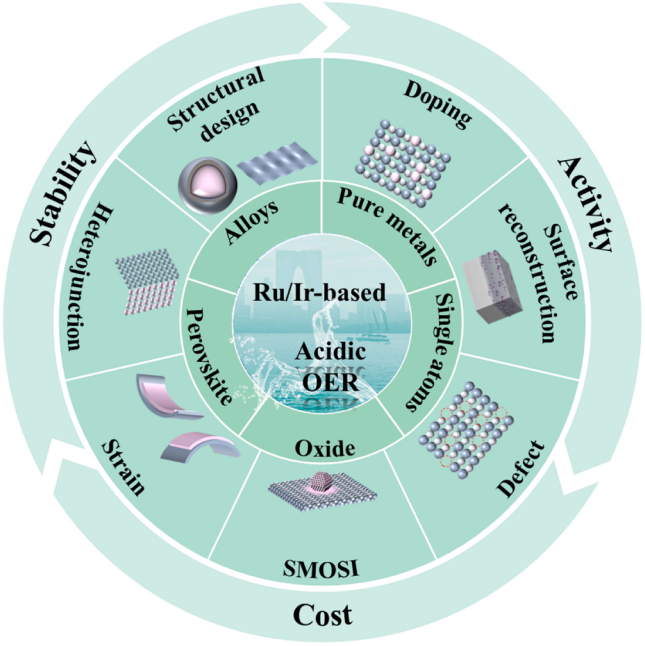

Scheme 1. Schematic illustration of classification, and modification strategy of Ru/Ir-based electrocatalysts.

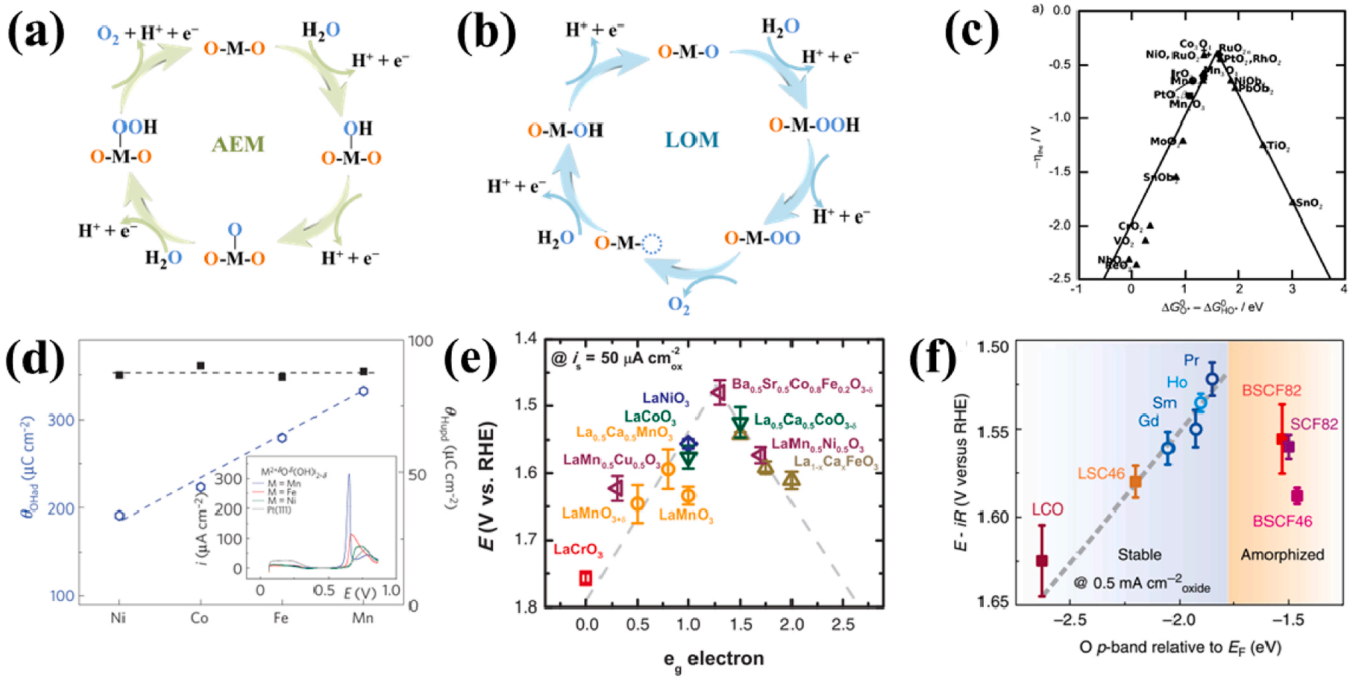

Fig. 1. (a) Adsorbate evolution mechanism. (b) Lattice oxygen participation mechanism. (c) Activity trends towards oxygen evolution [55]. (d) Comparison of OH_{ad} charge as a function of oxophilicity of the metal oxide cation. Inset displays the comparison of voltammograms [56]. (e) The relation between the OER activity and the occupancy of the transition metal [57]. (f) Evolution with IR-correction vs. the O *p*-band centre relative to E_F (eV) [58].

The AEM mechanism is characterized by theoretical calculations suggesting that the deprotonation of *OH or the generation of *OOH may serve as the rate-determining step (RDS). A linear correlation is observed between the adsorption energies of O* , *OH, and *OOH. Consequently, a volcano plot is constructed (Fig. 1**c**), which demonstrates the relationship between ΔG_{O^*}-ΔG_{HO^*} and activity. Notably, RuO_2 and IrO_2 exhibit proximity to ideal values on the plot, while maintaining relative stability in acidic OER conditions. The AEM mechanism explains the variability observed in OER activity (as determined by DFT) and provides a set of descriptors, including the ΔG_{O^*}-ΔG_{HO^*} (Fig. 1**c**) [55], strength of the OH–$M_{2+\delta}$ bond (Fig. 1**d**) [56], e_g orbital occupancy (Fig. 1**e**) [57], and O *p*-band center (Fig. 1**f**) [58].

Oxygen isotope labeling experiments have demonstrated the involvement of lattice oxygen in the OER catalytic cycle for certain metal oxide electrocatalysts [59,60]. Consequently, a second four-electron transfer mechanism, known as the LOM pathway, has been proposed and its catalytic cycle is illustrated in Fig. 1**b** [49]. When the electron state near the Fermi level corresponds to oxygen, the catalyst adheres to the LOM with lattice oxygen serving as the redox center [50,51]. Classical catalysts that follow LOM are RuO_2, perovskite, and spinel, among others. In the LOM pathway, the initial two steps entail hydrolytic dissociation leading to the adsorption of O on the surface lattice oxygen, followed by the generation of surface oxygen vacancies through the coupling of O_2(g) with the surface lattice oxygen in the third step. Finally, in the last two steps, the surface oxygen vacancy (V_O) is replenished through water dissociation [49]. LOM, or lattice oxygen migration, takes place on the lattice oxygen of oxides and is influenced by the covalency properties between metal and oxygen. Please refer to Eqs. (6) to (11) for specific reaction steps [61]. On one hand, the LOM process offers certain benefits as it circumvents the O-O velocity step necessary for the OER of AEM [53]. On the other hand, the generation of oxygen vacancies resulting from the LOM pathway accelerates metal dissolution, thereby causing catalyst structure collapse and rapid catalyst deactivation [62,63]. Consequently, catalysts that adhere to the LOM pathway exhibit comparatively inadequate stability.

$$H_2O(l) + M \rightarrow HO\text{-}M + H^+ + e^- \quad (6)$$

$$HO\text{-}M \rightarrow O\text{-}M + H^+ + e^- \quad (7)$$

$$O\text{-}M + O_L \rightarrow M_V + O_2(g) \quad (8)$$

$$M_V + H_2O(l) \rightarrow O_L + H\text{-}M + H^+ + e^- \quad (9)$$

$$H\text{-}M \rightarrow M + H^+ + e^- \quad (10)$$

$$\text{Overall } 2\,H_2O(l) \rightarrow O_2(g) + 4\,H^+ + 4e^- \quad (11)$$

M, O_L, and M_V represent the adsorption site, lattice oxygen, and surface oxygen vacancy, respectively.

Through the comparison of the two mechanisms, namely AEM and LOM, it is evident that AEM involves the coordinated transfer of proton-electron and the participation of multiple intermediates (*OH, *O, *OOH, and *O_2). On the other hand, the proton-electron transfer in LOM is not synchronized, resulting in its pH dependence. Additionally, the absence of *OOH formation in the LOM cycle breaks the constraint imposed by the scaling relationship between *OH and *OOH ($\Delta G_{*OOH} - \Delta G_{*OH} = 3.2 \pm 0.2$ eV), with the lowest theoretical overpotential in AEM being 0.37 V [64,65]. Furthermore, the presence of oxygen within the catalyst lattice serves as an intermediary, thereby diminishing the necessity for extensive coverage of the reaction intermediate. Consequently, the O-O binding step becomes less arduous (typically serving as the rate-determining step in AEM), thus suggesting that LOM exhibits superior performance in theory compared to AEM. Nevertheless, it is important to acknowledge that every situation has its pros and cons. Unlike the stable active center observed in AEM, the catalyst structure in LOM undergoes continuous dynamic changes throughout the reaction. The occurrence of oxygen vacancy in LOM can lead to the dissolution of metal, thereby diminishing the stability of the catalyst. The primary distinction between the two mechanisms lies in the involvement of active lattice oxygen in LOM during OER. In practice, AEM and LOM frequently coexist during the OER process, resulting in a certain level of competition [66], and even the occurrence of a transition between the two mechanisms [67,68]. Irrespective of the specific mechanism employed, the O-O bonding process in AEM and the deprotonation step

in LOM have a direct impact on the kinetics of OER [69]. Notably, in the case of acidic OER, the limited availability of OH^- ions for direct involvement in deprotonation necessitates the prior completion of H_2O adsorption and dissociation at the active site, thereby introducing additional steps and kinetic barriers [70].

3. Ru/Ir-based electrocatalysts

3.1. Pure metals

A noble metal catalyst is defined as a noble metal substance capable of altering the rate of a chemical reaction. Virtually all noble metals possess catalyst properties, with the Pt series metals (Pt, Ru, Ir) serving as the most extensively employed electrocatalysts. This preference is

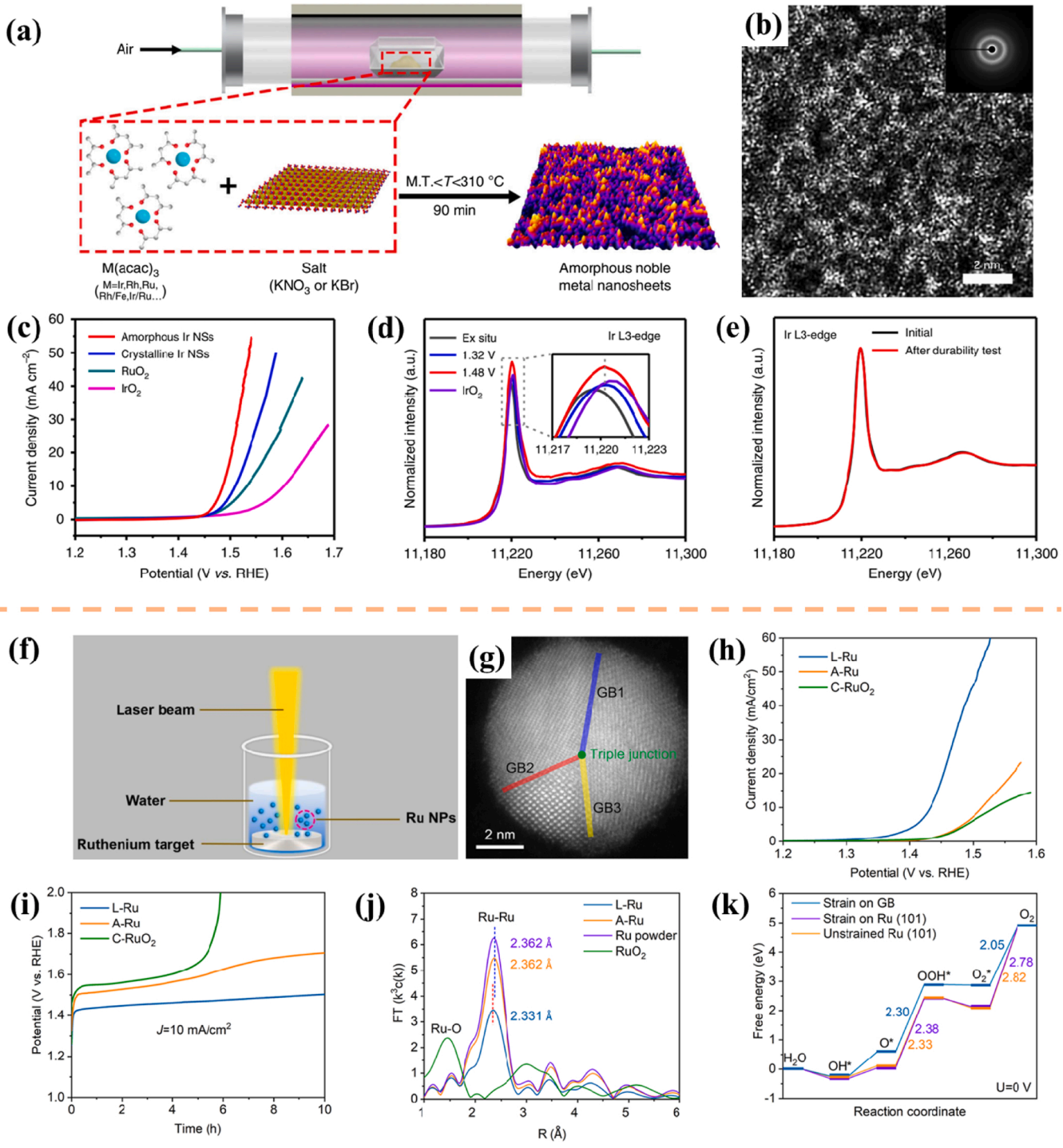

Fig. 2. (a) Diagram of the preparation process of amorphous noble metal NSs. (b) Aberration-corrected HAADF-STEM image of amorphous Ir NSs. (c) Polarization curves of the corresponding catalysts. (d) In situ XAFS spectra of the Ir L_3-edge. (e) XANES spectrum of amorphous Ir NSs [78]. (f) Preparation diagram of the Ru NPs. (g) HAADF-STEM image. (h) LSV curves of the corresponding catalysts. (i) Stability at 10 mA cm^{-2}. (j) FT k^3-weighted EXAFS spectra. (k) Free-energy landscape [81].

primarily attributed to their electron-deficient outermost *d*-orbitals, which facilitate electron acceptance and promote favorable chemisorption with reactants [71–73]. Noble metal catalysts possess a rich historical background, as they have been utilized in industrial settings since 1875 year for the production of sulfuric acid, employing Pt as a catalyst. In practice, the performance of the catalyst is not only determined by the catalyst itself, but also affected by the catalytic environment, thereby additional criteria are imposed on the selection of the catalyst. For instance, while Pt and Ru are widely recognized as the standard catalysts for acidic and alkaline HER, respectively, the employment of pure noble metal catalysts in acidic OER is susceptible to dissolution owing to the harsh acidic and oxidizing conditions, thereby diminishing their catalytic stability [74].

In comparison to noble metal crystal nanomaterials, amorphous noble metal nanomaterials show potential applications in the realm of catalysis owing to their distinct atomic arrangement, coordination environment, and altered bond length [75–77]. To generate a range of amorphous noble metal nanosheets (NSs), Li and colleagues employed direct annealing of a precursor metals mixture (Fig. 2**a**) [78]. The high-angle annular dark-field scanning transmission electron microscopy (HAADF-STEM) image (Fig. 2**b**) visually depicts the disordered atomic structure of the sample, thereby confirming its amorphous characteristics. Amorphous Ir nanosheets have demonstrated exceptional performance in the OER when exposed to O_2-saturated 0.1 M $HClO_4$ solution. These nanosheets require only a 255 mV overpotential to attain 10 mA cm^{-2}, which is lower than the current densities observed for crystalline Ir nanosheets (280 mV), RuO_2 (301 mV), and IrO_2 (373 mV) catalysts (Fig. 2**c**). The in situ X-ray absorption fine structure (XAFS) spectrum revealed the valence state of Ir remained below + 4 throughout the OER and returned to its original valence state after the reaction, demonstrating the stability of the amorphous Ir (Fig. 2**d**, **e**).

Grain boundaries (GBs) have the potential to induce strain and regulate the electron density and coordination number of the associated atoms, thereby influencing the catalytic performance and durability [79,80]. It is hypothesized that GBs can effectively enhance acidic OER. Du et al. conducted a study where they utilized a laser-ablation-in-liquid (PLAL) method to prepare Ru nanoparticles (NPs) enriched with GBs, referred to as L-Ru (Fig. 2**f**) [81]. To establish a comparison, L-Ru was subjected to further heat treatment in an inert gas, resulting in an prepared material denoted as A-Ru NPs. The HAADF-STEM images demonstrate that a polycrystalline structure exhibits three distinct grain boundaries (Fig. 2**g**). The L-Ru nanoparticles demonstrate remarkable catalytic efficiency and durability in 0.5 M H_2SO_4 as an OER catalyst, achieving a significantly low overpotential of 202 mV at 10 mA cm^{-2} (Fig. 2**h**). Furthermore, the catalyst exhibits a stability exceeding 10 h (Fig. 2**i**), surpassing that of commercially available RuO_2 (305 mV). These findings from the analysis of extended X-ray absorption fine structure (EXAFS) and density functional theory (DFT) calculations indicate that the utilization of a laser can induce the aggregation of GBs within ruthenium nanoparticles, consequently resulting in the development of compressive strain. This strain, in turn, leads to a notable improvement in both the activity and stability of the NPs (Fig. 2**j**, **k**).

The electrocatalytic efficacy of pure noble metals is undeniably assured; however, the substantial utilization of noble metals in industrial-scale production is evidently unfeasible, particularly considering the limited global mining of iridium, which amount to a mere 7 tons, significantly lower than other noble metals such as platinum, which recorded a production volume of 180 tons in 2021. Consequently, the utilization of pure noble metal catalysts poses challenges to the sustainable advancement of electrocatalysis. Furthermore, the Sabatier principle imposes constraints on the suitability of pure metals as catalysts for desired reactions [82].

3.2. Single-atomic-site catalysts

Reducing the size of the catalyst can greatly improve the mass activity of the catalyst and reduce its cost, but also. The utilization of cluster catalysts and single-atom catalysts (SACs) has been increasingly adopted in water splitting [46,83]. Since its initial proposal in 2011 [84], the concept of single-atom catalysis (SAC) has emerged as a prominent and highly sought-after catalytic frontier due to its exceptional activity, selectivity, optimal atom utilization (nearly 100%), and robust interaction between active atoms and the supporting material [85–87]. Nevertheless, the expeditious advancement of SACs is hindered by the intricacies associated with catalyst preparation, the propensity for single atoms to aggregate, and the consequential loss of active sites [88,89]. Consequently, the design of supported catalysts presents a viable solution, as it enhances the dispersion of noble metals and diminishes their overall quantity. Moreover, the synergistic interplay between the support and noble metals augments the intrinsic activity and stability of the catalyst.

In the actual electrocatalytic reaction process, the active site atomic and electronic structure of the catalyst may self-adjust and optimize, which is often the key of the catalytic reaction. Effectively capturing the changes of these reaction intermediates can better guide the design of the targeted OER catalysts [90]. Cao et al. [91] synthesized Ru_1-N_4 sites supported on the N-C framework (Ru-N-C) through thermal reduction. The utilization of HAADF-STEM and XAFS measurements confirmed the presence of ruthenium atoms distributed as single atoms on the N-C framework, demonstrating a remarkably uniform distribution (Fig. 3**a**, **b**). The obtained results revealed that the Ru_1-N_4 catalyst displayed exceptional acidic OER activity in an O_2-saturated 0.5 M H_2SO_4 solution, attaining 10 mA cm^{-2} with an overpotential of merely 267 mV. Furthermore, the mass activity and turnover frequency at this overpotential were found to be as high as 3571 A g^{-1}_{metal} and 3348 O_2 h^{-1}, respectively (Fig. 3**c, d**). The efficacy of electron transfer from Ru atom to O atom, which can prevent strong adsorption of reactive species and enhance catalytic activity, has been verified through the utilization of Operando synchrotron radiation infrared spectroscopy (Operando SR-FTIR) in conjunction with theoretical calculations (Fig. 3**e**, **f**).

Regulating the intrinsic activity of catalysts at the atomic level has proven to be a viable approach for enhancing their electrocatalytic performance; however, it remains a formidable challenge. The augmentation of intrinsic activity in SACs primarily relies on the regulation of local structure and the coupling effect with the support material [92]. A comprehensive comprehension of the formation mechanism, coordination environment, and stability of atomically dispersed metal species is pivotal in advancing the field of SACs [52]. Furthermore, it has been observed that the utilization of a supported catalyst can effectively diminish the quantity of noble metal. However, it is important to acknowledge that the corrosive and oxygen-rich nature of the acidic OER environment necessitates specific criteria for the substrate. Specifically, when employing a carbon substrate for acidic OER catalysts, the high oxidation potential poses a risk of carbon corrosion, resulting in the generation of CO_2, CO, and other byproducts, which subsequently contribute to a portion of the overall current [93,94]. In the aforementioned study, Yao et al. investigated the utilization of single-atom Ru on N-C substrate. However, no subsequent investigation was conducted to examine the impact of the carbon substrate on the obtained results. This necessitates considering the specific demands of catalyst design in acidic OER environments. By employing electrochemical equipment and gas chromatography to analyze Faraday efficiency in real time and assess catalyst selectivity, readers can gain a more comprehensive understanding of the rationale behind catalyst design. Researchers have used mass spectrometric analysis to show that carbon corrosion can be inhibited by modifying the structure of carbon [95].

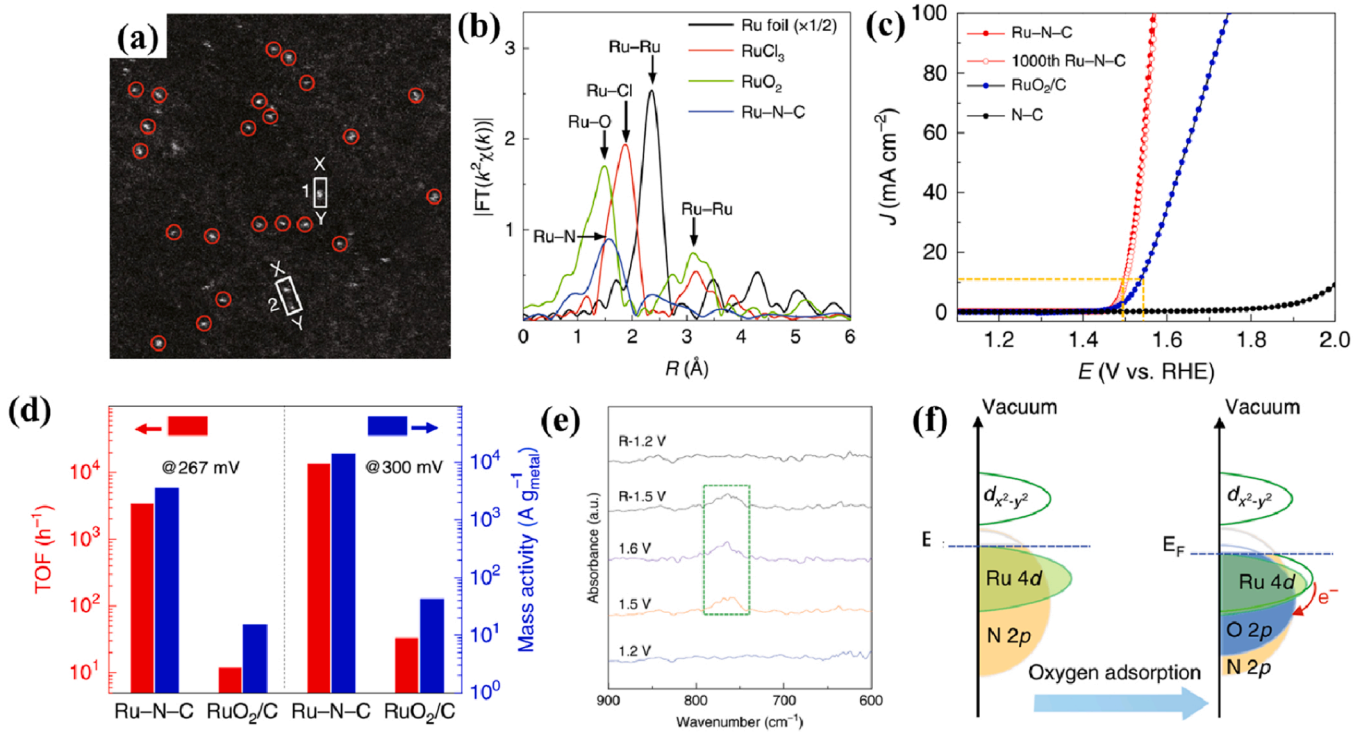

Fig. 3. (a) HAADF-STEM image of Ru-N-C. (b) The Ru K-edge k^2-weighted Fourier transform spectra. (c) OER properties of the catalysts. (d) TOF and mass activities for the electrocatalysts. (e) Operando SR-FTIR spectroscopy measurements for the Ru-N-C catalyst. (f) Diagram of oxygen adsorption process on Ru-N-C catalyst [91].

3.3. IrO_2 and RuO_2

Noble metal oxides, namely IrO_2 and RuO_2, have historically been regarded as optimal catalysts for the OER in acidic environments, located near the top of the OER active volcano plot (Fig. 1**c**). However, their limited availability, high cost, and inadequate stability have significantly hindered their utilization in extensive industrial applications. Given the subpar performance of non-noble metal catalysts currently available, enhancing the catalytic activity and stability of noble metal materials remains the most direct and efficient approach to mitigate catalyst expenses [96,97].

Compared with bulk catalysts, ultra-thin two-dimensional (2D) nanostructured catalysts can reveal more active sites and cut down the reactant diffusion path [98,99]. In view of this, Li's group employed a molten salt technique (Fig. 4**a**) to fabricate ultra-thin RuO_2 nanosheets (RuO_2 NSs) [100]. The atomic resolution STEM image (Fig. 4**b**) reveals the presence of numerous multi-scale defects within the nanosheets, which have the potential to modify the local electronic structure and consequently influence the catalytic activity. The X-ray photoelectron spectra (XPS) diagram demonstrates that, owing to the elevated defect density, the peak area corresponding to Ru^{5+} species in the synthesized RuO_2 NSs surpasses that of the annealed RuO_2 NSs and industrial RuO_2. Moreover, the Ru species exhibiting higher oxidation states exhibit enhanced capability in reducing overpotential (Fig. 4**c**). In the acidic OER test, it was observed that RuO_2 NSs displayed a lower overpotential of 199 mV in an O_2-saturated 0.5 M H_2SO_4 solution compared to other RuO_2 electrocatalysts, resulting in 10 mA cm^{-2}_{geo}. This finding is supported by DFT calculations, which demonstrate that the presence of a Ru vacancy defect on the surface of RuO_2 weakens the binding energy between O* and OOH* , leading to reduced energy consumption during the conversion from O* to OOH* . Consequently, the OER performance is significantly improved.

Metastable metal oxides possess promising potential for energy conversion catalysis; however, their synthesis methods have been largely limited [101–104]. In light of this, Shao et al.[105] fabricated a monoclinic layered IrO_2 nanoribbons (IrO_2 NRs) with a C2/m space group using the molten-alkali mechanochemical approach (Fig. 4**f, g**). The IrO_2 NRs exhibited remarkable OER activity and stability in an O_2-saturated 0.5 M H_2SO_4, demonstrating an overpotential of merely 205 mV at 10 mA cm^{-2} (Fig. 4**h, i**). Notably, the theoretical overpotential (η) of IrO_2 NRs was 0.34 V, which is lower than that of rutile IrO_2(110) (0.66 V). During the OER process, it is observed that the exposed Ir atoms of IrO_2NR are positioned below the *d*-band center of rutile IrO_2. This positioning is believed to be responsible for the weak adsorption of OER intermediates and potentially serves as the primary factor contributing to its high OER activity (Figs. 4**j** and 4**k**).

In practical commercial product applications, RuO_2 exhibits superior catalytic activity compared to IrO_2, albeit being susceptible to oxidation and possessing slightly lower stability. Currently, IrO_2 anode catalysts are more extensively employed in commercial PEM systems, boasting a load capacity of approximately 1 ~ 2 mg cm^{-2}. The industry is actively addressing the supply constraint of Ir material by reducing load and optimizing recycling processes.

3.4. Perovskite oxides

Several obstacles need to be overcome to successfully commercialize PEMWE. Two major challenges include the sluggish OER kinetics in acidic environments and the limited availability of oxygen evolution electrocatalysts that possess high activity, stability, and affordability. However, the utilization of perovskite catalysts in the form of polymetallic oxides can potentially address these difficulties. These catalysts not only reduce the reliance on noble metals but also allow for the adjustment of the electronic structure, thereby enhancing catalytic activity [106–109]. This approach has demonstrated promising application potential in various electrocatalytic reactions and holds particular promise for improving the acidic OER process.

Plentiful studies have found that cations or anions doping can adjust the surface structure and electronic configuration of electrocatalysts to improve OER performance [110,111]. Inspired by this, Zhao et al.

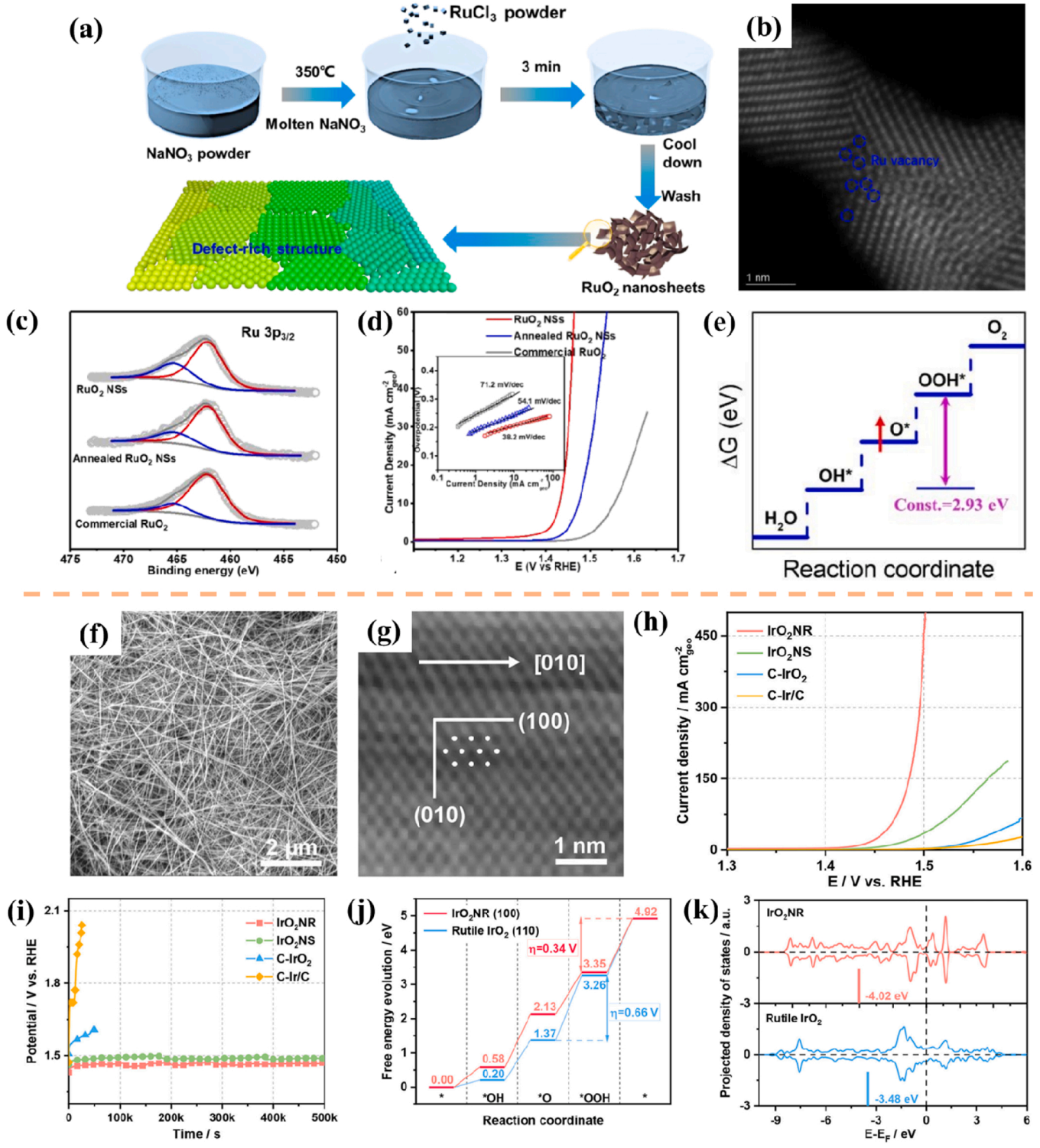

Fig. 4. (a) Diagram for the synthetical process of the RuO_2 NSs. (b) Atomic STEM images. (c) Ru $3p_{3/2}$ high-resolution XPS spectrum. (d) OER curves and the corresponding Tafel plots of the catalysts. (e) Schematic showing the origin of OER activity improvement upon introducing Ru vacancy [100]. (f) Scanning electron microscopy (SEM) image showing the uniform distribution of the IrO_2NR. (g) HAADF–STEM image for the IrO_2NR. (h) LSV curves, (i) Stability at 10 mA cm^{-2}. (j) $4e^-$ thermodynamic diagram. (k) Comparison of the d-orbital distribution of the Ir atoms in the rutile IrO_2 and IrO_2NR samples [105].

employed a sol-gel method combined with sulphuration treatment to synthesize S-doped M-$SrIrO_3$ nanosheets [112]. The electrocatalytic performance of the S-doped M-$SrIrO_3$ catalyst was evaluated in a 0.5 M H_2SO_4 solution, revealing an overpotential of 228 mV at 10 mA cm^{-2}, surpassing that of IrO_2 (Fig. 5**a**). Notably, the OER process resulted in the leaching of Sr from the surface, causing the surface reconstruction of the Ir(O, S)$_x$ amorphous layer (Fig. 5**b, c**). The results obtained from DFT calculations demonstrate that the inclusion of sulfur (S) in M-$SrIrO_3$ weakens the robust bonding of the reaction intermediates (O*/OH*/OOH*) on the surface. Consequently, this reduction in binding strength leads to a decrease in the activation energy required for OER kinetics and an enhancement in OER activity (Fig. 5**d**).

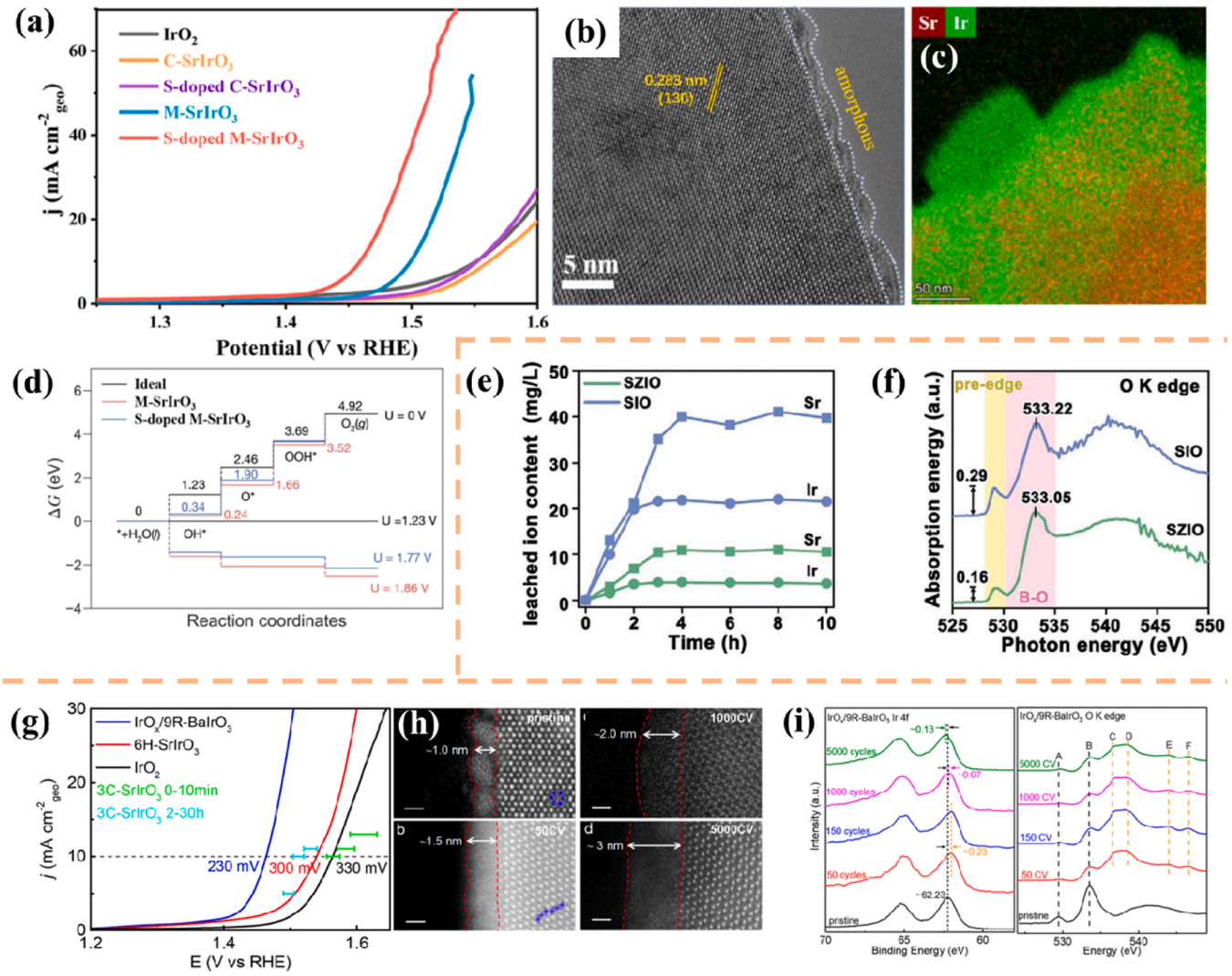

Fig. 5. (a) LSV curve of the corresponding electrocatalysts. (b) High resolution transmission electron microscopy (HRTEM) images, (c) X-ray energy spectrometer (EDS) elemental mapping after test. (d) Free-energy diagrams for acidic OER pathways [112]. (e) Contents of leached metals. (f) Normalized O K edge XAS spectra of SZIO and SIO [116]. (g) Polarization curves. (h) Lattice-resolved HAADF-STEM images of IrO_x/9R-$BaIrO_3$. Scale bars, 1 nm. (i) Ir 4 f XPS spectra (left), O K-edge XANES spectra of IrO_x/9R$BaIrO_3$ (right) [119].

Efforts have been made to enhance the catalytic activity and stability of acidic catalysts to meet the industry's requirements [112–115]. Zou et al.[116] introduced a novel approach by alloying catalytically inert $SrZrO_3$ (SZO) with $SrIrO_3$ (SIO) to create a perovskite-type $SrZrO_3$-S-$rIrO_3$ (SZIO) solid solution electrocatalyst. This innovative electrocatalyst demonstrated improved performance for acid OER (0.1 M $HClO_4$). One the one hand, the results of the inductively coupled plasma (ICP) test indicate that the cationic dissolution of SZIO material during the OER process is approximately five times lower compared to SIO. This finding indicates that the incorporation of SZO into SIO can significantly enhance the structural stability of the material (Fig. 5**e**). On the other hand, the X-ray absorption spectroscopy (XAS) at the O K-edge of SZIO and SIO indicate that the proper alloying of SZO-SIO effectively reduces the initially strong covalency of the Ir-O bond, thereby inhibiting the dissolution of cations on the surface of the material (Fig. 5**f**). Although iridium-based perovskites show excellent catalytic activity in acidic OER, their mass activity is still low.[117] In addition, because of the limitation of characterization means, the real structure of the active-layer formed on the surface of perovskite is still controversial [118]. Here, Yan et al.[119] employed solution calcination and strong acid treatment strategies to synthesize highly active IrO_x particles anchored on 9R-$BaIrO_3$ (IrO_x/9R-$BaIrO_3$). The resulting catalyst, IrO_x/9R-$BaIrO_3$, exhibited remarkable OER activity, requiring only 230 mV to afford 10 mA cm^{-2}_{geo} in O_2-saturated 0.5 M H_2SO_4 (Fig. 5**g**). Characterization means such as STEM, XPS, and XANES revealed that the IrO_x/9R-$BaIrO_3$ transformed into amorphous $Ir^{4+}O_xH_y/IrO_6$ during electrocatalysis, and subsequently evolved into amorphous $Ir^{5+}O_x/IrO_6$ (Fig. 5**h, i**). The exceptional catalytic activity of acidic OER can be ascribed to the presence of a substantial amount of amorphous $Ir^{5+}O_x$ species, which are derived from IrO_6 octahedrons, as well as the improved metal conductivity of the $Ir^{5+}O_x$/9R-$BaIrO_3$.

Our findings indicate that perovskite catalysts commonly undergo reconfiguration during the OER process. Furthermore, the objective of the aforementioned research is to improve the catalytic properties by modifying the existing catalysts. Through a comprehensive investigation of perovskites (ABO_3), Shao-Horn et al.[57] have successfully demonstrated a significant association between the OER performance under alkaline conditions and the occupation of eg orbitals by B-site metal cations. This relationship is visually depicted by a graph exhibiting a volcanic-shaped pattern. It is crucial to summarize similar descriptors that can predict the activity of perovskites in acidic environments, as this information holds significant guidance for the design of advanced catalysts.

3.5. Alloys

Based on the Sabatier principle, it is commonly observed that pure metal catalysts often exhibit a disparity with the optimal catalyst for the desired reaction [82,120]. Consequently, alloying has emerged as a viable approach for modifying the catalytic characteristics of active metals, as it enables the manipulation of their electronic and geometric states through the incorporation of diverse elements. Additionally, noble metal-based alloy catalysts offer the potential to reduce the reliance on noble metals by introducing less expensive counterparts [121–124].

The majority of the acidic OER catalysts reported do not meet the criteria of achieving high current density ($\geq$ 2 A cm_{geo}^{-2}) for industrial applications at a low overpotential ($\leq$ 500 mV) [125–127]. The design of a catalyst that possesses both good stability and the ability to achieve high current density remains a challenge. In a study conducted by Xiong et al.[128], biphasic IrW-W_2B (W-Ir-B) alloys were prepared through the arc-melting of high-purity elements under a high-purity Ar atmosphere. TEM images reveal that the separated crystalline phases in the alloy exhibit a discontinuous and interconnected structure (Fig. 6**a**). The phase separation of the prepared W-Ir-B alloy is further evidenced by STEM-EDS analysis (Fig. 6**b**). Moreover, the presence of distinct lattice streaks in the IrW and W_2B phases is observed in the HR-TEM images (Fig. 6**c**). Notably, the IrW-W_2B composite demonstrates remarkable OER activity 0.5 M H_2SO_4 aqueous solution, as verified by an overpotential of approximately 291 mV at 10 mA cm_{geo}^{-2}, as observed in the LSV after CV test (Fig. 6**d**). The utilization of both structural analysis and theoretical calculation demonstrates the significant contribution of IrW nanochannels in enhancing the stability of catalysts during OER electrocatalysis. The presence of IrW support effectively inhibits the aggregation of surface Ir atoms with additional O atoms, thereby preventing the formation of unstable Ir^{III} or Ir^{VI} species. Consequently, a layer of active IrO_2 clusters is preserved (Fig. 6**e, f**), enabling the catalyst to sustain high activity and stability within an acidic environment.

Traditional alloys typically consist of one or two metal elements, with their microstructure being modified through the addition of small quantities of alloying elements to fulfill specific performance criteria. Nevertheless, this design approach significantly restricts the range of elements that can be combined, and in practical scenarios, traditional alloys frequently enhance certain properties at the detriment of others [129,130]. To address these aforementioned challenges, the concept of high entropy alloy (HEA) was introduced in the year 2004 [131,132]. HEA materials have garnered significant attention in the realm of catalysis research because of their wide range of component combinations, remarkable stability, and distinctive physical and chemical properties [133]. Multiple studies have consistently shown that HEA structures possess heightened strength, stability, and corrosion resistance when compared to unalloyed metal materials or conventional low-element alloys, owing to the presence of four fundamental effects: high entropy effect, lattice distortion effect, sluggish diffusion effect, and cocktail effect [134–138]. Through the implementation of multi-component design and element regulation, HEAs have the capability to simultaneously attain high activity, high selectivity, stability, and low cost. Consequently, HEA catalysts hold considerable promise for application in acidic OER. Based on the aforementioned research background, Zhu et al.[139] implemented a study on the in situ synthesis of ultra-small size FeCoNiIrRu HEA NPs within electrospun carbon nanofibers (CNFs) (Fig. 7**a**). The FeCoNiIrRu/CNFs showed a low overpotential of 241 mV at 10 mA cm^{-2}, and demonstrated remarkable catalytic stability in 0.5 M H_2SO_4 solution (Fig. 7**b**, **c**). The primary factor contributing to this phenomenon is the sluggish diffusion effect, which hinders the process of metal leaching and dissolution, consequently enhancing the longevity of the catalyst during acidic OER. In situ Raman spectroscopy provided evidence for the presence of hydroxyl (OH) and superoxo (OO) intermediates on the surface of the HEA NPs, indicating the enhanced kinetics of the OER in acidic electrolytes (Fig. 7**d**, **e**).

Previous research has demonstrated that materials containing Ru exhibit notable catalytic activity in acidic environments, yet their

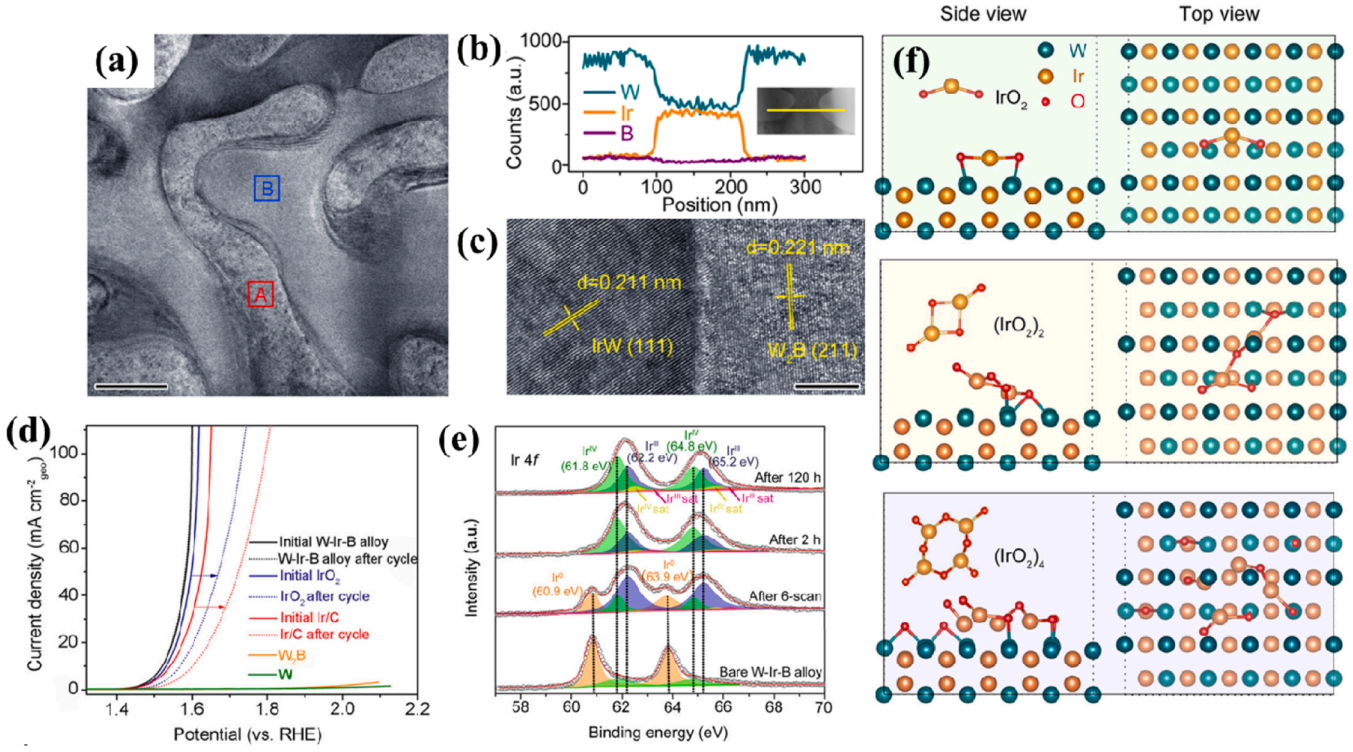

Fig. 6. (a) TEM image and (b) STEM-EDS line-scanning profile of the W-Ir-B alloy. (c) HRTEM image of the phase-separated W-Ir-B alloy. (d) LSV curves of the corresponding electrocatalysts. (e) Ir 4 f deconvoluted core-level peaks. (f) Optimized structures of the $(IrO_2)n$ (n = 1, 2, and 4) clusters adsorbed to the IrW (002) surface [128].

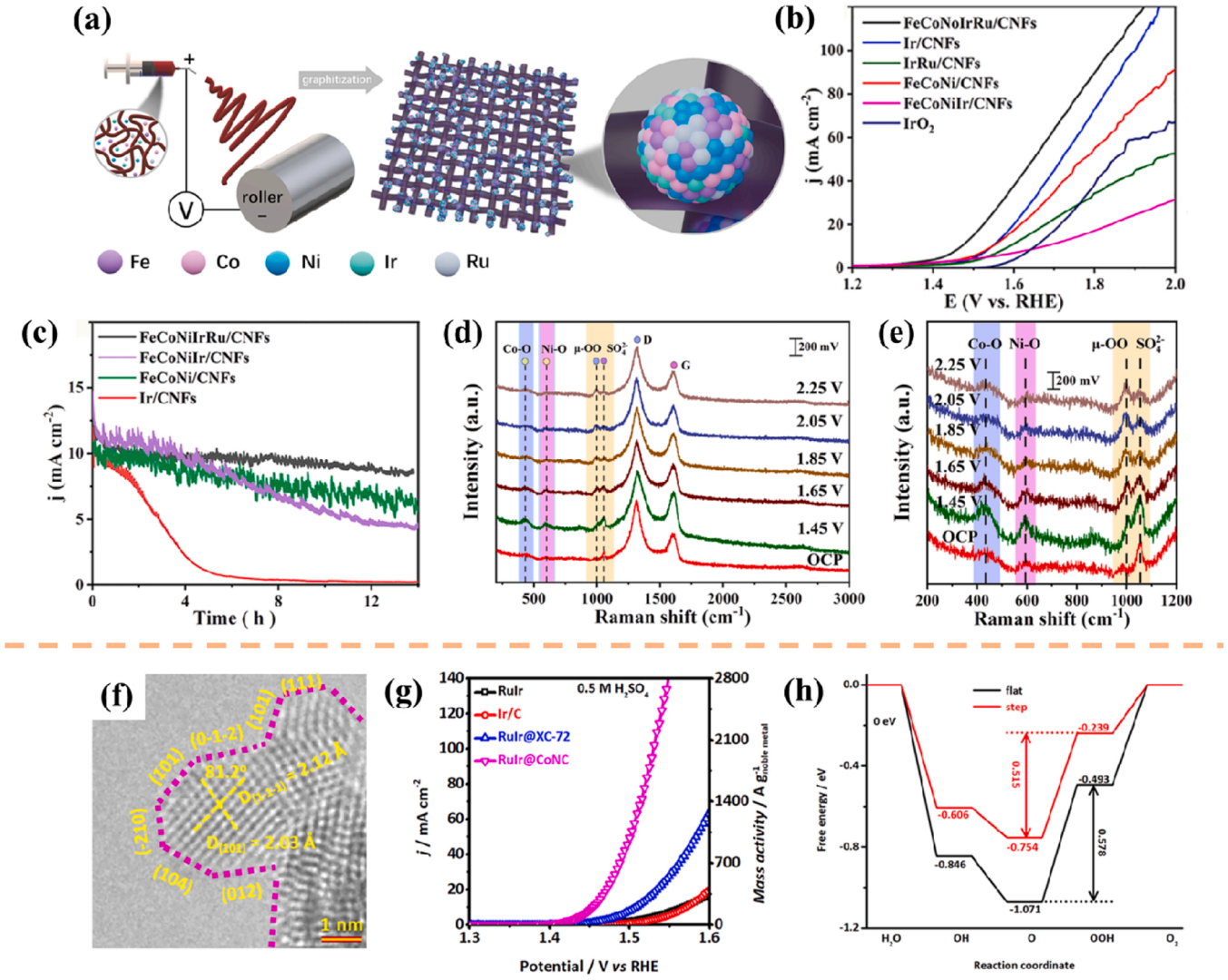

Fig. 7. (a) Preparation process for the FeCoNiIrRu/CNFs. (b) OER curves of the prepared catalysts. (c) i-t curves of the prepared catalysts at 10 mA cm^{-2}. (d, e) In situ Raman spectroelectrochemical study as the potential increases from 0 to 2.25 V (vs. RHE) [139]. (f) HRTEM images. (g) IR-corrected polarization curves. (h) Gibbs free-energy diagram [148].

stability is compromised because of the formation of soluble high-valent state oxides [33,140–142]. Conversely, materials containing Ir exhibit limited catalytic activity but demonstrate exceptional stability in acidic electrolytes [143–145]. By combining the advantageous catalytic activity of Ru with the superior acid stability of Ir, bimetallic RuIr and its mixed oxides present a promising solution for achieving both high activity and stability in the OER under acidic conditions [126,146,147]. Liu et al.[148] conducted a study in which they designed RuIr nanocrystals featuring a surface rich in atomic-step structures. These nanocrystals were successfully dispersed on carbon supports, resulting in the formation of RuIr@CoNC catalysts. This dispersion allowed for a greater number of catalytic active sites to be exposed (Fig. 7**f**). Comparative analysis revealed that RuIr@CoNC exhibited superior performance in the OER when compared to other catalysts and Ir/C. Specifically, it achieved the lowest η_{10} value of only 223 mV at 10 mA cm^{-2} in 0.5 M H_2SO_4 (Fig. 7**g**). Additionally, the findings from the DFT calculations indicate that the inclusion of atomic steps in the RuIr nanocrystals could potentially reduce the maximum potential of the rate-determining step, consequently augmenting the overall catalytic activity (Fig. 7**h**).

The current discourse in academia revolves around the subject of HEA material, with researchers commonly employing four fundamental effects to elucidate the remarkable catalytic performance of HEAs. Nevertheless, the investigation of the underlying mechanisms remains largely unexplored. The plausibility of this explanation warrants examination. For instance, as HEAs consist of a substantial proportion of Ru/Ir elements, it is imperative to ascertain the extent to which the inclusion of other supplementary elements contributes to the enhancement of the overall OER performance.

4. Modification strategies

When conducting laboratory research on OER electrocatalysts, it is crucial to take into account three essential factors: activity, stability, and cost. Thus far, the majority of studies on OER catalysts have primarily concentrated on enhancing catalytic activity and minimizing material expenses, with limited attention given to systematically devising approaches to improve the stability of OER catalysts, particularly in acidic conditions [149,150]. Nevertheless, the stability of OER catalysts holds significant importance in industrial applications, necessitating further scrutiny and consideration [151]. In the process of OER, the stability of the catalyst is predominantly influenced by mechanical and chemical factors. Mechanical stability is influenced by the strength of the catalyst's binding to the support/electrode and the stress caused by the

formation of O_2 bubbles. On the other hand, chemical stability pertains to the resistance of the active site of the catalyst and the support material against corrosion and oxidation. In the present research on acidic OER catalysts, the issue of stability has not received sufficient attention in comparison to catalytic activity [61].

4.1. Structural design

Morphological adjustment possesses a broad spectrum of potential applications within the realm of electrocatalysis, and its merits can be enumerated as follows: 1) it can significantly improve the exposure of reaction sites; 2) it facilitates the penetration of electrolytes and aids in the process of mass transfer; 3) it enables the adjustment of the electronic structure, thereby expediting the migration and transfer of charge [152–154].

Ir-based catalysts possess exceptional acidic OER properties; however, the scarcity and high cost of Ir elements pose significant challenges. To address this issue, the generation of a core-shell structure with

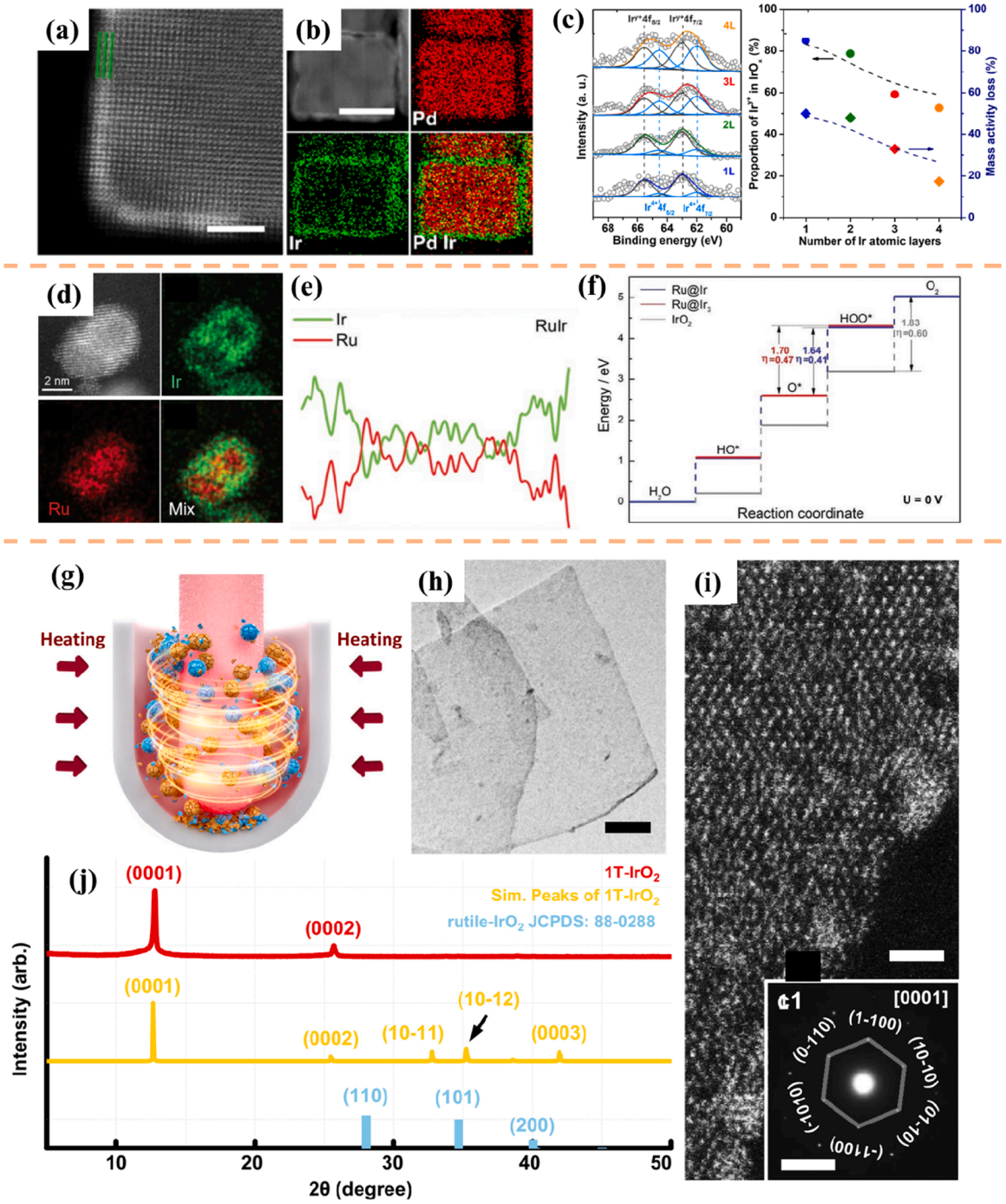

Fig. 8. (a) High-resolution HAADF−STEM images. (b) EDX mappings of Pd@Ir$_{3\,L}$. (c) Ir 4 f XPS spectra recorded from Pd@Ir$_{nL}$/C and effects of the number of Ir atomic layers on the proportion of Ir^{y+} ($y > 4$) in the oxidized IrO_x phase and the mass activity loss of Pd@Ir$_{nL}$/C [155]. (d) EDX elemental mapping of Ru@Ir–O. (e) EDX line-scan plot of Ru@Ir–O along a single particle. Scale bar: 1 nm. (f) Energy profile of OER on Ru@Ir–O, Ru@Ir$_3$-O, and IrO_2 at U = 0 V [156]. (g) Schematic representation for preparing 1 T-IrO_2. (h) TEM images of 1 T-IrO_2. (i) HAADF-STEM image of 1 T-IrO_2, inset: The SAED pattern of 1 T-IrO_2. (j) X-ray diffraction (XRD) patterns [158].

Ir serving as the shell can effectively expose the Ir active site, thereby enhancing atomic utilization and maximizing mass activity. Xia et al. [155] employed KBr to impede the reduction of Ir(III) precursor, enabling the precise preparation of Pd@Ir_{nL} (n: number of Ir atomic layers) core-shell nanocubes with varying thicknesses of Ir atomic layers (Fig. 8**a, b**). The optimization of OER mass activity and stability of Pd@Ir_{nL} nanocubes in acidic media was facilitated by precise control at the atomic level. The experimental results from the OER test indicated that a thicker Ir shell corresponded to enhanced stability in the OER performance of the material (Fig. 8**c, left**). Furthermore, the analysis of the Pd@Ir_{nL} nanocubes revealed that those with thicker Ir shells exhibited a higher proportion of Ir^{4+} (Fig. 8**c, right**). It is worth noting that Ir^{4+} ions are known to possess greater stability compared to Ir^{y+} ions, and the substantial increase in the Ir^{4+} ratio significantly contributed to the improved stability of the nanocubes.

In a comparable catalyst design, Yue et al. [156] prepared core-shell nanoparticles consisting of a Ru core and an O-incorporated Ir shell (Ru@Ir−O) (Fig. 8**d, e**). DFT calculations demonstrate the interaction between the core and shell, as well as the presence of tensile strain, can result in band displacement and charge redistribution. These electronic factors subsequently enhance the bonding strength between O* and HOO* intermediates on the catalyst surface, thereby augmenting the activity for the OER in 0.5 M H_2SO_4 (Fig. 8**f**). Metallene, possessing an ultra-thin two-dimensional graphene structure, exhibits distinctive physical and chemical characteristics due to the abundance of uncoordinated metal atoms [157]. These properties include a simple composition, a substantial specific surface area, enhanced conductivity, abundant metal active sites, and robust catalytic activity. Consequently, Metallene holds significant potential for various applications in the realm of electrocatalysis. Shao et al. [158] employed a combination of mechanical chemistry in a highly alkaline environment and heat treatment techniques to synthesize 1 T phase-iridium metal oxide (1 T-IrO_2) (Fig. 8**g**). The thin sheet structure of the sample (Fig. 8**h**) is confirmed by Fig. 8**i, j**, which provide evidence of its classification as belonging to the 1 T phase. Electrochemical tests demonstrate the remarkable acidic OER activity and cyclic stability of 1 T-IrO_2 in 0.1 M O_2-saturated $HClO_4$. Calculations further indicate that the enhanced catalytic performance of 1 T-IrO_2 in OER can be ascribed to the elevation of the optimal free energy of the hydroxyl group on the Ir atom.

The modification strategy of structural design is highly developed and effective. In the aforementioned example, precise control over the number of atomic layers in the shell is achievable when preparing the core-shell structure catalyst (Pd@Ir_{nL}). Deng's team has achieved significant progress in the design and utilization of "chainmail for catalyst" [159]. Nevertheless, there is limited documentation on whether the industrial-scale production of the target catalyst ensures structural

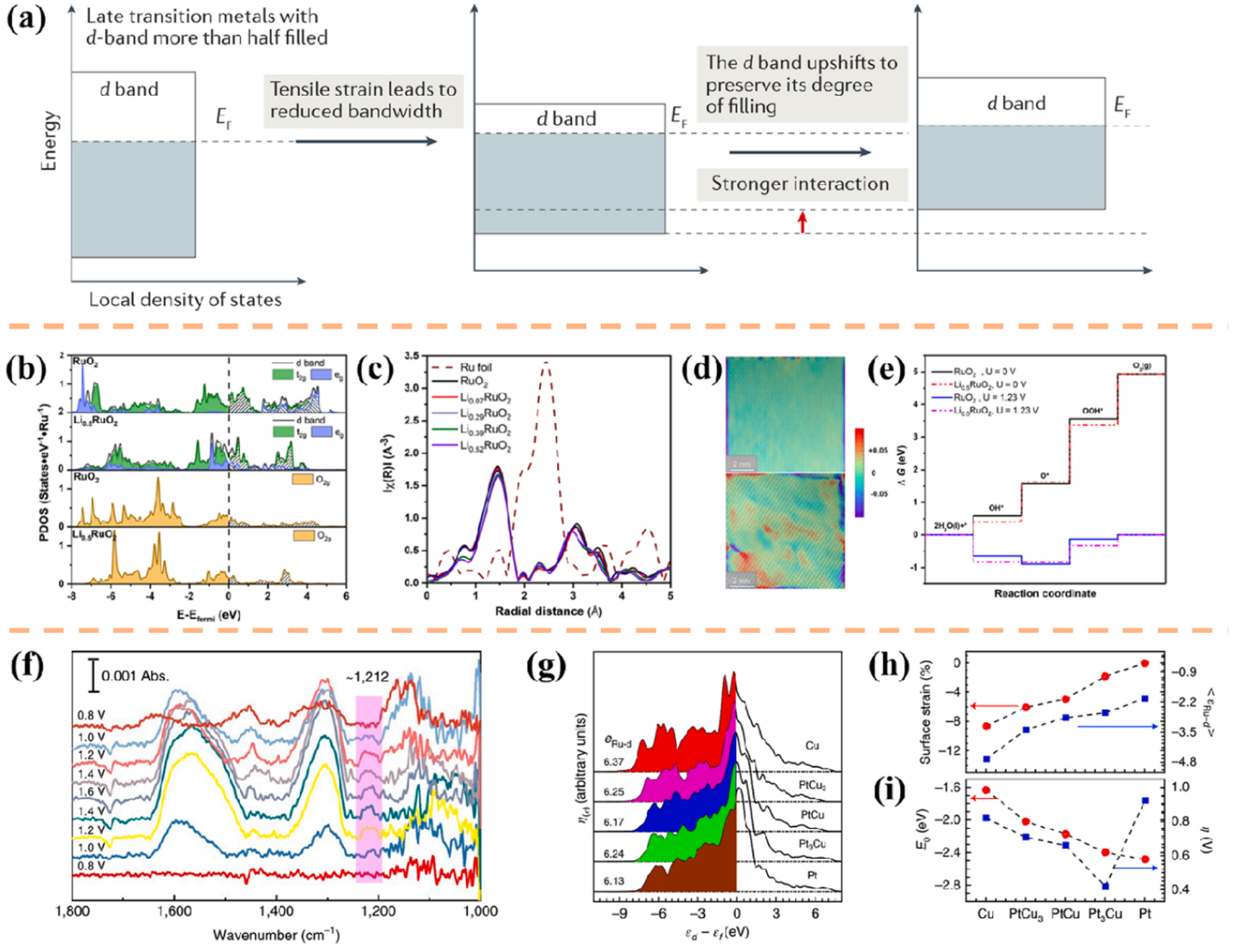

Fig. 9. (a) Energy diagrams explaining the effect of tensile strain on the *d*-band position of late transition metals [161]. (b) PDOS of the RuO_2 and $Li_{0.5}RuO_2$. (c) Fourier-transformed Ru K-edge EXAFS spectra. (d) Lattice strain (ε_{xx}) measured from GPA for RuO_2 (up) and for $Li_{0.56}RuO_2$ (down). (e) Calculated OER free-energy diagrams for RuO_2 and $Li_{0.5}RuO_2$ [41]. (f) In situ ATR-IR spectra. (g) PDOS of surface-embedded Ru_1 4*d* concerning the Fermi level. (h) In-plane lattice contraction. (i) Corresponding adsorption energy E_O [166].

uniformity.

4.2. Strain engineering

As widely known, strain engineering represents a potent approach for enhancing catalyst performance, as it involves the manipulation of the atomic spacing on the catalyst surface. This manipulation, in turn, leads to alterations in the electronic structure of the catalyst, thereby optimizing the adsorption of reactants and intermediates [79,160]. In the realm of mechanism, there is a widespread consensus regarding the influence of strain on the properties of metal surfaces, which can be attributed to the displacement of the metal *d*-band center. This phenomenon is illustrated in Fig. 9**a** [161], where it is observed that for late transition metals (with a *d*-band that is more than half-filled), tensile strain leads to a reduction in the coordination number (i.e., the number of neighboring metal atoms), consequently causing a decrease in bandwidth and an upward displacement of the *d*-band center. The presence of compressive lattice strain induces a widening of the band and a downward shift of the *d*-band center [162,163]. This shift in the *d*-band center has a notable impact on the adsorption energy of intermediates and the energy barrier of the RDS, consequently altering the reaction kinetics of the catalytic process.

The incorporation of foreign components into the host substance through electrochemical ion insertion has proven to be a successful approach for manipulating the electronic or crystal structure [164,165]. Nevertheless, the potential of strain engineering via electrochemical lithium insertion to enhance the OER performance of RuO_2 remains largely unexplored. Zhang et al.[41] have documented a technique involving the insertion of lithium ions into the lattice interstices of RuO_2, which effectively enhances both the acidic OER activity and stability in 0.5 M H_2SO_4 solution. The analysis of the partial density of states (PDOS) (Fig. 9**b**) demonstrates that the incorporation of lithium can effectively alter the *d*-band structure of Ru and the 2p-band structure of O. Consequently, the heightened OER activity resulting from lithium intercalation can be attributed to the modification of the electronic structure of Ru. Furthermore, the Fourier-transformed Ru K-edge EXAFS (Fig. 9**c**) reveals that the introduction of lithium intercalation induces lattice distortion and strain. The utilization of geometric phase analysis (GPA) in HRTEM images provides further evidence that the presence of Li_xRuO_2 induces a distribution of tensile-compressing strain, which is attributed to the lattice distortion of RuO_2 (Fig. 9**d**). Additionally, Fig. 3**e** illustrates the distribution of OER free energy for both RuO_2 and Li_xRuO_2. The obtained results indicate that the RDS for both RuO_2 and $Li_{0.5}RuO_2$ involves the formation of OOH* species. Furthermore, it is observed that the ΔG value for OOH* formation on $Li_{0.5}RuO_2$ is lower compared to that of RuO_2.

In a highly acidic and oxidative environment, RuO_2 undergoes facile oxidation to form soluble high oxidation state Ru oxides (such as RuO_4) at elevated working potentials, leading to its deactivation. The primary cause of Ru deactivation is typically attributed to the loss of lattice oxygen mobility, which plays a crucial role in the acidic OER. To address this issue, Wu et al. [166] employed acid etching and electrochemical leaching techniques to prepare Ru_1 supported on an alloy substrate, utilizing a Pt-based alloy as the carrier material. The in situ ATR-IR spectra demonstrate the capture of the OOH intermediate (Fig. 9**f**), suggesting that the AEM is the primary mechanism for the OER of the catalyst, thereby enhancing its stability in an O_2-saturated 0.1 M $HClO_4$. Additionally, theoretical analysis reveals that the compressive strain induced by the Pt skin shell can modulate the electronic structure of individual Ru sites and optimize the binding affinity of Ru with oxygen-containing intermediates. Consequently, the Ru_1 species supported on the alloy exhibits superior activity and stability (Fig. 9**g-i**).

The optimization of the equilibrium between stability and activity of electrocatalysts has consistently been of paramount importance in the field. Strain, which refers to the distortion of the lattice resulting from either local or global stress, induces deviations of atoms from their equilibrium positions. While a minimal level of strain fails to adequately regulate the electronic structure of the material, an excessive amount of strain detrimentally impacts the structural stability of the catalyst. Consequently, the quantitative description and introduction of strain hold immense significance in comprehending the relationship between the structure and activity of catalysts, with strain serving as a descriptor.

4.3. Doping

Heteroatom doping alter the *d*-band center's position concerning the Fermi level, leading to the optimization of adsorption energy for the intermediate and the regulation of intrinsic activity [167]. This process can be categorized into metal doping [168,169], non-metal doping [170,171] and co-doping [172,173], based on the types of doping atoms involved.

The distinctive LOM of Ru-based oxides exhibits significant OER activity. However, the involvement of lattice oxygen can result in the creation of soluble high oxygen vacancy intermediates (*Vo-RuO_4^{2-}), leading to the collapse and dissolution of the catalyst structure. Consequently, this leads to a sharp decline in catalytic activity and challenges in maintaining stability. Huang et al. [174] developed a single-site Pt--doped RuO_2 hollow nanospheres (SS Pt-RuO_2 HNSs) electrocatalyst for water splitting, which demonstrated exceptional OER performance in 0.5 M H_2SO_4. In this catalyst, carbon is effectively trapped within the gaps, and Pt replaces a portion of the Ru sites in the form of a single site (Fig. 10**a**). The results of the structural analysis demonstrate that the presence of interstitial carbon leads to elongation of the Ru-O and Pt-O bonds in SS-PT-RuO_2 HNSs (Fig. 10**b**, **c**). Furthermore, the incorporation of SS Pt significantly influences the electronic properties of RuO_2. The DFT calculation reveals that the inclusion of SS-Pt in RuO_2 hinders the dissociation of lattice oxygen, thereby enhancing the stability of OER (Fig. 10**d**). Additionally, it reduces the formation barrier of crucial intermediates (Fig. 10**e**), regulates the 4d orbitals of the Ru site, and consequently increases the catalytic activity (Fig. 10**f**).

Heteratom-doping is an impressive strategy to regulate the acidic OER properties of RuO_2, but the traditional dopants can only improve the performance of RuO_2 under low overpotential through static electron structure redistribution [33]. It is attractive to develop dopants that can adjust the performance of OER with dynamic electron distribution at different potentials. Qiao et al. [175] employed the molten salt method to introduce Re into RuO_2, resulting in the formation of $Re_{0.06}Ru_{0.94}O_2$. Notably, Re atoms were found to be uniformly distributed within the RuO_2 lattice (Fig. 10**g**, **h**). This catalyst displayed remarkable catalytic activity and stability towards acidic OER in O_2-saturated 0.1 M $HClO_4$. Operando XAS analysis further confirmed that Re dopants effectively acquired electrons from Ru sites under in-situ potential conditions, thereby facilitating OER activation. Moreover, these Re dopants contributed electrons back to the system, effectively preventing Ru dissolution even at high overpotentials (Fig. 10**i**, **j**). In contrast to the stationary redistribution of electrons observed in traditional dopants, the Re dopant present in $Re_{0.06}Ru_{0.94}O_2$ exhibits a dynamic process of electron acceptance and donation, which effectively enhances both the activity and stability of the material.

The prevailing consensus suggests that doping does not induce a shift in the OER mechanism from AEM to LOM. Rather, the observed increase in activity can be attributed to the optimization of the binding energy of oxygen intermediates. However, given that doping modulates the electronic structure of the metal, consequently altering the *d*-band center, there exists a theoretical possibility of altering the OER reaction mechanism. The most recent study revealed that the introduction of P-doping in $NiFeO_x$ during the experiment resulted in an enhancement of the basic OER activity of the catalysts. The doping of P atoms led to an increase in the covalent bonding between the metal and oxygen in the in-situ generated NiOOH, thereby activating the lattice oxygen. This activation subsequently triggered the LOM process, disrupting the linear relationship of the original AEM between *OH and *OOH species.

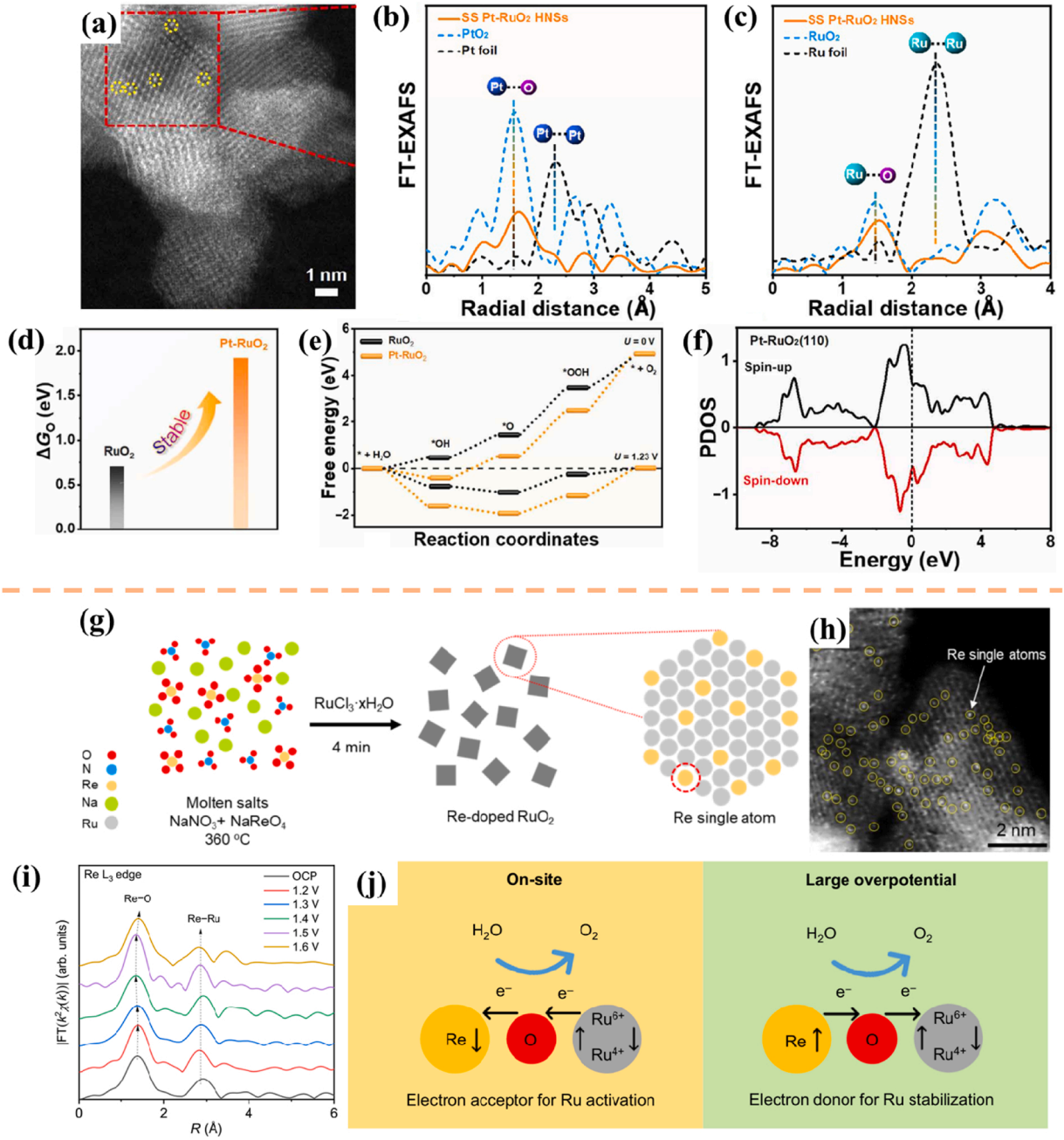

Fig. 10. (a) High-resolution HAADF-STEM image of SS Pt-RuO_2 HNSs. (b) Pt L3-edge EXAFS spectra. (c) Ru K-edge EXAFS spectra. (d) The dissociation energy of *O in RuO_2 and Pt-RuO_2. (e) The free energy profiles. (f) The PDOS of 4d orbitals of surface Ru atoms in Pt-RuO_2 [174]. (g) Schematic for the molten-salt synthesis of Re-RuO_2. (h) HRSTEM image of pristine $Re_{0.06}Ru_{0.94}O_2$. (e, f) HAADF-STEM image of $Re_{0.06}Ru_{0.94}O_2$ after test. (i) FT-EXAFS signals for $Re_{0.06}Ru_{0.94}O_2$. (j) Schematic for dynamic electron transfer in $Re_{0.06}Ru_{0.94}O_2$ [175].

Consequently, the overall activity of the catalyst was significantly improved [176]. Further investigation is necessary to determine if this transformation occurs in acidic OER and if it is a prevalent occurrence in heteroatom-doped OER catalysts. Additionally, while doping proves to be an effective method for catalyst modification, there remain numerous challenges including achieving quantitative doping of heteroatoms, controlling the types and proportions of multiple heteroatom doping, and precise doping based on various locations (e.g., depth, edge) of the primary catalyst.

Numerous studies have demonstrated that the degradation of Ru-based catalysts in acidic electrolytes primarily stems from the oxidation of lattice oxygen [177,178]. The liberation of oxygen from the electrocatalyst's lattice leads to the generation of oxygen vacancies (V_O), which, in turn, expedite the over-oxidation of the exposed Ru. Consequently, it can be postulated that enhancing the energy required for V_O formation and impeding direct O-O coupling from the lattice would prove advantageous in preserving the stability of Ru-based materials in acidic electrolytes. According to the findings presented in Fig. 11**a**, the energy required for the formation of V_O (ΔG) in $W_mEr_nRu_{1-m-n}O_{2-\delta}$ exhibits a significant increase when the center of the O 2p band is shifted downward, thereby preventing the formation of soluble $Ru^{x>4}$. Building upon this theoretical analysis, Wang et al. [179] synthesized $W_mEr_nRu_{1-m-n}O_{2-\delta}$ nanosheets through the combination of a hydrothermal method and calcination. These nanosheets were subsequently employed as catalysts to evaluate their acidic OER properties. By incorporating tungsten (W) and erbium (Er), the electronic structure of

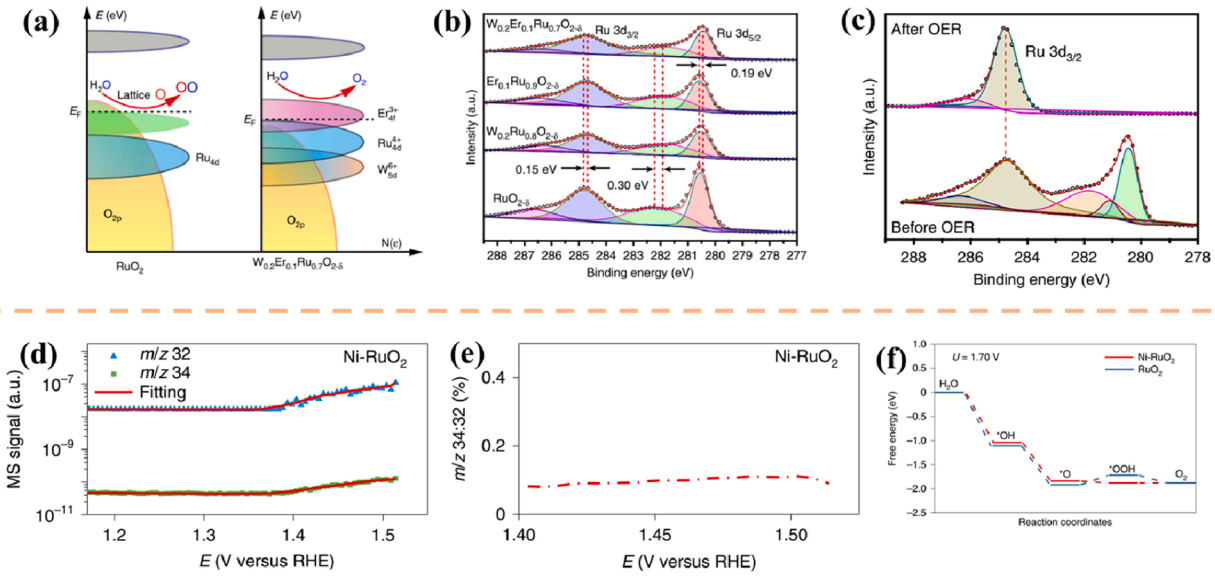

Fig. 11. (a) Schematic diagrams of rigid band models for RuO_2 and $W_{0.2}Er_{0.1}Ru_{0.7}O_{2-\delta}$. (b) Ru 3d spectra for the prepared electrocatalysts. (c) Ru 3d spectra for $W_{0.2}Er_{0.1}Ru_{0.7}O_{2-\delta}$ before and after 500 h stability [179]. (d) DEMS signals of $^{32}O_2$ ($^{16}O + {}^{16}O$) and $^{34}O_2$ ($^{16}O + {}^{18}O$), (e) Ratio of $^{34}O_2$:$^{32}O_2$. (f) Computed free energy evolution of OER via AEM on surfaces of RuO_2 (110) and Ni-RuO_2 (110) [33].

RuO_2 was adjusted to enhance its catalytic performance. The electrochemical test demonstrates the catalyst (denoted as $W_{0.2}Er_{0.1}Ru_{0.7}O_{2-\delta}$), exhibits exceptional stability for a duration exceeding 500 h in 0.5 M H_2SO_4. XPS analysis reveals that the incorporation of both W and Er in the catalyst effectively inhibits the overoxidation of Ru from Ru^{4+} to $Ru^{x>4}$, achieved by modulating the electronic structure of RuO_2 (Fig. 11**b**, **c**).

As a recognized alternative to Ir-based catalysts, Ru-based catalysts have cost advantages, but the stability of Ru-based catalysts at low current densities is far from the requirements of industrial applications [166,180]. To overcome this limitation, Wang et al. [33] conducted a three-step synthesis method to prepare a Ni-stabilized RuO_2 catalyst (Ni-RuO_2). The catalytic activity and stability of Ni-RuO_2 were found to be excellent, with a duration of over 200 h in an O_2-saturated 0.1 M $HClO_4$ electrolyte. Theoretical and experimental investigations, including DFT studies and *operando* differential electrochemical mass spectroscopy (DEMS) analysis, support the notion that the Ni-RuO_2 catalysts are more inclined towards the AEM mechanism rather than the LOM mechanism. The incorporation of Ni dopants significantly improves the lattice stability of the surface Ru and subsurface oxygen, thereby exerting a pivotal influence on enhancing the durability of the OER (Fig. 11**d-f**).

In conclusion, there exist two mechanisms for improving the OER performance of RuO_2 through the implementation of doping strategies. The first mechanism involves the creation of an electron-rich environment at Ru sites or the provision of electrons to Ru under high potential conditions, thereby restraining the overoxidation of the Ru active center. The second mechanism aims to impede the LOM mechanism to enhance stability. The quantification of Ru loss by measuring the Ru content in the electrolyte after the reaction serves as a means to evaluate the structural stability of the catalyst. The regulation of doping on OER catalyst materials primarily centers on the examination of physical properties such as wettability and conductivity [181,182], reaction path analysis including AEM and LOM, electronic band structure evaluation focusing on the O 2p band, local charge distribution analysis utilizing SPS, adsorption energy assessment using DFT, and other pertinent aspects of the catalyst. These investigations have yielded significant advancements. Doping engineering stands as a prevalent and effective approach for enhancing catalytic performance. Nevertheless, the precise control of doping concentration and placement remains a formidable obstacle.

4.4. Creation of oxygen vacancies

The catalytic process is influenced by the physicochemical properties of the active site situated on the surface of the catalyst, thereby directly influencing the adsorption and desorption processes of the reaction molecules. This interaction assumes a crucial role in determining the characteristics of the catalytic reaction. Defect engineering is employed to enhance the electronic structure of the catalyst by modifying the surface microstructure, resulting in improved electron transfer rates and reduced adsorption-free energy of substrate molecules. Defects can be categorized as anionic or cationic, depending on their species [183,184].

Vacancy defects, such as oxygen vacancies in oxides, have been found to have several effects, including reducing the O 2p band and Fermi level, increasing the covalency of metal-oxygen bonds, and activating lattice oxygen, ultimately leading to enhanced OER activity [167]. Zhang et al. [185] propose a functionalization strategy involving the activation of Ru clusters with superior OER catalytic activity. This is achieved by wrapping the Ru nanoclusters/carbon hybrid microsheet with sub-nanometer RuO_2 that is rich in oxygen vacancy (referred to as Ru@V-RuO_2/C HMS). The HAADF-STEM image (Fig. 12**a**) reveals a core-shell nanostructure. XPS reveals the existence of oxygen vacancies (Fig. 12**b**). DFT calculations indicate that the introduction of an oxygen-vacancy-enriched RuO_2 sub-nanometer skin on the coated Ru core can attenuate the adsorption of oxygen-based intermediates, thereby expediting the reaction kinetics (Fig. 12**c**).

In another study using defect engineering to modify catalysts, Chen et al. [186] fabricated Zn-doped RuO_2 materials, utilizing metal doping to regulate conductivity and electronic structure, reduce nanoparticle size to expose more active sites, and enhance the intrinsic activity of catalysts in 0.5 M H_2SO_4 by introducing defects/vacancies. Through acid treatment, they obtained ultrafine RuO_2 NPs with abundant defects on carbon cloth, referred to as UfD-RuO_2/CC (Fig. 12**d**). The catalyst exhibits several advantages. Firstly, the partial substitution of Ru with divalent Zn leads to the generation of oxygen vacancies and a decrease in the crystallinity of RuO_2. Secondly, during the acid treatment process, Zn can be readily eliminated, thereby creating defects and further reducing the size of RuO_2 particles. The remarkable catalytic properties of the catalysts can be primarily attributed to the existence of oxygen

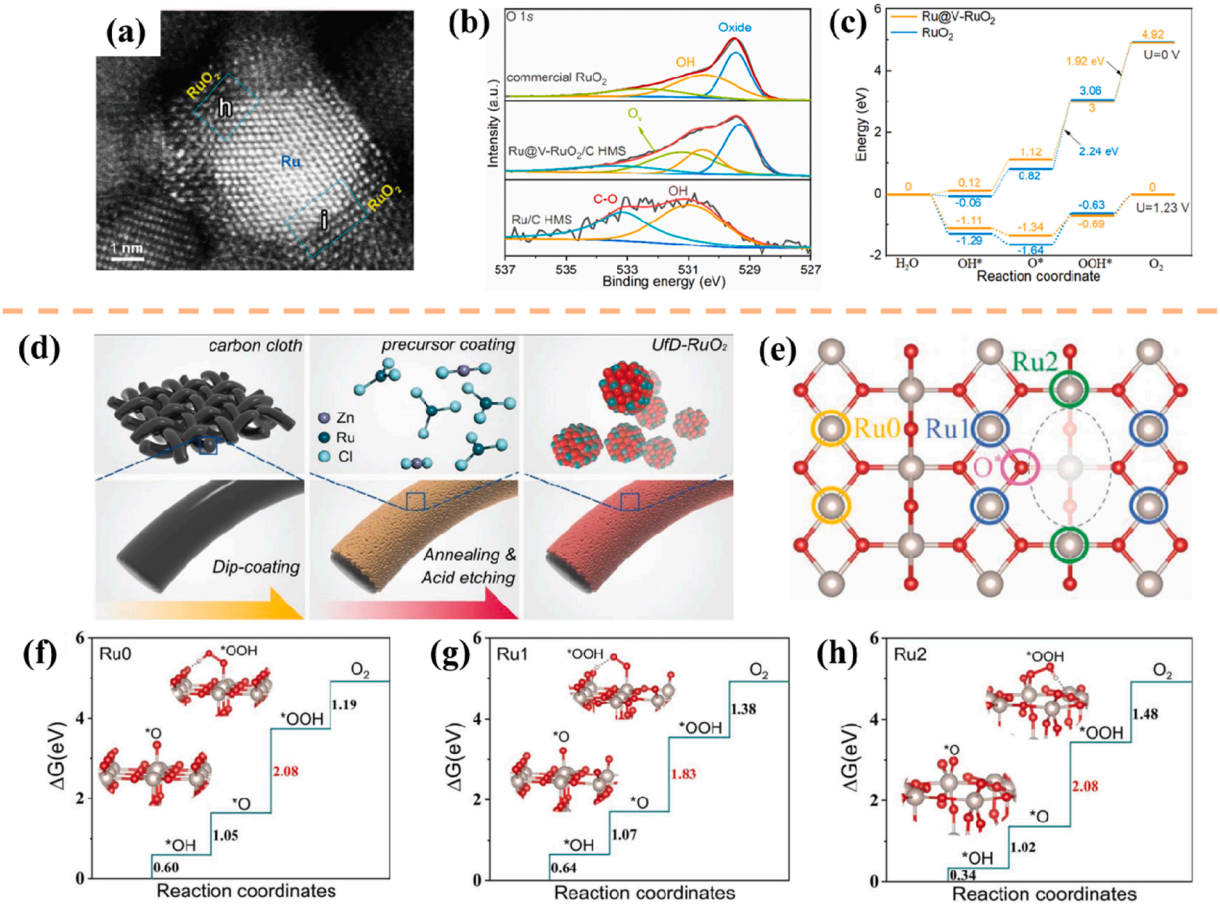

Fig. 12. (a) Aberration-corrected HAADF-STEM of Ru@V-RuO_2/C HMS. (b) The O 2p high-resolution XPS spectra of the electrocatalysts. (c) Free energy diagrams [185]. (d) The preparation route for the UfD-RuO_2/CC. (e) The top view of defective RuO_2 structure. The calculated free-energy profiles of OER on the (f) Ru0, (g) Ru1, and (h) Ru2 sites [186].

defects, which promote the creation of supplementary active sites and regulate the electronic structure of 5-coordinated Ru (Fig. 12**e-h**).

In the realm of electrocatalysis, it has been observed that the presence of oxygen vacancies alters the local coordination environment of the electrocatalyst through its influence on the energy band structure of the material, consequently enhancing its intrinsic activity. Furthermore, oxygen vacancies can also furnish supplementary active sites for electrode reactions, thereby augmenting the overall catalytic performance.

Parts **4.3 Doping** and **4.4 Creation of oxygen vacancies** are surface defects, which will create strain. In addition, the current preparation method is to achieve the addition of defects by in-situ method or post-treatment method, which leads to the random arrangement of defects and the existence of multiple types of defects [187]. There will be synergies between the multiple types of defects and the induced strains, which hinder the understanding of how they improve in the catalytic process. How to isolate these complex factors is the premise of maximizing synergy.

4.5. Strong metal oxide-support interaction (SMOSI)

The phenomenon known as the strong metal-support interaction (SMSI) was initially observed and defined in 1978 [188]. SMSI is commonly understood as the interplay between metal and transition metal oxides, with its scope gradually expanding to encompass non-metallic oxide substrates. This interaction has the potential to enhance the performance of catalysts, particularly in thermal catalysis, by improving their activity, selectivity, and stability. Building upon the foundation of SMSI, the strong metal oxide-support interaction (SMOSI) has been identified, offering a novel avenue for the advancement of supported catalysts. Numerous studies have verified that the deposition of noble metal catalysts onto robust substrates can enhance the dispersion of noble metals while reducing the loading [189]. Additionally, the interaction between the noble metal and the substrates can optimize the stability and specific activity of the catalyst. Consequently, this approach holds promise for addressing the limitations of Ru/Ir-based catalysts in the context of acidic OER [165,190].

In their study, Song et al. [191] employed the template method to synthesize RuO_2-WC NPs and demonstrated their exceptional OER properties in 0.5 M H_2SO_4 (Fig. 13**a**). The presence of two lattices, WC and RuO_2, along with the observable interface between them (Fig. 13**b**). Furthermore, Fig. 13**c** reveals that the change in the characteristic peak of WC before and after the incorporation of RuO_2 suggests electron transfer from WC to RuO_2, thus confirming the presence of interaction at the interface. The strong interaction between the catalyst RuO_2-WC and its support optimizes the electronic structure surrounding the Ru active site, leading to favorable adsorption of OER intermediates. This, in turn, reduces the reaction barrier for the RDS (Fig. 13**d**). Additionally, the WC support contributes a greater number of electrons to the catalyst surface, safeguarding the Ru active site against overoxidation and enhancing overall stability. Similarly, Cho et al. [192] conducted a study on the electrocatalyst IrO_x/Zr_2ON_2, utilizing Zr_2ON_2 as the support, to address the inherent conflict between catalyst activity and stability. Through XPS analysis, it can be deduced that the strong interaction between IrO_x and Zr_2ON_2 leads to the transfer of electrons from the support to the catalyst (Fig. 13**e**). Furthermore, the longer Ir-O bond length observed in IrO_x/Zr_2ON_2 compared to IrO_2 suggests the presence of tensile strain in

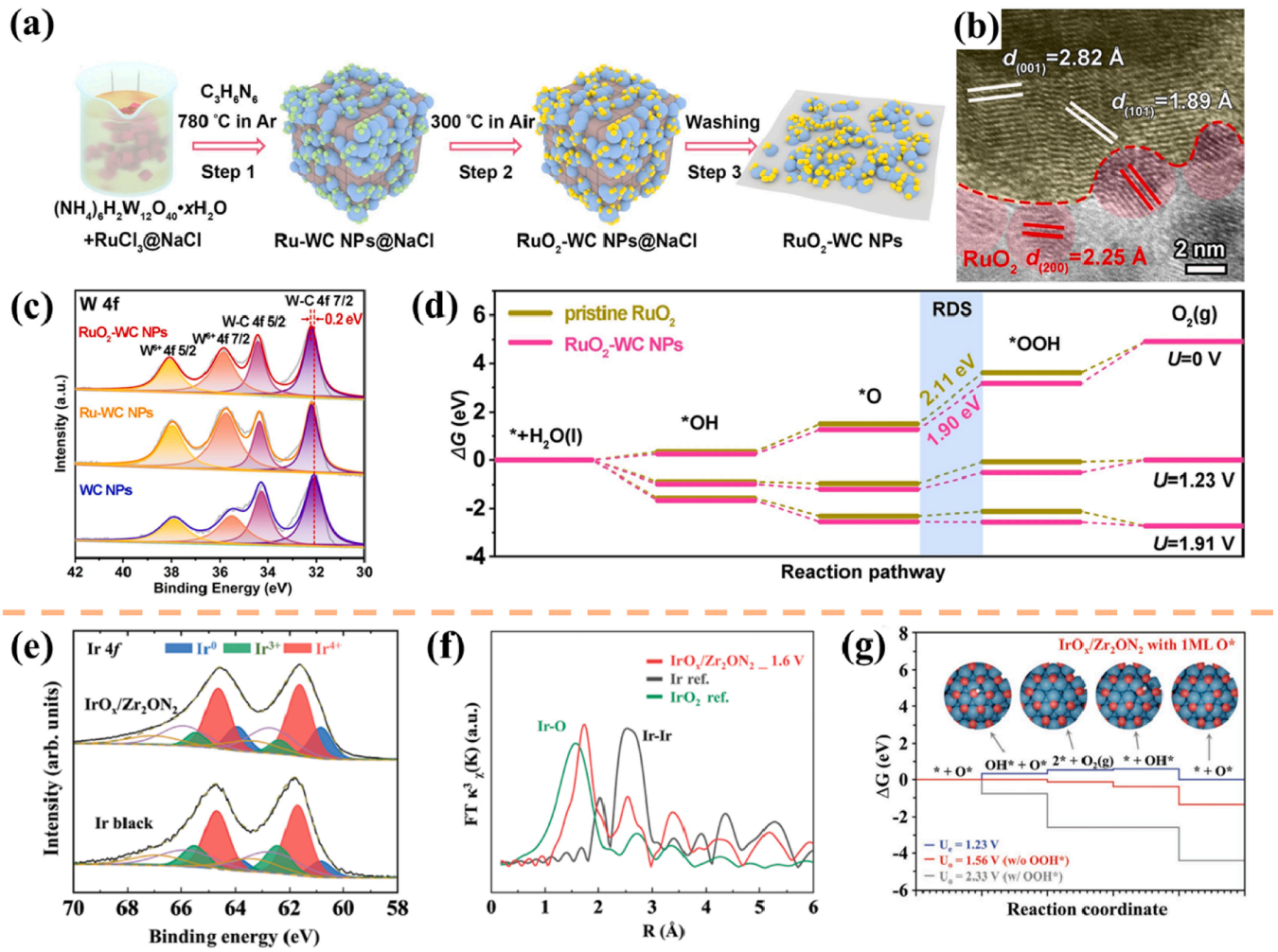

Fig. 13. (a) Diagram for the fabrication procedure, and (b) HRTEM image of RuO_2-WC NPs. (c) High-resolution XPS spectra of W 4 f. (d) Free-energy landscape of pristine RuO_2 and RuO_2-WC NPs [191]. (e) Ir 4 f XPS spectra. (f) Fourier transformed EXAFS analysis. (g) DFT-estimated reaction energy diagram for the OER on on IrO_x/Zr_2ON_2 with 1 ML O* [192].

the oxidized Ir catalyst (Fig. 13**f**). The experimental and theoretical findings demonstrate that the diminished oxidation state of Ir and the elongated Ir-O bond length in IrO_x/Zr_2ON_2 effectively improve the activity and stability of the catalysts in an Ar-saturated 0.5 M H_2SO_4 solution. Additionally, the reaction pathway shifts from the conventional AEM to the LOM (Fig. 13**g**).

The occurrence of electron transfer is influenced by the disparate chemical potential between the metal and the support, leading to charge redistribution at the metal site and subsequent impact on catalytic activity. The positioning of metal species on the support and the characteristics of the carrier plays a role in determining the extent of electron transfer [193]. In the process of choosing a suitable support material, it is observed that traditional carbon-based materials and transition metal oxides demonstrate a common trade-off between their structural stability and electronic conductivity, rendering them incapable of fulfilling the criteria for both electrical conductivity and corrosion resistance. Consequently, WC and Zr_2ON_2 were individually selected for the aforementioned studies. The interaction between the catalyst and support enhances the electronic structure of the surrounding active site, resulting to enhanced catalytic activity and stability, and potentially modifying the pathway of the OER. The efficacy of the SMOSI in reducing the noble metal content in catalysts, while maintaining catalytic performance and reducing costs, has been demonstrated.

4.6. *Heterojunctions*

The utilization of multiple materials in the construction of heterogeneous structures presents a viable approach for enhancing catalyst activity. Through the amalgamation of distinct components, the interface undergoes electronic redistribution, leading to the attainment of synergistic effects such as the ensemble effect and electron effect. Additionally, by altering the composition and crystal phase of the same component, a novel interface structure can be generated [194]. Numerous studies have demonstrated the benefits of heterojunction electron transport in effectively maintaining the equilibrium between the activity and stability of acidic OER [195,196].

Su et al. [197] have reported a low Ir electrocatalyst, known as Ir-NCT/CC, which involves the embedding of Ir nanocrystals (Ir-NCT) into 3D carbon clothes (CC) using a "graphene nanoflake amino-induced" strategy. The HAADF-TEM images of Ir-NCT/CC, both before and after the OER, reveal the formation of amorphous oxides (IrO_x) on the surface of Ir-NCT/CC. These oxides then form heterojunctions with the internal Ir nanocrystals (Fig. 14**a**, **b**). The stability of the IrO_x active phase is demonstrated by in-situ SRIR measurements, which reveal the presence of a dynamically-evolved surface heterojunction. This heterojunction facilitates the formation of *OOH intermediates, thereby enhancing the efficiency and speed of the four-electron OER process (Fig. 14**c**). This approach has led to the achievement of excellent acidic OER activity and stability in 0.1 M

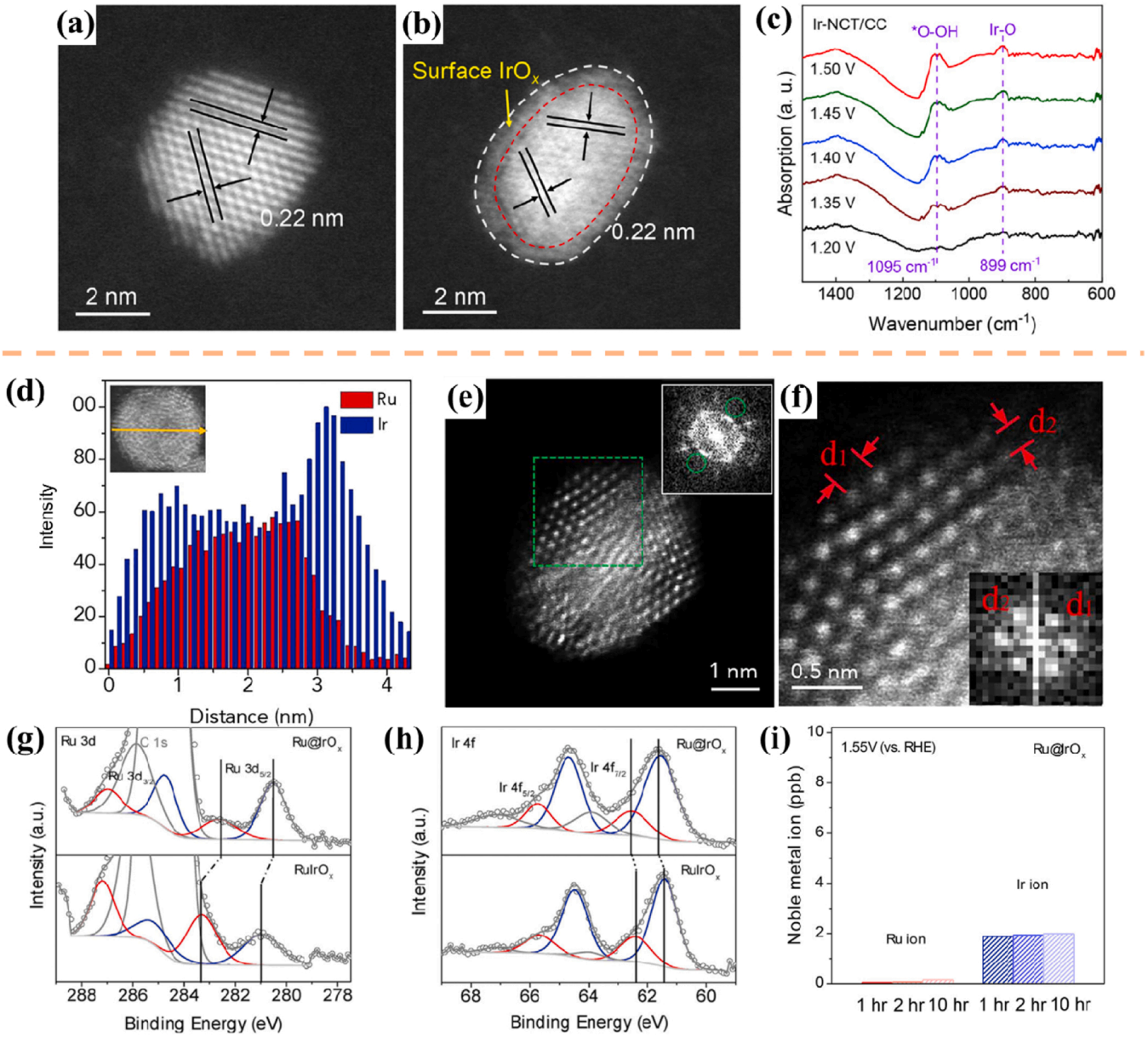

Fig. 14. HAADF-TEM images (a) before and (b) after OER process. (c) In-situ SRIR for Ir-NCT/CC [197]. (d) EDX line profile across an individual Ru@IrO_x nanocrystal. (e) HAADF-STEM image of Ru@IrO_x. (f) An enlarged view of the rectangular region in (e). (g) Ru 3d, and (h) Ir 4 f XPS spectra of Ru@IrO_x and $RuIrO_x$. (i) ICP-MS analysis data for Ru@IrO_x [198].

$HClO_4$.

The catalytic activity of Ru-based oxides was found to be high, but their stability was poor. In contrast, Ir-based oxides exhibited relatively high stability but lower catalytic activity compared to Ru-based oxides. To improve the overall catalytic properties of acidic OER, the fusion of Ru and Ir was proposed as a potentially effective strategy. In line with this idea, Qiao et al. [198] designed a heterostructured bimetallic electrocatalyst composed of Ru and Ir (Ru@IrO_x). The core-shell nanostructure of Ru@IrO_x was observed in Fig. 14**d**, where heterojunctions were formed and strains were generated in the shell region (Fig. 14**e, f**). The electrocatalytic tests demonstrate that the acidic OER properties of Ru@IrO_x core-shell nanocrystals surpass those of homogeneous RuIr oxide alloys in 0.05 M H_2SO_4 solutions. This superiority can be ascribed to the charge redistribution occurring at the core-shell heterojunction, leading to a favorable surface valence state of the Ru@IrO_x nanocrystals (Fig. 14**g, h**). Conversely, the core-shell nanostructures exhibit enhanced structural stability and offer more efficient protection for the IrO_x shell, resulting in a significant reduction in the dissolution rate of metal cations and the maintenance of high activity (Fig. 14**i**).

The presence of diverse chemical compositions and crystal structures within heterogeneous structures has been observed to induce lattice strain, thereby influencing the adsorption energy of intermediates at specific sites and enhancing catalytic activity. Heterojunctions can be generated in-situ through the surface reconstruction phenomenon observed during electrocatalysis [199], representing a non-conventional approach to constructing heterojunctions. By elucidating the process and mechanism of reconstruction, it becomes possible to design heterojunctions in a rational manner.

4.7. *Surface reconstruction*

The reconstruction of a catalyst involves various processes such as surface/subsurface atomic rearrangement, phase transformation, component change, intermediate adsorption, defect formation, and

oxidation. These processes represent spontaneous changes in the morphology, geometry, and electronic structure of the initial material (pre-catalyst) within a given reaction environment and potential [61]. In the context of electrochemical processes, the dynamic nature of surface sites in electrocatalysts can induce the phenomenon of surface reconstruction [200,201]. During the process of OER, surface reconstruction can be employed to establish a correlation between the electrocatalyst's surface and the active site engaged in the reaction. Furthermore, surface reconstruction plays a regulatory role in the behavior of electrocatalysts, encompassing adsorption, activation, and desorption, thereby exerting an influence on the overall performance of OER. Consequently, an increasing number of investigations demonstrate the efficacy of surface reconstruction engineering as a viable approach to enhance the catalytic efficacy of OER electrocatalysts [202–205].

A range of noble metal and non-noble metal-based materials have demonstrated exceptional performance in alkaline OER. However, in the case of acidic OER, catalysts such as RuO_x and IrO_x remain the most effective. Enhancing the performance of Ru/Ir-based catalysts poses a significant challenge. In a study conducted by Jaramillo et al.[117], an epitaxial $SrIrO_3$ film was grown on $SrTiO_3$ substrates using the pulsed laser deposition (PLD) technique. The researchers observed that this catalyst displayed excellent OER performance and stability in 0.5 M H_2SO_4. Subsequently, they investigated and analyzed the factors contributing to the catalyst's high activity. The catalyst underwent structural changes, as evidenced by a series of characterizations. The AFM results indicated an increase in surface roughness following the reaction (Fig. 15**a**). Conversely, the XPS results revealed no significant alteration in the Ir element content on the catalyst surface before and after the reaction, but a notable decrease in Sr element content was observed (Fig. 15**b, c**). The characterization results and theoretical calculations have confirmed the leaching of Sr and the formation of highly active IrO_x during the reaction process. The resulting $IrO_x/SrIrO_3$ compound may account for the catalyst's exceptional level of activity.

The primary obstacle to the widespread implementation of proton exchange membranes is the inadequate longevity of electrocatalysts during the acidic OER process. To address this issue, Zhang et al. [206] synthesize Ru-based alloys by introducing various non-noble metals onto carbon fiber papers (CFPs) and subsequently dealloying them. Through cyclic voltammetry (CV) testing, the RuMn alloy exhibited remarkable resistance to acid corrosion and overoxidation. The analysis of concentration evolution demonstrated that the steady-state dissolution was effectively inhibited during the later stage (Fig. 15**d**). Furthermore, the XRD and TEM findings demonstrated the formation of an amorphous RuO_x shell after CV scanning (Fig. 15**e, f**). The findings of

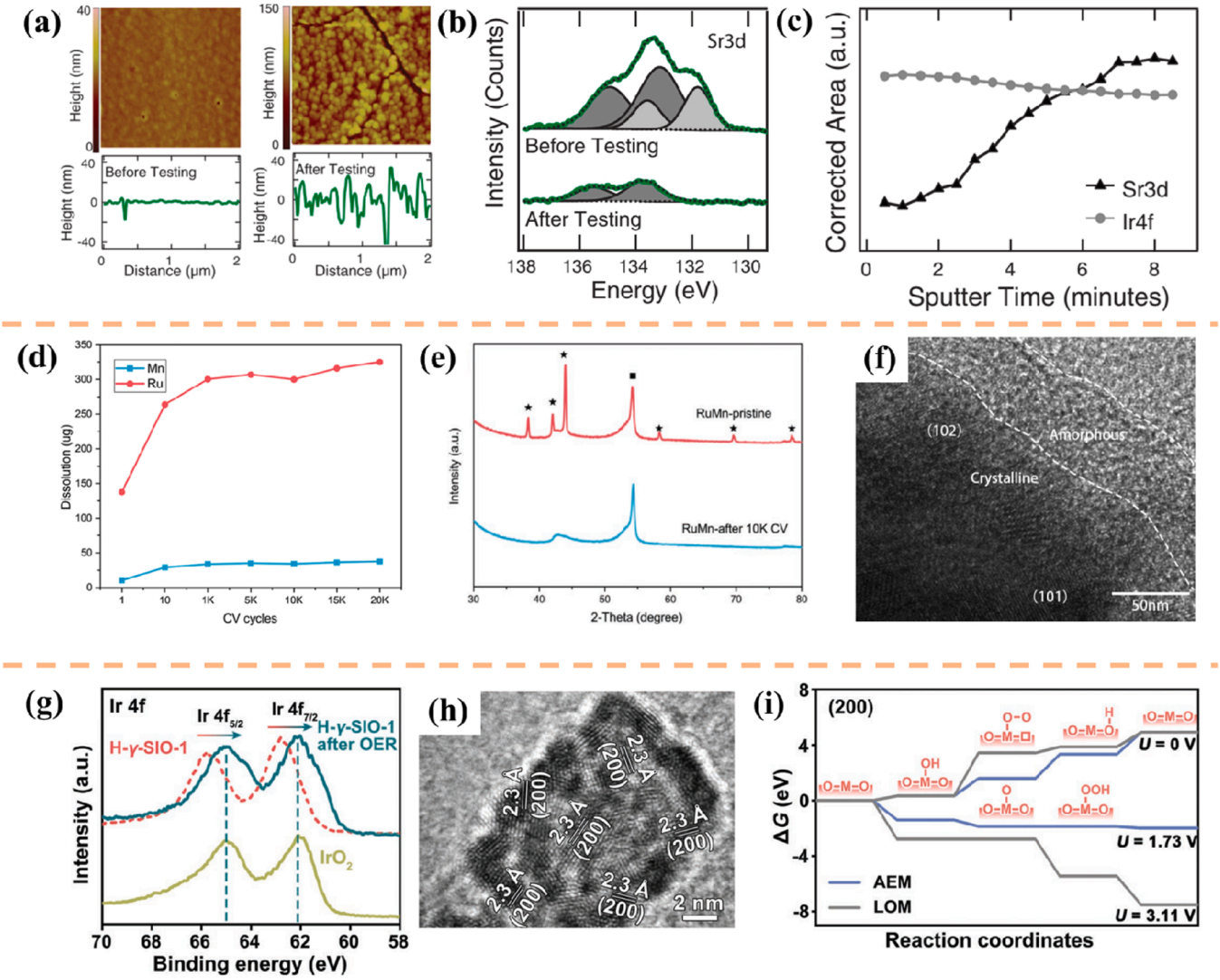

Fig. 15. (a) AFM maps and line scans for a 100-nm $SrIrO_3$ film. (b) XPS on the Sr 3d peaks for a 100-nm $SrIrO_3$ film. (c) Depth sputter profile indicating the relative quantities of each element near the surface [117]. (d) Ru and Mn dissolution condition. (e) XRD patterns of RuMn. (f) HRTEM figure of the RuMn after 1000 CV cycles [206]. (g) Ir 4 f XPS spectrum of H-γ-SIO-1. (h) HRTEM image of H-γ-SIO-1. (i) Diagram of four stages' free energies [207].

this study suggest that rational surface reconstruction serves as a viable approach for developing stable catalysts for the OER in acidic conditions.

As commonly understood, the reconstruction phenomenon in the process of OER typically results in the active phase of the final catalyst differing from the structure of the pre-catalyst. Researchers aim to develop appropriate pre-catalysts to achieve a highly efficient catalytic active phase. For instance, Zou et al. [207] reported the phase-selective synthesis of metastable strontium iridium, which serves as a nano-catalyst exhibiting exceptional catalytic activity and stability in acidic conditions. The post-OER characterization of H-γ-SIO-1 was conducted to investigate potential structural reconstruction during electrocatalysis. The XPS analysis of H-γ-SIO-1 revealed a reduction in the oxidation state of Ir after the catalytic reaction (Fig. 15**g**). Furthermore, the HRTEM images of H-γ-SIO-1 demonstrated the presence of diminutive nanoparticles measuring 1–2 nm, exhibiting a lattice spacing of approximately 0.23 nm, which corresponds to the (200) plane of IrO_2 (Fig. 15**h**). The findings of this study suggest that H-γ-SIO-1 experienced recombination, resulting in the formation of (200) oriented IrO_2 nanoparticles. Additionally, the analysis of the reaction paths of AEM and LOM on the IrO_2 (200) surface indicates that the OER of H-γ-SIO-1 predominantly follows the AEM pathway, rather than the LOM pathway. This preference can be ascribed to the presence of the active phase, which consists of (200) plane-oriented IrO_2 (Fig. 15**i**).

Structural reconstruction presents a promising approach for enhancing the catalytic activity of electrocatalysts. Nevertheless, the deep comprehension of the underlying factors responsible for the remarkable OER performance of reconstructed materials remains elusive, and the comprehensive and precise descriptors for the reconstruction phenomenon are lacking. This significant knowledge gap significantly impedes the advancement of efficient electrocatalysts founded on structural reconstruction. Generally, surface reconstruction is voltage dependent, examining the reconstruction behavior through in-situ characterization and theoretical simulation can potentially serve as an effective approach to uncovering the underlying chemical and structural factors contributing to the efficient OER of electrocatalysts [197]. A thorough analysis of the structural transformations and the subsequent elucidation of the connection between the initial structure and the active phase are essential prerequisites for the design of appropriate pre-electrocatalysts.

Surface reconstruction takes place during the electrocatalytic reaction process, wherein the catalyst synthesized beforehand acts as a pre-catalyst. Can the reconstruction process be intentionally manipulated through the design of the pre-catalyst? For instance, research has demonstrated that the introduction of heteroatom doping can lead to the formation of lattice strain, thereby promoting the reconstruction process [208]. Phase segregation is accomplished via thermal induction, resulting in the transformation of the catalyst into a phase that exhibits a higher susceptibility to surface reconfiguration [209]. Enhancing catalyst performance through structural reconstruction holds great importance. For instance, in the context of **4.6 Heterojunctions**, the formation of amorphous oxide (IrO_x) shells during electrocatalysis enhances catalyst stability.

Through the comprehensive analysis of numerous modification measures, it is evident that various strategies for modification exert mutual influence on one another. For instance, in the field of structural engineering, the conventional approach involves the design of core-shell structures to safeguard the internal active substances against electrolyte-induced corrosion. However, recent advancements in characterization equipment have facilitated extensive research, revealing that the dissimilarity between the lattice structures of the shell and core can result in a discernible level of strain at the interface of the core-shell structure [210]. Extensive literature has substantiated that lattice mismatches induce significant strain, thereby exerting a pivotal influence on the modification of the electronic structure and consequent electrocatalytic behavior [211].

Table 1 presents a comprehensive overview of the aforementioned instances alongside additional advanced Ru/Ir-based electrocatalysts. These instances collectively demonstrate the viability and efficacy of enhancing and optimizing Ru/Ir-based materials as a means to develop acidic OER electrocatalysts exhibiting commendable activity and stability.

5. Summary and outlook

The growing importance of PEM has sparked a heightened interest in the field of acidic oxygen evolution. This article commences by introducing two established mechanisms for OER, namely AEM and LOM. Subsequently, the paper provides a summary of the recent experimental

Table 1
Summary of the acidic OER performance of recent reported Ru/Ir-based electrocatalysts.

Catalysts	Electrolyte	η_{10} (mV)	Stability (mV/ mA cm^{-2}- h)	Strategies
Ir NSs	0.1 M $HClO_4$	255	255 mV - 8	crystal phase [78]
L-Ru	0.5 M H_2SO_4	202	10 mA cm^{-2} - 10	strain[81]
Ir-Co_3O_4	0.5 M H_2SO_4	236	10 mA cm^{-2} - 30	single atoms [212]
Ru-N-C	0.5 M H_2SO_4	267	260 mV - 30	single atoms [91]
RuO_2 NSs	0.5 M H_2SO_4	199	10 mA cm^{-2} - 0.61	defect[100]
IrO_2 NRs	0.5 M H_2SO_4	205	10 mA cm^{-2} - 138.9	crystal phase [105]
S-doped M-$SrIrO_3$	0.5 M H_2SO_4	228	10 mA cm^{-2} - 20	doping[112]
$SrZrO_3$-$SrIrO_3$	0.1 M $HClO_4$	240	/	alloying[116]
IrO_x/9R-$BaIrO_3$	0.5 M H_2SO_4	230	10 mA cm^{-2} - 48	reconstruction [119]
IrW-W_2B	0.5 M H_2SO_4	291	100 mA cm^{-2} - 120	structure[128]
FeCoNiIrRu	0.5 M H_2SO_4	241	/ - 14	HEA[139]
RuIr@CoNC	0.5 M H_2SO_4	223	10 mA cm^{-2} - 40	crystal phase [148]
Pd@Ir_{nL}	0.1 M $HClO_4$	245	/	structure[155]
Ru@Ir–O	0.5 M H_2SO_4	238	/	structure[156]
1 T-IrO_2	0.1 M $HClO_4$	197	50 mA cm^{-2} - 45	structure[158]
SS Pt-RuO_2 HNSs	0.5 M H_2SO_4	228	10 mA cm^{-2} - 100	doping[174]
$Re_{0.06}Ru_{0.94}O_2$	0.1 M $HClO_4$	190	10 mA cm^{-2} - 200	doping[175]
$W_{0.2}Er_{0.1}Ru_{0.7}O_{2-\delta}$	0.5 M H_2SO_4	168	10 mA cm^{-2} - 500	doping[179]
Ni-RuO_2	0.1 M $HClO_4$	214	10 mA cm^{-2} - 200	doping[213]
Ru@V-RuO_2/C HMS	0.5 M H_2SO_4	176	/	defect[185]
UfD-RuO_2/CC	0.5 M H_2SO_4	179	10 mA cm^{-2} - 20	defect[186]
RuO_2-WC NPs	0.5 M H_2SO_4	347	10 mA cm^{-2} - 20	SMOSI[191]
IrO_x/Zr_2ON_2	0.5 M H_2SO_4	255	10 mA cm^{-2} - 5	SMOSI[192]
$Li_{0.52}RuO_2$	0.5 M H_2SO_4	156	10 mA cm^{-2} - 70	strain[41]
Ru_1–Pt_3Cu	0.1 M $HClO_4$	220	10 mA cm^{-2} - 28	strain[166]
Ir-NCT/CC	0.1 M $HClO_4$	202	10 mA cm^{-2} - 50	heterojunction [197]
Ru@IrO_x	0.05 M H_2SO_4	282	320 mV - 30	heterojunction [198]
IrO_x/$SrIrO_3$	0.5 M H_2SO_4	340	10 mA cm^{-2} - 30	reconstruction [117]
RuMn	0.5 M H_2SO_4	239	10 mA cm^{-2} - 720	reconstruction [206]
H-γ-SIO-1	0.1 M $HClO_4$	220	10 mA cm^{-2} - 1080	reconstruction [207]

advancements in Ru/Ir-based catalysts for acidic OER, encompassing various forms such as pure metals, single atoms, oxides, alloys, and others. Additionally, an overview is presented regarding the modification strategies employed to enhance the stability, activity, and cost-effectiveness of Ru/Ir-based catalysts, including techniques such as doping, strain engineering, and surface reconstruction. Specifically, this study examines the viability, benefits, and drawbacks of various strategies employed for modification. Despite progress made in the development of OER mechanisms and catalyst design, certain challenges remain unresolved. Herein, we provide an overview of the existing obstacles encountered in the acidic OER process, identify potential avenues for further investigation, and propose potential solutions (Fig. 16).

5.1. Modification strategies

This review presents an extensive compilation of cases pertaining to modification strategies. While the enhancement of catalytic performance is notable, the identification and implementation of structural alterations (such as stresses, defects, heterojunctions, etc.) have reached a relatively advanced stage. However, advancements in achieving precise and controllable introduction of these modifications have been sluggish. The activity of a catalyst can be significantly influenced by various factors, including the distribution, concentration, and type of stress, defects, and heteroatoms, as well as the shell thickness and curvature in a core-shell structure. Exploring advancements in these areas could potentially lead researchers to discover novel approaches for enhancing catalytic performance.

5.2. In-situ/Operando characterization

During the process of OER, surface reconstruction of oxides, hydroxides, and alloys commonly take place. This reconstructed product is regarded as an authentic active site. Nevertheless, the lack of clarity regarding the reconstruction mechanism hinders the exploration and accurate identification of the genuine catalytic active sites. Gaining insight into the genuine active site of the catalyst under real operating conditions is of utmost importance to unveil its intrinsic catalytic mechanism. In the context of dynamic evolution, the utilization of in-situ/operando characterization enables the identification of the catalytic catalyst, monitoring the transfer of reactants and intermediates [214,215]. By surpassing the constraints associated with conventional vacuum test conditions, vacuum interconnected near atmospheric pressure test instruments offer a viable solution [216,217]. Furthermore, the experimental observation of the transformation of the catalyst OER mechanism can be achieved by employing ^{18}O isotope labeling in conjunction with in-situ characterization [218,219].

5.3. Catalyst

In contrast to nanocatalysts, model catalysts possess a more distinct structure, and their characterization techniques are more extensive and well-established. By examining catalysts at the atomic or molecular level, the structure-activity principles can be derived, thereby providing valuable insights for the development of practical catalysts. For instance, catalysts consisting of dispersed single atoms possess several benefits, including a homogeneous structure of active centers, a high utilization rate of active center atoms, and a low coordination number of said atoms. These characteristics make them an ideal model system for investigating catalytic mechanisms such as the optimization mechanism of SMSI [220] and the interface effect [221]. To examine the surface reconstruction process during the OER, cobalt single crystals were employed as a model catalyst [222].

The primary objective of catalyst research should focus on its practical implementation. To effectively bridge the disparity between laboratory-scale experiments and large-scale performance, it is imperative to thoroughly examine the reaction environment and industrial production of the catalyst. The advancement of catalysts utilizing low noble metal or non-noble metal materials holds immense importance for promoting the sustainable development of electrolytic water. The anode reaction environment in PEM fuel cells is characterized by its harshness, particularly in high-potential, oxygen-rich, and acidic conditions, which makes non-noble metals and carbon support materials susceptible to corrosion degradation. In terms of both activity and stability, the current and short-term most suitable catalyst material remains to be Ru/Ir-based catalyst. However, the future research direction should primarily focus on reducing the number of noble metals in catalysts, considering the limitations imposed by the cost of Ru/Ir and the constraints associated with mining. One aspect entails the discovery of appropriate support materials for the preparation of noble metal catalysts that are highly dispersed. These support materials must satisfy specific criteria such as corrosion resistance, favorable electrical conductivity, and a substantial specific surface area. Conversely, an innovative catalyst structure is devised, inspired by the prevalent utilization of core-shell structure catalysts in fuel cells [5,223,224]. Non-noble metal materials may be employed within the inner core, while noble metal materials may be utilized in the outer shell. The approach may involve a singular step method, or alternatively, the noble metal alloy can be initially prepared, followed by the subsequent formation of the core-shell structure through the process of high-temperature surface segregation.

5.4. Descriptor

Descriptors play a crucial role in elucidating the influence of electricity and its associated physical and chemical factors on the

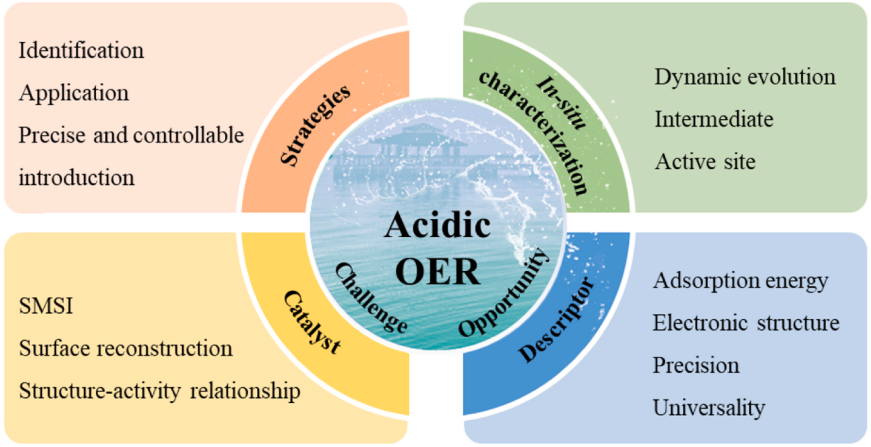

Fig. 16. Schematic illustration of challenges and opportunities in acidic OER.

enhancement of catalyst activity. The disparity between these descriptors serves as a guiding principle for the rational design of electric catalysts [225]. One category of descriptors primarily elucidates the interaction between the catalyst and the adsorption intermediate, encompassing *H, *OH, and *OOH. Another category of descriptors pertains to the electronic structure of the catalyst, encompassing electronegativity, charge density, and *d*-band center. The advancement of precise and comprehensive descriptors can elucidate the correlation between the catalyst's structure and its electrocatalytic efficacy, thereby facilitating the examination, prognostication, and selection of catalysts with superior performance. For example, Ge et al. [226] proposed an intuitive descriptor (Ru charge) to describe the acidic OER activity of RuO_2. Further, the reaction mechanism is modulated by controlling the M-O-Ru structure (selecting whether lattice oxygen is involved in the reaction (LOM)).

Declaration of Competing Interest

The authors declare the following financial interests/personal relationships which may be considered as potential competing interests: Zixu Sun reports was provided by National Natural Science Foundation of China. Yusuke Yamauchi reports a relationship with University of Queensland that includes: employment. Yusuke Yamauchi has patent none pending to none. We have no conflict of interest.

Data availability

Data will be made available on request.

Acknowledgements

We gratefully acknowledge the financial support by the Doctor of Suzhou University Scientific Research Foundation (2022BSK019), and National Natural Science Foundation of China (No. 52102241). Y. Yamauchi would like to gratefully acknowledge the financial support from the Australian National Fabrication Facility's Queensland Node (ANFF-Q), the UQ-Yonsei International Research Project, and the JST-ERATO Yamauchi Materials Space-Tectonics Project (JPMJER2003). S. Liu. gratefully acknowledges the financial support by National Natural Science Foundation of China (No. 52302223).

Appendix A. Supporting information

Supplementary data associated with this article can be found in the online version at doi:10.1016/j.apcatb.2023.123584.

References

[1] P.Y. Kuang, M. Sayed, J.J. Fan, B. Cheng, J.G. Yu, 3D graphene-based H-2-production photocatalyst and electrocatalyst, Adv. Energy Mater. 10 (2020) 1903802.
[2] J. Qian, Y. Xing, Y. Yang, Y. Li, K.X. Yu, W.L. Li, T. Zhao, Y.S. Ye, L. Li, F. Wu, R. J. Chen, Enhanced electrochemical kinetics with highly dispersed conductive and electrocatalytic mediators for lithium-sulfur batteries, Adv. Mater. 33 (2021) 2100810.
[3] Q. Niu, M. Yang, D.Y. Luan, N.W. Li, L. Yu, X.W. Lou, Construction of Ni-Co-Fe Hydr(oxy)oxide@Ni-Co Layered Double Hydroxide Yolk-Shelled Microrods for Enhanced Oxygen Evolution, Angew. Chem. -Int. Ed. 61 (2022), e202213049.
[4] J.L. Du, D.L. Xiang, K.X. Zhou, L.C. Wang, J.Y. Yu, H.H. Xia, L.L. Zhao, H. Liu, W. J. Zhou, Electrochemical hydrogen production coupled with oxygen evolution, organic synthesis, and waste reforming, Nano Energy 104 (2022), 107875.
[5] F. Xiao, Y.C. Wang, Z.P. Wu, G.Y. Chen, F. Yang, S.Q. Zhu, K. Siddharth, Z. J. Kong, A.L. Lu, J.C. Li, C.J. Zhong, Z.Y. Zhou, M.H. Shao, Recent advances in electrocatalysts for proton exchange membrane fuel cells and alkaline membrane fuel cells, Adv. Mater. 33 (2021) 2006292.
[6] A. Dhakshinamoorthy, S. Navalon, A. Primo, H. Garcia, Selective gas-phase hydrogenation of CO_2 to methanol catalysed by metal-organic frameworks, Angew. Chem. -Int. Ed. (2023), e202311241.
[7] K. Rechberger, A. Spanlang, A.S. Conde, H. Wolfmeir, C. Harris, Green hydrogen-based direct reduction for low-carbon steelmaking, Steel Res. Int. 91 (2020) 2000110.
[8] J. Wang, F. Xu, H.Y. Jin, Y.Q. Chen, Y. Wang, Non-noble metal-based carbon composites in hydrogen evolution reaction: fundamentals to applications, Adv. Mater. 29 (2017) 1605838.
[9] J. Zhu, L.S. Hu, P.X. Zhao, L.Y.S. Lee, K.Y. Wong, Recent advances in electrocatalytic hydrogen evolution using nanoparticles, Chem. Rev. 120 (2020) 851–918.
[10] X.C. Wang, K. Maeda, A. Thomas, K. Takanabe, G. Xin, J.M. Carlsson, K. Domen, M. Antonietti, A metal-free polymeric photocatalyst for hydrogen production from water under visible light, Nat. Mater. 8 (2009) 76–80.
[11] J. Lee, H. Cho, J. Kim, Techno-economic analysis of on-site blue hydrogen production based on vacuum pressure adsorption: practical application to real-world hydrogen refueling stations, J. Environ. Chem. Eng. 11 (2023), 109549.
[12] R.W. Howarth, M.Z. Jacobson, How green is blue hydrogen? Energy Sci. Eng. 9 (2021) 1676–1687.
[13] J.M. Serra, J.F. Borras-Morell, B. Garcia-Banos, M. Balaguer, P. Plaza-Gonzalez, J. Santos-Blasco, D. Catalan-Martinez, L. Navarrete, J.M. Catala-Civera, Hydrogen production via microwave-induced water splitting at low temperature, Nat. Energy 5 (2020) 910–919.
[14] D.M. Zhao, Y.Q. Wang, C.L. Dong, Y.C. Huang, J. Chen, F. Xue, S.H. Shen, L. J. Guo, Boron-doped nitrogen-deficient carbon nitride-based Z-scheme heterostructures for photocatalytic overall water splitting, Nat. Energy 6 (2021) 388–397.
[15] J.M. Li, J. Li, J. Ren, H. Hong, D.X. Liu, L.Z. Liu, D.H. Wang, Electric-Field-Treated Ni/Co3O4 Film as High-Performance Bifunctional Electrocatalysts for Efficient Overall Water Splitting, Nano-Micro Lett. 14 (2022) 148.
[16] Z.W. Lei, T.Y. Wang, B.T. Zhao, W.B. Cai, Y. Liu, S.H. Jiao, Q. Li, R.G. Cao, M. L. Liu, Recent progress in electrocatalysts for acidic water oxidation, Adv. Energy Mater. 10 (2020) 2000478.
[17] C.F. Du, E. Hu, H. Yu, Q. Yan, Strategies for local electronic structure engineering of two-dimensional electrocatalysts, Chin. J. Catal. 48 (2023) 1–14.
[18] F.C. Yang, M.J. Kim, M. Brown, B.J. Wiley, Alkaline water electrolysis at 25 a cm-2 with a microfibrous flow-through electrode, Adv. Energy Mater. 10 (2020) 2001174.
[19] C. Niether, S. Faure, A. Bordet, J. Deseure, M. Chatenet, J. Carrey, B. Chaudret, A. Rouet, Improved water electrolysis using magnetic heating of FeC-Ni core-shell nanoparticles, Nat. Energy 3 (2018) 476–483.
[20] X.M. Yuan, T. Yan, Z.K. Liu, P. Kang, Highly efficient alkaline water electrolysis using alkanolamine- functionalized zirconia-blended separators, ACS Sustain. Chem. Eng. 11 (2023) 4269–4278.
[21] B.H. Zhou, R.J. Gao, J.J. Zou, H.M. Yang, Surface design strategy of catalysts for water electrolysis, Small 18 (2022) 2202336.
[22] S. Yuan, C. Zhao, X. Cai, L. An, S. Shen, X. Yan, J. Zhang, Bubble evolution and transport in PEM water electrolysis: mechanism, impact, and management, Prog. Energ. Combust. 96 (2023), 101075.
[23] Z.C. Chen, L. Guo, L. Pan, T.Q. Yan, Z.X. He, Y. Li, C.X. Shi, Z.F. Huang, X. W. Zhang, J.J. Zou, Advances in oxygen evolution electrocatalysts for proton exchange membrane water electrolyzers, Adv. Energy Mater. 12 (2022) 2103670.
[24] C. Wang, A. Schechter, L. Feng, Iridium-based catalysts for oxygen evolution reaction in acidic media: mechanism, catalytic promotion effects and recent progress, Nano Res, Energy 2 (2023), e9120056.
[25] W. Zhang, D.H. Li, L.Z. Zhang, X.L. She, D.J. Yang, NiFe-based nanostructures on nickel foam as highly efficiently electrocatalysts for oxygen and hydrogen evolution reactions, J. Energy Chem. 39 (2019) 39–53.
[26] L.B. Liu, Y.J. Ji, W.T. You, S.H. Liu, Q. Shao, Q.Y. Kong, Z.W. Hu, H.B. Tao, L. Z. Bu, X.Q. Huang, Trace Lattice S Inserted RuO2 Flexible Nanosheets for Efficient and Long-Term Acidic Oxygen Evolution Catalysis, Small 19 (2023) 2208202.
[27] T.Z. Wang, X.J. Cao, L.F. Jiao, Progress in hydrogen production coupled with electrochemical oxidation of small molecules, Angew. Chem. -Int. Ed. 61 (2022), e202213328.
[28] Q.L. Qi, J. Hu, S.T. Guo, H.C. Song, S.X. Wang, Y.C. Yao, T. Le, W. Li, C.X. Zhang, L.B. Zhang, Large-scale synthesis of low-cost bimetallic polyphthalocyanine for highly stable water oxidation, Appl. Catal. B-Environ. 299 (2021), 120637.
[29] Y. Huang, L.W. Jiang, X.L. Liu, T. Tan, H. Liu, J.J. Wang, Precisely engineering the electronic structure of active sites boosts the activity of iron-nickel selenide on nickel foam for highly efficient and stable overall water splitting, Appl. Catal. B-Environ. 299 (2021), 120678.
[30] Y.K. Bai, Y. Wu, X.C. Zhou, Y.F. Ye, K.Q. Nie, J.O. Wang, M. Xie, Z.X. Zhang, Z. J. Liu, T. Cheng, C.B. Gao, Promoting nickel oxidation state transitions in single-layer NiFeB hydroxide nanosheets for efficient oxygen evolution, Nat. Commun. 13 (2022) 6094.
[31] L.J. Zhang, W.W. Cai, N.Z. Bao, Top-level design strategy to construct an advanced high-entropy Co-Cu-Fe-Mo (Oxy)hydroxide electrocatalyst for the oxygen evolution reaction, Adv. Mater. 33 (2021) 2100745.
[32] J.W. Su, R.X. Ge, K.M. Jiang, Y. Dong, F. Hao, Z.Q. Tian, G.X. Chen, L. Chen, Assembling ultrasmall copper-doped ruthenium oxide nanocrystals into hollow porous polyhedra: highly robust electrocatalysts for oxygen evolution in acidic media, Adv. Mater. 30 (2018) 1801351.
[33] Z.Y. Wu, F.Y. Chen, B. Lie, S.W. Yu, Y.Z. Finfrock, D.M. Meira, Q.Q. Yan, P. Zhu, M.X. Chen, T.W. Song, Z. Yin, H.W. Liang, S. Zhang, G. Wang, H. Wang, Non-iridium-based electrocatalyst for durable acidic oxygen evolution reaction in proton exchange membrane water electrolysis, Nat. Mater. 22 (2023) 100–108.
[34] X.M. Xu, H.N. Sun, S. Jiang, Z.P. Shao, Modulating metal-organic frameworks for catalyzing acidic oxygen evolution for proton exchange membrane water electrolysis, SusMat 1 (2021) 460–481.

[35] J. Bai, N.A. Lei, L.M. Wang, Y.Q. Gong, In situ generated Cu-Co-Zn trimetallic sulfide nanoflowers on copper foam: a highly efficient OER electrocatalyst, Nanoscale 14 (2022) 17976–17984.
[36] Y.D. Hu, G. Luo, L.G. Wang, X.K. Liu, Y.T. Qu, Y.S. Zhou, F.Y. Zhou, Z.J. Li, Y. F. Li, T. Yao, C. Xiong, B. Yang, Z.Q. Yu, Y. Wu, Single Ru Atoms Stabilized by Hybrid Amorphous/Crystalline FeCoNi Layered Double Hydroxide for Ultraefficient Oxygen Evolution, Adv. Energy Mater. 11 (2021) 2002816.
[37] Z.P. Shi, J. Li, J.D. Jiang, Y.B. Wang, X. Wang, Y. Li, L.T. Yang, Y.Y. Chu, J.S. Bai, J.H. Yang, J. Ni, Y. Wang, L.J. Zhang, Z. Jiang, C.P. Liu, J.J. Ge, W. Xing, Enhanced Acidic Water Oxidation by Dynamic Migration of Oxygen Species at the Ir/Nb2O5-x Catalyst/Support Interfaces, Angew. Chem. -Int. Ed. 61 (2022), e202212341.
[38] H. Chen, L. Shi, X. Liang, L.N. Wang, T. Asefa, X.X. Zou, Optimization of active sites via crystal phase, composition, and morphology for efficient low-iridium oxygen evolution catalysts, Angew. Chem. -Int. Ed. 59 (2020) 19654–19658.
[39] B.B. Sheng, D.F. Cao, H.W. Shou, W.J. Xu, C.Q. Wu, P.J. Zhang, C.J. Liu, Y.J. Xia, X.J. Wu, S.Q. Chu, J. Zhang, L. Song, S.M. Chen, Anomalous Ru dissolution enabling efficient integrated CO_2 electroreduction in strong acid, Chem. Eng. J. 454 (2023), 140245.
[40] C.X. Liu, Y.B. Jiang, T. Wang, Q.S. Li, Y.Z. Liu, Nano Si-doped ruthenium oxide particles from caged precursors for high-performance acidic oxygen evolution, Adv. Sci. 10 (2023) 2207429.
[41] Y. Qin, T.T. Yu, S.H. Deng, X.Y. Zhou, D.M. Lin, Q. Zhang, Z.Y. Jin, D.F. Zhang, Y. B. He, H.J. Qiu, L.H. He, F.Y. Kang, K.K. Li, T.Y. Zhang, RuO2 electronic structure and lattice strain dual engineering for enhanced acidic oxygen evolution reaction performance, Nat. Commun. 13 (2022) 3784.
[42] J.Z. Huang, H.Y. Sheng, R.D. Ross, J.C. Han, X.J. Wang, B. Song, S. Jin, Modifying redox properties and local bonding of Co3O4 by CeO2 enhances oxygen evolution catalysis in acid, Nat. Commun. 12 (2021) 3036.
[43] J.H. Yu, F.A. Garces-Pineda, J. Gonzalez-Cobos, M. Pena-Diaz, C. Rogero, S. Gimenez, M.C. Spadaro, J. Arbiol, S. Barja, J.R. Galan-Mascaros, Sustainable oxygen evolution electrocatalysis in aqueous 1 M H2SO4 with earth abundant nanostructured Co3O4, Nat. Commun. 13 (2022) 4341.
[44] L. An, C. Wei, M. Lu, H.W. Liu, Y.B. Chen, G.G. Scherer, A.C. Fisher, P.X. Xi, Z.C. J. Xu, C.H. Yan, Recent development of oxygen evolution electrocatalysts in acidic environment, Adv. Mater. 33 (2021) 2006328.
[45] Y.C. Lin, Y. Dong, X.Z. Wang, L. Chen, Electrocatalysts for the oxygen evolution reaction in acidic media, Adv. Mater. 35 (2023) 2210565.
[46] N. Ismail, F.J. Qin, C.H. Fang, D. Liu, B.H. Liu, X.Y. Liu, Z.L. Wu, Z. Chen, W. X. Chen, Electrocatalytic acidic oxygen evolution reaction: from nanocrystals to single atoms, Aggregate 2 (2021), e106.
[47] F. Zhou, L.J. Zhang, J. Li, Q. Wang, Y.R. Chen, H.L. Chen, G.L. Lu, G. Chen, H. L. Jin, S. Wang, J.C. Wang, Novel engineering of ruthenium-based electrocatalysts for acidic water oxidation: A mini review, Eng, Rep 3 (2021), e12437.
[48] Q. Shi, C. Zhu, D. Du, Y. Lin, Robust noble metal-based electrocatalysts for oxygen evolution reaction, Chem. Soc. Rev. 48 (2019) 3181–3192.
[49] X.K. Gu, J.C.A. Camayang, S. Samira, E. Nikolla, Oxygen evolution electrocatalysis using mixed metal oxides under acidic conditions: challenges and opportunities, J. Catal. 388 (2020) 130–140.
[50] H.Y. Zhong, Q. Zhang, J.C. Yu, X. Zhang, C. Wu, Y.F. Ma, H. An, H. Wang, J. Zhang, X.P. Wang, J.M. Xue, Fundamental understanding of structural reconstruction behaviors in oxygen evolution reaction electrocatalysts, Adv. Energy Mater. 13 (2023) 2301391.
[51] Q. Ma, S. Mu, Acidic oxygen evolution reaction: mechanism, catalyst classification, and enhancement strategies, Interdisciplinary, Materials 2 (2023) 53–90.
[52] S. Iqbal, B. Safdar, I. Hussain, K.L. Zhang, C. Chatzichristodoulou, Trends and prospects of bulk and single-atom catalysts for the oxygen evolution reaction, Adv. Energy Mater. 13 (2023) 2203913.
[53] X.P. Wang, H.Y. Zhong, S.B. Xi, W.S.V. Lee, J.M. Xue, Understanding of oxygen redox in the oxygen evolution reaction, Adv. Mater. 34 (2022) 2107956.
[54] Z.P. Shi, X. Wang, J.J. Ge, C.P. Liu, W. Xing, Fundamental understanding of the acidic oxygen evolution reaction: mechanism study and state-of-the-art catalysts, Nanoscale 12 (2020) 13249–13275.
[55] I.C. Man, H.Y. Su, F. Calle-Vallejo, H.A. Hansen, J.I. Martinez, N.G. Inoglu, J. Kitchin, T.F. Jaramillo, J.K. Norskov, J. Rossmeisl, Universality in oxygen evolution electrocatalysis on oxide surfaces, ChemCatChem 3 (2011) 1159–1165.
[56] R. Subbaraman, D. Tripkovic, K.C. Chang, D. Strmcnik, A.P. Paulikas, P. Hirunsit, M. Chan, J. Greeley, V. Stamenkovic, N.M. Markovic, Trends in activity for the water electrolyser reactions on 3d M(Ni,Co,Fe,Mn) hydr(oxy)oxide catalysts, Nat. Mater. 11 (2012) 550–557.
[57] J. Suntivich, K.J. May, H.A. Gasteiger, J.B. Goodenough, Y. Shao-Horn, A perovskite oxide optimized for oxygen evolution catalysis from molecular orbital principles, Science 334 (2011) 1383–1385.
[58] A. Grimaud, K.J. May, C.E. Carlton, Y.L. Lee, M. Risch, W.T. Hong, J.G. Zhou, Y. Shao-Horn, Double perovskites as a family of highly active catalysts for oxygen evolution in alkaline solution, Nat. Commun. 4 (2013) 2439.
[59] S. Lee, K. Banjac, M. Lingenfelder, X.L. Hu, Oxygen isotope labeling experiments reveal different reaction sites for the oxygen evolution reaction on nickel and nickel iron oxides, Angew. Chem. -Int. Ed. 58 (2019) 10295–10299.
[60] L.S. Zhang, L.P. Wang, Y.Z. Wen, F.L. Ni, B. Zhang, H.S. Peng, Boosting neutral water oxidation through surface oxygen modulation, Adv. Mater. 32 (2020) 2002297.
[61] Q.L. Wang, Y.Q. Cheng, H.B. Tao, Y.H. Liu, X.H. Ma, D.S. Li, H.B. Yang, B. Liu, Long-term stability challenges and opportunities in acidic oxygen evolution electrocatalysis, Angew. Chem. -Int. Ed. 62 (2023), e202216645.
[62] N. Yao, H. Jia, J. Zhu, Z. Shi, Hengjiang Cong, J. Ge, W. Luo, Atomically dispersed Ru oxide catalyst with lattice oxygen participation for efficient acidic water oxidation, Chem 9 (2023) 1–15.
[63] Z.P. Shi, Y. Wang, J. Li, X. Wang, Y.B. Wang, Y. Li, W.L. Xu, Z. Jiang, C.P. Liu, W. Xing, J.J. Ge, Confined Ir single sites with triggered lattice oxygen redox: Toward boosted and sustained water oxidation catalysis, Joule 5 (2021) 2164–2176.
[64] C. Fang, J. Zhou, L.L. Zhang, W.C. Wan, Y.X. Ding, X.Y. Sun, Synergy of dual-atom catalysts deviated from the scaling relationship for oxygen evolution reaction, Nat. Commun. 14 (2023) 4449.
[65] C. Lin, J.L. Li, X.P. Li, S. Yang, W. Luo, Y.J. Zhang, S.H. Kim, D.H. Kim, S. S. Shinde, Y.F. Li, Z.P. Liu, Z. Jiang, J.H. Lee, In-situ reconstructed Ru atom array on α-MnO2 with enhanced performance for acidic water oxidation, Nat. Catal. 4 (2021) 1012–1023.
[66] Y.-H. Wang, L. Li, J. Shi, M.-Y. Xie, J. Nie, G.-F. Huang, B. Li, W. Hu, A. Pan, W.-Q. Huang, Oxygen defect engineering promotes synergy between adsorbate evolution and single lattice oxygen mechanisms of OER in transition metal-based (oxy)hydroxide, Adv. Sci. (2023), e2303321.
[67] X.H. Tan, M.K. Zhang, D. Chen, W.B. Li, W.Y. Gou, Y.Q. Qu, Y.Y. Ma, Electrochemical etching switches electrocatalytic oxygen evolution pathway of IrOx/Y2O3 from adsorbate evolution mechanism to lattice-oxygen-mediated mechanism, Small (2023), 2303249.
[68] R.Z. Chen, Z.C. Wang, S.H. Chen, W. Wu, Y. Zhu, J. Zhong, N.C. Cheng, Activating lattice oxygen in spinel oxides via engineering octahedral sites for oxygen evolution, ACS Energy Lett. 8 (2023) 3504–3511.
[69] X.P. Wang, S.B. Xi, P.R. Huang, Y.H. Du, H.Y. Zhong, Q. Wang, A. Borgna, Y. W. Zhang, Z.B. Wang, H. Wang, Z.G. Yu, W.S.V. Lee, J.M. Xue, Pivotal role of reversible NiO6 geometric conversion in oxygen evolution, Nature 611 (2022) 702–708.
[70] C. Rong, K. Dastafkan, Y. Wang, C. Zhao, Breaking the activity and stability bottlenecks of electrocatalysts for oxygen evolution reactions in acids, Adv. Mater. (2023), e2211884.
[71] B. Chen, Z.N. Zhou, Y.Z. Li, K.B. Tan, Y.T. Wang, X.P. Rao, J.L. Huang, X. D. Zhang, Q.B. Li, G.W. Zhan, Catalytic pyrolysis of fatty acids and oils into liquid biofuels and chemicals over supported Ni catalysts on biomass-derived carbon, Appl. Catal. B-Environ. 338 (2023), 123067.
[72] Y. Sun, J. Wang, T. Shang, Z. Li, K. Li, X. Wang, H. Luo, W. Lv, L. Jiang, Y. Wan, Counting d-Orbital Vacancies of Transition-Metal Catalysts for the Sulfur Reduction Reaction, Angew. Chem. (Int. Ed. Engl.) (2023), e202306791.
[73] Q. Wang, M. Ming, S. Niu, Y. Zhang, G.Y. Fan, J.S. Hu, Scalable Solid-State Synthesis of Highly Dispersed Uncapped Metal (Rh, Ru, Ir) Nanoparticles for Efficient Hydrogen Evolution, Adv. Energy Mater. 8 (2018) 1801698.
[74] W. Zhu, X. Song, F. Liao, H. Huang, Q. Shao, K. Feng, Y. Zhou, M. Ma, J. Wu, H. Yang, H. Yang, M. Wang, J. Shi, J. Zhong, T. Cheng, M. Shao, Y. Liu, Z. Kang, Stable and oxidative charged Ru enhance the acidic oxygen evolution reaction activity in two-dimensional ruthenium-iridium oxide, Nat. Commun. 14 (2023) 5365.
[75] Y.Y. Ge, J.J. Ge, B. Huang, X.X. Wang, G.G. Liu, X.H. Shan, L. Ma, B. Chen, G. H. Liu, S.M. Du, A. Zhang, H.F. Cheng, Q. Wa, S.Y. Lu, L.J. Li, Q.B. Yun, K. Yuan, Q.X. Luo, Z.J. Xu, Y.H. Du, H. Zhang, Synthesis of amorphous Pd-based nanocatalysts for efficient alcoholysis of styrene oxide and electrochemical hydrogen evolution, Nano Res 16 (2023) 4650–4655.
[76] M.H. Jiang, A.Y. Tao, Y. Hu, L. Wang, K.Q. Zhang, X.M. Song, W. Yan, Z.X. Tie, Z. Jin, Crystalline Modulation Engineering of Ru Nanoclusters for Boosting Ammonia Electrosynthesis from Dinitrogen or Nitrate, ACS Appl. Mater. Interfaces 14 (2022) 17470–17478.
[77] H.F. Cheng, N.L. Yang, G.G. Liu, Y.Y. Ge, J.T. Huang, Q.B. Yun, Y.H. Du, C.J. Sun, B. Chen, J.W. Liu, H. Zhang, Ligand-exchange-induced amorphization of Pd nanomaterials for highly efficient electrocatalytic hydrogen evolution reaction, Adv. Mater. 32 (2020) 1902964.
[78] G. Wu, X.S. Zheng, P.X. Cui, H.Y. Jiang, X.Q. Wang, Y.T. Qu, W.X. Chen, Y. Lin, H. Li, X. Han, Y.M. Hu, P.G. Liu, Q.H. Zhang, J.J. Ge, Y.C. Yao, R.B. Sun, Y. Wu, L. Gu, X. Hong, Y.D. Li, A general synthesis approach for amorphous noble metal nanosheets, Nat. Commun. 10 (2019) 4855.
[79] L. Dubau, J. Nelayah, S. Moldovan, O. Ersen, P. Bordet, J. Drnec, T. Asset, R. Chattot, F. Maillard, Defects do catalysis: CO monolayer oxidation and oxygen reduction reaction on hollow PtNi/C nanoparticles, ACS Catal. 6 (2016) 4673–4684.
[80] Z. Chen, T. Wang, B. Liu, D. Cheng, C. Hu, G. Zhang, W. Zhu, H. Wang, Z.J. Zhao, J. Gong, Grain-boundary-rich copper for efficient solar-driven electrochemical CO_2 reduction to ethylene and ethanol, J. Am. Chem. Soc. 142 (2020) 6878–6883.
[81] J.Q. Wang, C. Xi, M. Wang, L. Shang, J. Mao, C.K. Dong, H. Liu, S.A. Kulinich, X. W. Du, Laser-generated grain boundaries in ruthenium nanoparticles for boosting oxygen evolution reaction, ACS Catal. 10 (2020) 12575–12581.
[82] Y. Nakaya, S. Furukawa, Catalysis of alloys: classification, principles, and design for a variety of materials and reactions, Chem. Rev. 123 (2023) 5859–5947.
[83] X.F. Bai, X.P. Zhang, Y.J. Sun, M.C. Huang, J.T. Fan, S.Y. Xu, H. Li, Low Ruthenium Content Confined on Boron Carbon Nitride as an Efficient and Stable Electrocatalyst for Acidic Oxygen Evolution Reaction, Angew. Chem. -Int. Ed. 62 (2023), e202308704.
[84] B.T. Qiao, A.Q. Wang, X.F. Yang, L.F. Allard, Z. Jiang, Y.T. Cui, J.Y. Liu, J. Li, T. Zhang, Single-atom catalysis of CO oxidation using Pt1/FeOx, Nat. Chem. 3 (2011) 634–641.

[85] J. Chang, Q. Zhang, J. Yu, W. Jing, S. Wang, G. Yin, G.I.N. Waterhouse, S. Lu, A Fe Single Atom Seed-Mediated Strategy Toward Fe3C/Fe-N-C Catalysts with Outstanding Bifunctional ORR/OER Activities, Adv. Sci. (2023), e2301656.
[86] K. Shah, R. Dai, M. Mateen, Z. Hassan, Z. Zhuang, C. Liu, M. Israr, W.C. Cheong, B. Hu, R. Tu, C. Zhang, X. Chen, Q. Peng, C. Chen, Y. Li, Cobalt Single Atom Incorporated in Ruthenium Oxide Sphere: A Robust Bifunctional Electrocatalyst for HER and OER, Angew. Chem. -Int. Ed. Engl. 61 (2022), e202114951.
[87] Z. Pei, H. Zhang, Z.-P. Wu, X.F. Lu, D. Luan, X.W.D. Lou, Atomically dispersed Ni activates adjacent Ce sites for enhanced electrocatalytic oxygen evolution activity, Sci. Adv. 9 (2023), eadh1320.
[88] X.C. Liu, C.Y. Wang, J.L. Meng, X.D. Yue, Q.Y. Wang, J.T. Lu, J.K. Wang, X. C. Wang, Y.X. Zong, X.F. Jiang, Single-atom cobalt catalysts for chemoselective hydrogenation of nitroarenes to anilines, Chin. Chem. Lett. 34 (2023), 108745.
[89] J.F. Sun, Q.Q. Xu, J.L. Qi, D. Zhou, H.Y. Zhu, J.Z. Yin, Isolated single atoms anchored on N-doped carbon materials as a highly efficient catalyst for electrochemical and organic reactions, ACS Sustain. Chem. Eng. 8 (2020) 14630–14656.
[90] Z.W. Seh, J. Kibsgaard, C.F. Dickens, I.B. Chorkendorff, J.K. Norskov, T. F. Jaramillo, Combining theory and experiment in electrocatalysis: Insights into materials design, Science 355 (2017), eaad4998.
[91] L.L. Cao, Q.Q. Luo, J.J. Chen, L. Wang, Y. Lin, H.J. Wang, X.K. Liu, X.Y. Shen, W. Zhang, W. Liu, Z.M. Qi, Z. Jiang, J.L. Yang, T. Yao, Dynamic oxygen adsorption on single-atomic Ruthenium catalyst with high performance for acidic oxygen evolution reaction, Nat. Commun. 10 (2019) 4849.
[92] D. Liu, Q. He, S. Ding, L. Song, Structural regulation and support coupling effect of single-atom catalysts for heterogeneous catalysis, Adv. Energy Mater. 10 (2020) 2001482.
[93] Y.R. Zheng, J. Vernieres, Z.B. Wang, K. Zhang, D. Hochfilzer, K. Krempl, T. W. Liao, F. Presel, T. Altantzis, J. Fatermans, S.B. Scott, N.M. Secher, C. Moon, P. Liu, S. Bals, S. Van Aert, A. Cao, M. Anand, J.K. Norskov, J. Kibsgaard, I. Chorkendorff, Monitoring oxygen production on mass-selected iridium-tantalum oxide electrocatalysts, Nat. Energy 7 (2022) 55–64.
[94] H.D. Xu, J. Yang, R.Y. Ge, J.J. Zhang, Y. Li, M.Y. Zhu, L.M. Dai, S. Li, W.X. Li, Carbon-based bifunctional electrocatalysts for oxygen reduction and oxygen evolution reactions: optimization strategies and mechanistic analysis, J. Energy Chem. 71 (2022) 234–265.
[95] K. Mamtani, D. Jain, D. Dogu, V. Gustin, S. Gunduz, A.C. Co, U.S. Ozkan, Insights into oxygen reduction reaction (ORR) and oxygen evolution reaction (OER) active sites for nitrogen-doped carbon nanostructures (CNx) in acidic media, Appl. Catal. B-Environ. 220 (2018) 88–97.
[96] H. Yan, Z. Jiang, B. Deng, Y. Wang, Z.J. Jiang, Ultrathin carbon coating and defect engineering promote ruo2 as an efficient catalyst for acidic oxygen evolution reaction with super-high durability, Adv. Energy Mater. (2023), 2300152.
[97] G. Zhao, Z. Luo, B. Zhang, Y. Chen, X. Cui, J. Chen, Y. Liu, M. Gao, H. Pan, W. Sun, Epitaxial interface stabilizing iridium dioxide toward the oxygen evolution reaction under high working potentials, Nano Res 16 (2023) 4767–4774.
[98] X.K. Kong, K. Xu, C.L. Zhang, J. Dai, S.N. Oliaee, L.Y. Li, X.C. Zeng, C.Z. Wu, Z. M. Peng, Free-standing two-dimensional ru nanosheets with high activity toward water splitting, ACS Catal. 6 (2016) 1487–1492.
[99] D. Takimoto, K. Fukuda, S. Miyasaka, T. Ishida, Y. Ayato, D. Mochizuki, W. Shimizu, W. Sugimoto, Synthesis and oxygen electrocatalysis of iridium oxide nanosheets, Electrocatalysis 8 (2017) 144–150.
[100] Z.L. Zhao, Q. Wang, X. Huang, Q. Feng, S. Gu, Z. Zhang, H. Xu, L. Zeng, M. Gu, H. Li, Boosting the oxygen evolution reaction using defect-rich ultra-thin ruthenium oxide nanosheets in acidic media, Energy Environ. Sci. 13 (2020) 5143–5151.
[101] C. Liu, L.R. Zheng, Q. Song, Z.J. Xue, C.H. Huang, L. Liu, X.Z. Qiao, X. Li, K.Y. Liu, T. Wang, A metastable crystalline phase in two-dimensional metallic oxide nanoplates, Angew. Chem. -Int. Ed. 58 (2019) 2055–2059.
[102] Z.Y. Wang, J.Y. Chen, E.H. Song, N. Wang, J.C. Dong, X. Zhang, P.M. Ajayan, W. Yao, C.F. Wang, J.J. Liu, J.F. Shen, M.X. Ye, Manipulation on active electronic states of metastable phase beta-NiMoO4 for large current density hydrogen evolution, Nat. Commun. 12 (2021) 5960.
[103] X.L. Zheng, X. Gao, R.A. Vila, Y. Jiang, J.Y. Wang, R. Xu, R. Zhang, X. Xiao, P. Zhang, L.C. Greenburg, Y.F. Yang, H.L.L. Xin, X.L. Zheng, Y. Cui, Hydrogen-substituted graphdiyne-assisted ultrafast sparking synthesis of metastable nanomaterials, Nat. Nanotechnol. 18 (2023) 153–159.
[104] Z. Sun, X.H. Zhao, W.J. Qiu, C.S. Yang, O. Yamamoto, N. Imanishi, J.J. Liu, T. Zhang, Partial disproportionation gallium-oxygen reaction boosts lithium-oxygen batteries, Energy Storage Mater. 41 (2021) 475–484.
[105] F. Liao, K. Yin, Y.J. Ji, W.X. Zhu, Z.L. Fan, Y.Y. Li, J. Zhong, M.W. Shao, Z. H. Kang, Q. Shao, Iridium oxide nanoribbons with metastable monoclinic phase for highly efficient electrocatalytic oxygen evolution, Nat. Commun. 14 (2023) 1248.
[106] X.M. Hu, Y.T. Sun, S.Y. Guo, J.W. Sun, Y.S. Fu, S. Chen, S.L. Zhang, J.W. Zhu, Identifying electrocatalytic activity and mechanism of Ce1/3NbO3 perovskite for nitrogen reduction to ammonia at ambient conditions, Appl. Catal. B-Environ. 280 (2021), 119419.
[107] J. Hwang, R.R. Rao, L. Giordano, Y. Katayama, Y. Yu, Y. Shao-Horn, Perovskites in catalysis and electrocatalysis, Science 358 (2017) 751–756.
[108] J. Liu, T. Zhang, F. Ji, Z. Liu, Z. Wang, High-performance perovskite bifunctional electrocatalysts for oxygen reduction reaction and oxygen evolution reaction, ACS Appl. Energ. Mater. 5 (2022) 8852–8861.
[109] N. Han, S. Feng, W. Guo, O.M. Mora, X. Zhao, W. Zhang, S. Xie, Z. Zhou, Z. Liu, Q. Liu, K. Wan, X. Zhang, J. Fransaer, Rational design of Ruddlesden–Popper perovskite electrocatalyst for oxygen reduction to hydrogen peroxide, SusMat 2 (2022) 456–465.
[110] S. Geiger, O. Kasian, M. Ledendecker, E. Pizzutilo, A.M. Mingers, W.T. Fu, O. Diaz-Morales, Z.Z. Li, T. Oellers, L. Fruchter, A. Ludwig, K.J.J. Mayrhofer, M.T. M. Koper, S. Cherevko, The stability number as a metric for electrocatalyst stability benchmarking, Nat. Catal. 1 (2018) 508–515.
[111] S.J. Peng, X.P. Han, L.L. Li, S.L. Chou, D.X. Ji, H.J. Huang, Y.H. Du, J. Liu, S. Ramakrishna, Electronic and defective engineering of electrospun CaMnO3 nanotubes for enhanced oxygen electrocatalysis in rechargeable zinc-air batteries, Adv. Energy Mater. 8 (2018) 1800612.
[112] M. You, L. Gui, X. Ma, Z. Wang, Y. Xu, J. Zhang, J. Sun, B. He, L. Zhao, Electronic tuning of SrIrO3 perovskite nanosheets by sulfur incorporation to induce highly efficient and long-lasting oxygen evolution in acidic media, Appl. Catal. B-Environ. 298 (2021), 120562.
[113] S. Hu, S. Ge, H. Liu, X. Kang, Q. Yu, B. Liu, Low-dimensional electrocatalysts for acidic oxygen evolution: intrinsic activity, high current density operation, and long-term stability, Adv. Funct. Mater. 32 (2022) 2201726.
[114] Y. Zhang, X. Zhu, G. Zhang, P. Shi, A.-L. Wang, Ration. Catal. Des. Oxyg. Evol. acidic Cond.: Strateg. Enhanc. Electro Perform., J. Mater. Chem. A 9 (2021) 5890–5914.
[115] D. Zhang, M. Li, X. Yong, H. Song, G.I.N. Waterhouse, Y. Yi, B. Xue, D. Zhang, B. Liu, S. Lu, Construction of Zn-doped RuO2 nanowires for efficient and stable water oxidation in acidic media, Nat. Commun. 14 (2023) 2517.
[116] X. Liang, L. Shi, R. Cao, G. Wan, W. Yan, H. Chen, Y. Liu, X. Zou, Perovskite-Type Solid Solution Nano-Electrocatalysts Enable Simultaneously Enhanced Activity and Stability for Oxygen Evolution, Adv. Mater. 32 (2020), e2001430.
[117] L.C. Seitz, C.F. Dickens, K. Nishio, Y. Hikita, J. Montoya, A. Doyle, C. Kirk, A. Vojvodic, H.Y. Hwang, J.K. Norskov, T.F. Jaramillo, A highly active and stable IrOx/SrIrO3 catalyst for the oxygen evolution reaction, Science 353 (2016) 1011–1014.
[118] Y.B. Chen, H.Y. Li, J.X. Wang, Y.H. Du, S.B. Xi, Y.M. Sun, M. Sherburne, J. W. Ager, A.C. Fisher, Z.C.J. Xu, Exceptionally active iridium evolved from a pseudo-cubic perovskite for oxygen evolution in acid, Nat. Commun. 10 (2019) 572.
[119] N. Li, L. Cai, C. Wang, Y. Lin, J. Huang, H. Sheng, H. Pan, W. Zhang, Q. Ji, H. Duan, W. Hu, W. Zhang, F. Hu, H. Tan, Z. Sun, B. Song, S. Jin, W. Yan, Identification of the Active-Layer Structures for Acidic Oxygen Evolution from 9R-BaIrO3 Electrocatalyst with Enhanced Iridium Mass Activity, J. Am. Chem. Soc. 143 (2021) 18001–18009.
[120] T. Xiong, X. Yao, Z. Zhu, R. Xiao, Yw Hu, Y. Huang, S. Zhang, M.S. Balogun, In Situ Grown Co-Based Interstitial Compounds: Non-3d Metal and Non-Metal Dual Modulation Boosts Alkaline and Acidic Hydrogen Electrocatalysis, Small 18 (2021) 2105331.
[121] T. Shen, S. Wang, T.H. Zhao, Y.Z. Hu, D.L. Wang, Recent Advances of Single-Atom-Alloy for Energy Electrocatalysis, Adv. Energy Mater. 12 (2022) 2201823.
[122] X.X. Wang, J. Sokolowski, H. Liu, G. Wu, Pt alloy oxygen-reduction electrocatalysts: Synthesis, structure, and property, Chin. J. Catal. 41 (2020) 739–755.
[123] J.D. Lee, J.B. Miller, A.V. Shneidman, L. Sun, J.F. Weaver, J. Aizenberg, J. Biener, J.A. Boscoboinik, A.C. Foucher, A.I. Frenkel, J.E.S. van der Hoeven, B. Kozinsky, N. Marcella, M.M. Montemore, H.T. Ngan, C.R. O'Connor, C.J. Owen, D. J. Stacchiola, E.A. Stach, R.J. Madix, P. Sautet, C.M. Friend, Dilute Alloys Based on Au, Ag, or Cu for Efficient Catalysis: From Synthesis to Active Sites, Chem. Rev. 122 (2022) 8758–8808.
[124] C. Yang, Y. Gao, T. Ma, M. Bai, C. He, X. Ren, X. Luo, C. Wu, S. Li, C. Cheng, Metal alloys-structured electrocatalysts: metal-metal interactions, coordination microenvironments, and structural property-reactivity relationships, Adv. Mater. (2023), e2301836.
[125] M. Zhu, Q. Shao, Y. Qian, X. Huang, Superior overall water splitting electrocatalysis in acidic conditions enabled by bimetallic Ir-Ag nanotubes, Nano Energy 56 (2019) 330–337.
[126] J. Xu, Z. Lian, B. Wei, Y. Li, O. Bondarchuk, N. Zhang, Z. Yu, A. Araujo, I. Amorim, Z. Wang, B. Li, L. Liu, Strong Electronic Coupling between Ultrafine Iridium–Ruthenium Nanoclusters and Conductive, Acid-Stable Tellurium Nanoparticle Support for Efficient and Durable Oxygen Evolution in Acidic and Neutral Media, ACS Catal. 10 (2020) 3571–3579.
[127] J. Gao, X. Huang, W. Cai, Q. Wang, C. Jia, B. Liu, Rational design of an iridium-tungsten composite with an iridium-rich surface for acidic water oxidation, ACS Appl. Mater. Interfaces 12 (2020) 25991–26001.
[128] R. Li, H. Wang, F. Hu, K.C. Chan, X. Liu, Z. Lu, J. Wang, Z. Li, L. Zeng, Y. Li, X. Wu, Y. Xiong, IrW nanochannel support enabling ultrastable electrocatalytic oxygen evolution at 2 A cm-2 in acidic media, Nat. Commun. 12 (2021) 3540.
[129] K.X. Song, Y. Feng, W. Zhang, W.T. Zheng, MOFs fertilized transition-metallic single-atom electrocatalysts for highly-efficient oxygen reduction: Spreading the synthesis strategies and advanced identification, J. Energy Chem. 67 (2022) 391–422.
[130] C. Xie, C.L. Fu, S.S. Li, L.M. Liao, G.T. Chen, C.X. Pan, A special ancient bronze sword and its possible manufacturing technique from materials science analysis, Materials 15 (2022) 2491.
[131] B. Cantor, I.T.H. Chang, P. Knight, A.J.B. Vincent, Microstructural development in equiatomic multicomponent alloys, Mater. Sci. Eng. A-Struct. Mater. Prop. Microstruct. Process. 375 (2004) 213–218.

[132] J.W. Yeh, S.K. Chen, S.J. Lin, J.Y. Gan, T.S. Chin, T.T. Shun, C.H. Tsau, S. Y. Chang, Nanostructured high-entropy alloys with multiple principal elements: Novel alloy design concepts and outcomes, Adv. Eng. Mater. 6 (2004) 299–303.
[133] X. Huang, G. Yang, S. Li, H. Wang, Y. Cao, F. Peng, H. Yu, Noble-metal-based high-entropy-alloy nanoparticles for electrocatalysis, J. Energy Chem. 68 (2022) 721–751.
[134] Y.T. He, X.H. Zhu, C.X. Zhang, Z.Q. Liu, B.B. Cao, L.Y. Sheng, Y. Yang, Q.G. Feng, N. Wang, J.Z. Ou, Y. Xu, Self-circulating adsorption-desorption structure of non-noble high-entropy alloy electrocatalyst facilitates efficient water splitting, ACS Sustain. Chem. Eng. 11 (2023) 5055–5064.
[135] Y.J. Ma, Y. Ma, Q.S. Wang, S. Schweidler, M. Botros, T.T. Fu, H. Hahn, T. Brezesinski, B. Breitung, High-entropy energy materials: challenges and new opportunities, Energy Environ. Sci. 14 (2021) 2883–2905.
[136] H. Li, J. Lai, Z. Li, L. Wang, Multi-sites electrocatalysis in high-entropy alloys, Adv. Funct. Mater. 31 (2021) 2106715.
[137] Y. Xin, S. Li, Y. Qian, W. Zhu, H. Yuan, P. Jiang, R. Guo, L. Wang, High-entropy alloys as a platform for catalysis: progress, challenges, and opportunities, ACS Catal. 10 (2020) 11280–11306.
[138] A.L. Maulana, P.C. Chen, Z.X. Shi, Y. Yang, C. Lizandara-Pueyo, F. Seeler, H. D. Abruña, D. Muller, K. Schierle-Arndt, P.D. Yang, Understanding the structural evolution of IrFeCoNiCu High-entropy alloy nanoparticles under the acidic oxygen evolution reaction, Nano Lett. 23 (2023) 6637–6644.
[139] H. Zhu, Z. Zhu, J. Hao, S. Sun, S. Lu, C. Wang, P. Ma, W. Dong, M. Du, High-entropy alloy stabilized active Ir for highly efficient acidic oxygen evolution, Chem. Eng. J. 431 (2022), 133251.
[140] H. Liu, Z. Zhang, J. Fang, M. Li, M.G. Sendeku, X. Wang, H. Wu, Y. Li, J. Ge, Z. Zhuang, D. Zhou, Y. Kuang, X. Sun, Eliminating over-oxidation of ruthenium oxides by niobium for highly stable electrocatalytic oxygen evolution in acidic media, Joule 7 (2023) 558–573.
[141] K. Du, L. Zhang, J. Shan, J. Guo, J. Mao, C.C. Yang, C.H. Wang, Z. Hu, T. Ling, Interface engineering breaks both stability and activity limits of RuO2 for sustainable water oxidation, Nat. Commun. 13 (2022) 5448.
[142] Q. Yao, B. Huang, Y. Xu, L. Li, Q. Shao, X. Huang, A chemical etching strategy to improve and stabilize RuO2-based nanoassemblies for acidic oxygen evolution, Nano Energy 84 (2021), 105909.
[143] Z. Xu, L. Zhou, G. Zhou, S. Wu, P. Wang, H. Li, P. Huang, L. Liu, Light-driven orderly assembly of ir-atomic chains to integrate a dynamic reaction pathway for acidic oxygen evolution, Angew. Chem. -Int. Ed. 62 (2023), e202301128.
[144] Z. Liu, G. Wang, J. Guo, S. Wang, S.-q Zang, Sub-2 nm IrO2/Ir nanoclusters with compressive strain and metal vacancies boost water oxidation in acid, Nano Res 16 (2022) 334–342.
[145] C. Wang, A. Schechter, L. Feng, Iridium-based catalysts for oxygen evolution reaction in acidic media: mechanism, catalytic promotion effects and recent progress, Nano Res, Energy 2 (2023), e9120056.
[146] V.A. Saveleva, L. Wang, W. Luo, S. Zafeiratos, C. Ulhaq-Bouillet, A.S. Gago, K. A. Friedrich, E.R. Savinova, Uncovering the Stabilization Mechanism in Bimetallic Ruthenium-Iridium Anodes for Proton Exchange Membrane Electrolyzers, J. Phys. Chem. Lett. 7 (2016) 3240–3245.
[147] G. Li, S. Li, J. Ge, C. Liu, W. Xing, Discontinuously covered IrO2–RuO2@Ru electrocatalysts for the oxygen evolution reaction: how high activity and long-term durability can be simultaneously realized in the synergistic and hybrid nano-structure, J. Mater. Chem. A 5 (2017) 17221–17229.
[148] J. Xu, J. Li, Z. Lian, A. Araujo, Y. Li, B. Wei, Z. Yu, O. Bondarchuk, I. Amorim, V. Tileli, B. Li, L. Liu, Atomic-step enriched ruthenium–iridium nanocrystals anchored homogeneously on MOF-derived support for efficient and stable oxygen evolution in acidic and neutral media, ACS Catal. 11 (2021) 3402–3413.
[149] D.A. Kuznetsov, B. Han, Y. Yu, R.R. Rao, J. Hwang, Y. Román-Leshkov, Y. Shao-Horn, Tuning redox transitions via inductive effect in metal oxides and complexes, and implications in oxygen electrocatalysis, Joule 2 (2018) 225–244.
[150] A.L. Li, S. Kong, C.X. Guo, H. Ooka, K. Adachi, D. Hashizume, Q.K. Jiang, H. X. Han, J.P. Xiao, R. Nakamura, Enhancing the stability of cobalt spinel oxide towards sustainable oxygen evolution in acid, Nat. Catal. 5 (2022) 109–118.
[151] F.-Y. Chen, Z.-Y. Wu, Z. Adler, H. Wang, Stability challenges of electrocatalytic oxygen evolution reaction: from mechanistic understanding to reactor design, Joule 5 (2021) 1704–1731.
[152] Y. Xie, Z. Yang, Morphological and coordination modulations in iridium electrocatalyst for robust and stable acidic OER catalysis, Chem. Rec. (2023), e202300129.
[153] X. Li, J. Hu, M. Wu, C. Guo, L. Bai, J. Li, Y. Li, D. Luo, J. Duan, X. Li, Z. Li, Fabrication and morphological effect of waxberry-like carbon for high-performance aqueous zinc-ion electrochemical storage, Carbon 205 (2023) 226–235.
[154] K. Zhang, J. Qiu, J. Wu, Y. Deng, Y. Wu, L. Yan, Morphological tuning engineering of Pt@TiO2/graphene catalysts with optimal active surfaces of support for boosting catalytic performance for methanol oxidation, J. Mater. Chem. A 10 (2022) 4254–4265.
[155] J. Zhu, Z. Lyu, Z. Chen, M. Xie, M. Chi, W. Jin, Y. Xia, Facile synthesis and characterization of Pd@IrnL (n = 1–4) core–shell nanocubes for highly efficient oxygen evolution in acidic media, Chem. Mat. 31 (2019) 5867–5875.
[156] J. Zhang, X. Fu, F. Xia, W. Zhang, D. Ma, Y. Zhou, H. Peng, J. Wu, X. Gong, D. Wang, Q. Yue, Core-shell nanostructured Ru@Ir-O electrocatalysts for superb oxygen evolution in acid, Small 18 (2022), e2108031.
[157] B. Jiang, Y. Guo, F. Sun, S. Wang, Y. Kang, X. Xu, J. Zhao, J. You, M. Eguchi, Y. Yamauchi, H. Li, Nanoarchitectonics of metallene materials for electrocatalysis, ACS Nano 17 (2023) 13017–13043.
[158] Q. Dang, H. Lin, Z. Fan, L. Ma, Q. Shao, Y. Ji, F. Zheng, S. Geng, S.Z. Yang, N. Kong, W. Zhu, Y. Li, F. Liao, X. Huang, M. Shao, Iridium metallene oxide for acidic oxygen evolution catalysis, Nat. Commun. 12 (2021) 6007.
[159] J. Deng, D.H. Deng, X.H. Bao, Robust catalysis on 2D materials encapsulating metals: concept, application, and perspective, Adv. Mater. 29 (2017) 1606967.
[160] Z. Li, J.-Y. Fu, Y. Feng, C.-K. Dong, H. Liu, X.-W. Du, A silver catalyst activated by stacking faults for the hydrogen evolution reaction, Nat. Catal. 2 (2019) 1107–1114.
[161] M.C. Luo, S.J. Guo, Strain-controlled electrocatalysis on multimetallic nanomaterials, Nat. Rev. Mater. 2 (2017) 17059.
[162] B. You, M.T. Tang, C. Tsai, F. Abild-Pedersen, X.L. Zheng, H. Li, Enhancing electrocatalytic water splitting by strain engineering, Adv. Mater. 31 (2019) 1807001.
[163] X.B. Yang, Y.Y. Wang, X.L. Tong, N.J. Yang, Strain engineering in electrocatalysts: fundamentals, progress, and perspectives, Adv. Energy Mater. 12 (2022), 2102261.
[164] J. Wang, K.P. Hou, Y. Wen, H. Liu, H. Wang, K. Chakarawet, M. Gong, X. Yang, Interlayer structure manipulation of iron oxychloride by potassium cation intercalation to steer H2O2 activation pathway, J. Am. Chem. Soc. 144 (2022) 4294–4299.
[165] Y. He, Z. Kang, J. Li, Y. Li, X. Tian, Recent progress of manganese dioxide based electrocatalysts for the oxygen evolution reaction, Ind. Chem. Mater. 1 (2023) 312–331.
[166] Y. Yao, S. Hu, W. Chen, Z.-Q. Huang, W. Wei, T. Yao, R. Liu, K. Zang, X. Wang, G. Wu, W. Yuan, T. Yuan, B. Zhu, W. Liu, Z. Li, D. He, Z. Xue, Y. Wang, X. Zheng, J. Dong, C.-R. Chang, Y. Chen, X. Hong, J. Luo, S. Wei, W.-X. Li, P. Strasser, Y. Wu, Y. Li, Engineering the electronic structure of single atom Ru sites via compressive strain boosts acidic water oxidation electrocatalysis, Nat. Catal. 2 (2019) 304–313.
[167] L. Zhang, H. Jang, H. Liu, M.G. Kim, D. Yang, S. Liu, X. Liu, J. Cho, Sodium-decorated amorphous/crystalline RuO2 with rich oxygen vacancies: a robust pH-universal oxygen evolution electrocatalyst, Angew. Chem. -Int. Ed. 60 (2021) 18821–18829.
[168] Y. Wei, L. Yi, R. Wang, J. Li, D. Li, T. Li, W. Sun, W. Hu, A unique etching-doping route to Fe/Mo Co-doped Ni oxyhydroxide catalyst for enhanced oxygen evolution reaction, Small (2023), e2301267.
[169] S. Kader, M.R. Al-Mamun, M.B.K. Suhan, S.B. Shuchi, M.S. Islam, Enhanced photodegradation of methyl orange dye under UV irradiation using MoO3 and Ag doped TiO2 photocatalysts, Environ. Technol. Innov. 27 (2022), 102476.
[170] K. Huang, C. Lin, G. Yu, P. Du, X. Xie, X. He, Z. Zheng, N. Sun, H. Tang, X. Li, M. Lei, H. Wu, Ru/Se-RuO2 Composites via Controlled Selenization Strategy for Enhanced Acidic Oxygen Evolution, Adv. Funct. Mater. 33 (2022) 2211102.
[171] Y. Shen, C. Chen, Z. Zou, Z. Hu, Z. Fu, W. Li, S. Pan, Y. Zhang, H. Zhang, Z. Yu, H. Zhao, G. Wang, Geometric and electronic effects of Co@NPC catalyst in chemoselective hydrogenation: Tunable activity and selectivity via N,P co-doping, J. Catal. 421 (2023) 65–76.
[172] H.J. Qiu, P. Du, K. Hu, J. Gao, H. Li, P. Liu, T. Ina, K. Ohara, Y. Ito, M. Chen, Metal and Nonmetal Codoped 3D Nanoporous Graphene for Efficient Bifunctional Electrocatalysis and Rechargeable Zn-Air Batteries, Adv. Mater. 31 (2019), e1900843.
[173] A. Baktash, Y. Fang, M. Xiao, M. Hunter, Q. Yuan, L. Wang, Enhanced hydrogen evolution performance of carbon nitride using transition metal and boron Co-dopants, Small Struct. 4 (2022) 2200264.
[174] J. Wang, H. Yang, F. Li, L.G. Li, J.B. Wu, S.H. Liu, T. Cheng, Y. Xu, Q. Shao, X. Q. Huang, Single-site Pt-doped RuO2 hollow nanospheres with interstitial C for high-performance acidic overall water splitting, Sci. Adv. 8 (2022), eabl9271.
[175] H.Y. Jin, X.Y. Liu, P.F. An, C. Tang, H.M. Yu, Q.H. Zhang, H.J. Peng, L. Gu, Y. Zheng, T.S. Song, K. Davey, U. Paik, J.C. Dong, S.Z. Qiao, Dynamic rhenium dopant boosts ruthenium oxide for durable oxygen evolution, Nat. Commun. 14 (2023) 354.
[176] X. Li, C. Deng, Y. Kong, Q. Huo, L. Mi, J. Sun, J. Cao, J. Shao, X. Chen, W. Zhou, M. Lv, X. Chai, H. Yang, Q. Hu, C. He, Unlocking the transition of electrochemical water oxidation mechanism induced by heteroatom doping, Angew. Chem. Int. Ed. 62 (2023), e202309732.
[177] A. Grimaud, O. Diaz-Morales, B.H. Han, W.T. Hong, Y.L. Lee, L. Giordano, K. A. Stoerzinger, M.T.M. Koper, Y. Shao-Horn, Activating lattice oxygen redox reactions in metal oxides to catalyse oxygen evolution, Nat. Chem. 9 (2017) 828.
[178] J. Kim, P.C. Shih, K.C. Tsao, Y.T. Pan, X. Yin, C.J. Sun, H. Yang, High-performance pyrochlore-type yttrium ruthenate electrocatalyst for oxygen evolution reaction in acidic media, J. Am. Chem. Soc. 139 (2017) 12076–12083.
[179] S. Hao, M. Liu, J. Pan, X. Liu, X. Tan, N. Xu, Y. He, L. Lei, X. Zhang, Dopants fixation of ruthenium for boosting acidic oxygen evolution stability and activity, Nat. Commun. 11 (2020) 5368.
[180] Y.C. Lin, Z.Q. Tian, L.J. Zhang, J.Y. Ma, Z. Jiang, B.J. Deibert, R.X. Ge, L. Chen, Chromium-ruthenium oxide solid solution electrocatalyst for highly efficient oxygen evolution reaction in acidic media, Nat. Commun. 10 (2019) 162.
[181] J. Liao, Z. Liu, Y. Ling, Q. Zhang, S. Qiu, J. Gu, J. Li, H. Dong, J. Song, T. Wang, Electronic and surface engineering of Mo doped Ni@C nanocomposite boosting catalytic upgrading of aqueous bio-ethanol to bio-jet fuel precursors, Chem. Eng. J. 461 (2023), 141888.
[182] W. Luo, Y. Yu, Y. Wu, Z. Ma, X. Ma, Y. Jiang, W. Shen, R. He, W. Su, M. Li, Realizing efficient oxygen evolution at low overpotential via dopant-induced interfacial coupling enhancement effect, Appl. Catal. B-Environ. 336 (2023), 122928.
[183] Q. Dang, S. Tang, T. Liu, X. Li, X. Wang, W. Zhong, Y. Luo, J. Jiang, Regulating Electronic Spin Moments of Single-Atom Catalyst Sites via Single-Atom Promoter

Tuning on S-Vacancy MoS(2) for Efficient Nitrogen Fixation, J. Phys. Chem. Lett. 12 (2021) 8355–8362.
[184] F. Ye, S. Zhang, Q. Cheng, Y. Long, D. Liu, R. Paul, Y. Fang, Y. Su, L. Qu, L. Dai, C. Hu, The role of oxygen-vacancy in bifunctional indium oxyhydroxide catalysts for electrochemical coupling of biomass valorization with CO_2 conversion, Nat. Commun. 14 (2023) 2040.
[185] Y. Li, W. Wang, M. Cheng, Y. Feng, X. Han, Q. Qian, Y. Zhu, G. Zhang, Arming Ru with Oxygen-Vacancy-Enriched RuO2 Sub-Nanometer Skin Activates Superior Bifunctionality for pH-Universal Overall Water Splitting, Adv. Mater. (2023), e2206351.
[186] R.X. Ge, L. Li, J.W. Su, Y.C. Lin, Z.Q. Tian, L. Chen, Ultrafine Defective RuO2 Electrocatayst Integrated on Carbon Cloth for Robust Water Oxidation in Acidic Media, Adv. Energy Mater. 9 (2019) 1901313.
[187] S.L. Liu, Z. Hu, Y.Z. Wu, J.F. Zhang, Y. Zhang, B.H. Cui, C. Liu, S. Hu, N.Q. Zhao, X.P. Han, A.Y. Cao, Y.N. Chen, Y.D. Deng, W.B. Hu, Dislocation-Strained IrNi Alloy Nanoparticles Driven by Thermal Shock for the Hydrogen Evolution Reaction, Adv. Mater. 32 (2020) 2006034.
[188] S.J. Tauster, S.C. Fung, R.L. Garten, Strong metal-support interactions. group 8 noble metals supported on titanium dioxide, J. Am. Chem. Soc. 100 (1978) 170–175.
[189] H. Yan, N.Q. Zhang, D.S. Wang, Highly efficient CeO2-supported noble-metal catalysts: from single atoms to nanoclusters, Chem, Catalysis 2 (2022) 1594–1623.
[190] Y.H. Liu, Q.L. Wang, J.C. Zhang, J. Ding, Y.Q. Cheng, T. Wang, J. Li, F.X. Hu, H. B. Yang, B. Liu, Recent advances in carbon-supported noble-metal electrocatalysts for hydrogen evolution reaction: syntheses, structures, and properties, Adv. Energy Mater. 12 (2022), 2200928.
[191] S.C. Sun, H. Jiang, Z.Y. Chen, Q. Chen, M.Y. Ma, L. Zhen, B. Song, C.Y. Xu, Bifunctional WC-Supported RuO2 Nanoparticles for Robust Water Splitting in Acidic Media, Angew. Chem. Int. Ed. Engl. 61 (2022), e202202519.
[192] C. Lee, K. Shin, Y. Park, Y.H. Yun, G. Doo, G.H. Jung, M. Kim, W.C. Cho, C.H. Kim, H.M. Lee, H.Y. Kim, S. Lee, G. Henkelman, H.S. Cho, Catalyst-support interactions in Zr2ON2–supported IrOx electrocatalysts to break the trade-off relationship between the activity and stability in the acidic oxygen evolution reaction, Adv. Funct. Mater. 33 (2023) 2301557.
[193] P. Hu, Z. Huang, Z. Amghouz, M. Makkee, F. Xu, F. Kapteijn, A. Dikhtiarenko, Y. Chen, X. Gu, X. Tang, Electronic metal-support interactions in single-atom catalysts, Angew. Chem. Int. Ed. Engl. 126 (2014) 3486–3489.
[194] D. Zheng, L. Yu, W. Liu, X. Dai, X. Niu, W. Fu, W. Shi, F. Wu, X. Cao, Structural advantages and enhancement strategies of heterostructure water-splitting electrocatalysts, Cell Rep. Phys. Sci. 2 (2021), 100443.
[195] L.M. Deng, S.Y. Liu, D. Liu, Y.M. Chang, L.L. Li, C.S. Li, Y. Sun, F. Hu, H.Y. Chen, H. Pan, S.J. Peng, Activity-stability balance: the role of electron supply effect of support in acidic oxygen evolution, Small 19 (2023) 10.
[196] Z.X. Wu, Y.L. Wang, D.Z. Liu, B.W. Zhou, P.F. Yang, R.Z. Liu, W.P. Xiao, T.Y. Ma, J.S. Wang, L. Wang, Hexagonal Defect-Rich MnOx/RuO2 with Abundant Heterointerface to Modulate Electronic Structure for Acidic Oxygen Evolution Reaction, Adv. Funct. Mater. (2023) 2307010.
[197] C. Yang, X. Zhang, Q. An, M. Liu, W. Zhou, Y. Li, F. Hu, Q. Liu, H. Su, Dynamically-evolved surface heterojunction in iridium nanocrystals boosting acidic oxygen evolution and overall water splitting, J. Energy Chem. 78 (2023) 374–380.
[198] J. Shan, C. Guo, Y. Zhu, S. Chen, L. Song, M. Jaroniec, Y. Zheng, S.-Z. Qiao, Charge-redistribution-enhanced nanocrystalline Ru@IrOx electrocatalysts for oxygen evolution in acidic media, Chem 5 (2019) 445–459.
[199] X. Luo, X. Tan, P.X. Ji, L. Chen, J. Yu, S.C. Mu, Surface reconstruction-derived heterostructures for electrochemical water splitting, EnergyChem 5 (2023), 100091.
[200] H. Jiang, L. Yan, S. Zhang, Y. Zhao, X. Yang, Y. Wang, J. Shen, X. Zhao, L. Wang, Electrochemical surface restructuring of phosphorus-doped carbon@MoP electrocatalysts for hydrogen evolution, Nano-Micro Lett. 13 (2021) 215.
[201] Z. Han, D. Han, Z. Chen, J. Gao, G. Jiang, X. Wang, S. Lyu, Y. Guo, C. Geng, L. Yin, Z. Weng, Q.H. Yang, Steering surface reconstruction of copper with electrolyte additives for CO_2 electroreduction, Nat. Commun. 13 (2022) 3158.
[202] D. Guan, G. Ryu, Z. Hu, J. Zhou, C.L. Dong, Y.C. Huang, K. Zhang, Y. Zhong, A. C. Komarek, M. Zhu, X. Wu, C.W. Pao, C.K. Chang, H.J. Lin, C.T. Chen, W. Zhou, Z. Shao, Utilizing ion leaching effects for achieving high oxygen-evolving performance on hybrid nanocomposite with self-optimized behaviors, Nat. Commun. 11 (2020) 3376.
[203] Y. Duan, S.N. Sun, Y.M. Sun, S.B. Xi, X. Chi, Q.H. Zhang, X. Ren, J.X. Wang, S.J. H. Ong, Y.H. Du, L. Gu, A. Grimaud, Z.C.J. Xu, Mastering surface reconstruction of metastable spinel oxides for better water oxidation, Adv. Mater. 31 (2019) 1807898.
[204] L. Trotochaud, S.L. Young, J.K. Ranney, S.W. Boettcher, Nickel-iron oxyhydroxide oxygen-evolution electrocatalysts: the role of intentional and incidental iron incorporation, J. Am. Chem. Soc. 136 (2014) 6744–6753.
[205] J. Huang, Y. Li, Y. Zhang, G. Rao, C. Wu, Y. Hu, X. Wang, R. Lu, Y. Li, J. Xiong, Identification of key reversible intermediates in self-reconstructed nickel-based hybrid electrocatalysts for oxygen evolution, Angew. Chem. Int. Ed. Engl. 58 (2019) 17458–17464.
[206] L. An, F. Yang, C. Fu, X. Cai, S. Shen, G. Xia, J. Li, Y. Du, L. Luo, J. Zhang, A functionally stable rumn electrocatalyst for oxygen evolution reaction in acid, Adv. Funct. Mater. 32 (2022) 2200131.
[207] L. Yang, L. Shi, H. Chen, X. Liang, B. Tian, K. Zhang, Y. Zou, X. Zou, A Highly Active, Long-Lived Oxygen Evolution Electrocatalyst Derived from Open-Framework Iridates, Adv. Mater. 35 (2023) 2208539.
[208] Z.M. Wei, J. Ding, X.X. Duan, G.L. Chen, F.Y. Wu, L. Zhang, X.J. Yang, Q. Zhang, Q.Y. He, Z.Y. Chen, J. Huang, S.F. Hung, X. Yang, Y.M. Zhai, Enhancing Selective Electrochemical CO_2 Reduction by In Situ Constructing Tensile-Strained Cu Catalysts, ACS Catal. 13 (2023) 4711–4718.
[209] D.Q. Guan, C.L. Shi, H.Y. Xu, Y.X. Gu, J. Zhong, Y.C. Sha, Z.W. Hu, M. Ni, Z. P. Shao, Simultaneously mastering operando strain and reconstruction effects via phase-segregation strategy for enhanced oxygen-evolving electrocatalysis, J. Energy Chem. 82 (2023) 572–580.
[210] G. Meng, W. Sun, A.A. Mon, X. Wu, L. Xia, A. Han, Y. Wang, Z. Zhuang, J. Liu, D. Wang, Y. Li, Strain regulation to optimize the acidic water oxidation performance of atomic-layer IrOx, Adv. Mater. 31 (2019), e1903616.
[211] Q. Yao, Z. Yu, L. Li, X. Huang, Strain and surface engineering of multicomponent metallic nanomaterials with unconventional phases, Chem. Rev. 123 (2023) 9676–9717.
[212] Y. Zhu, J. Wang, T. Koketsu, M. Kroschel, J.-M. Chen, S.-Y. Hsu, G. Henkelman, Z. Hu, P. Strasser, J. Ma, Iridium single atoms incorporated in Co3O4 efficiently catalyze the oxygen evolution in acidic conditions, Nat. Commun. 13 (2022) 7754.
[213] Z.Y. Wu, F.Y. Chen, B. Lie, S.W. Yu, Y.Z. Finfrock, D.M. Meira, Q.Q. Yan, P. Zhu, M.X. Chen, T.W. Song, Z. Yin, H.W. Liang, S. Zhang, G. Wang, H. Wang, Non-iridium-based electrocatalyst for durable acidic oxygen evolution reaction in proton exchange membrane water electrolysis, Nat. Mater. 22 (2023) 100–108.
[214] Y. Zhao, D.P. Adiyeri Saseendran, C. Huang, C.A. Triana, W.R. Marks, H. Chen, H. Zhao, G.R. Patzke, Oxygen evolution/reduction reaction catalysts: from in situ monitoring and reaction mechanisms to rational design, Chem. Rev. 123 (2023) 6257–6358.
[215] S.-K. Geng, Y. Zheng, S.-Q. Li, H. Su, X. Zhao, J. Hu, H.-B. Shu, M. Jaroniec, P. Chen, Q.-H. Liu, S.-Z. Qiao, Nickel ferrocyanide as a high-performance urea oxidation electrocatalyst, Nat. Energy 6 (2021) 904–912.
[216] N. Yang, Z. Chen, D. Ding, C. Zhu, X. Gan, Y. Cui, Tungsten–nickel alloy boosts alkaline hydrogen evolution reaction, J. Phy. Chem. C. 125 (2021) 27185–27191.
[217] Z.G. Chen, Y.F. Xu, D. Ding, G. Song, X.X. Gan, H. Li, W. Wei, J. Chen, Z.Y. Li, Z. M. Gong, X.M. Dong, C.F. Zhu, N.N. Yang, J.Y. Ma, R. Gao, D. Luo, S. Cong, L. Wang, Z.G. Zhao, Y. Cui, Thermal migration towards constructing W-W dual-sites for boosted alkaline hydrogen evolution reaction, Nat. Commun. 13 (2022) 763.
[218] F. Wang, P. Zou, Y. Zhang, W. Pan, Y. Li, L. Liang, C. Chen, H. Liu, S. Zheng, Activating lattice oxygen in high-entropy LDH for robust and durable water oxidation, Nat. Commun. 14 (2023) 6019.
[219] N. Yao, H.N. Jia, J. Zhu, Z.P. Shi, H.J. Cong, J.J. Ge, W. Luo, Atomically dispersed Ru oxide catalyst with lattice oxygen participation for efficient acidic water oxidation, Chem 9 (2023) 1882–1896.
[220] B. Han, Y. Guo, Y. Huang, W. Xi, J. Xu, J. Luo, H. Qi, Y. Ren, X. Liu, B. Qiao, T. Zhang, Strong metal-support interactions between Pt single atoms and TiO2, Angew. Chem. Int. Ed. Engl. 59 (2020) 11824–11829.
[221] T. Gao, X. Tang, X. Li, S. Wu, S. Yu, P. Li, D. Xiao, Z. Jin, Understanding the atomic and defective interface effect on ruthenium clusters for the hydrogen evolution reaction, ACS Catal. 13 (2022) 49–59.
[222] C. Luan, M. Corva, U. Hagemann, H. Wang, M. Heidelmann, K. Tschulik, T. Li, Atomic-scale insights into morphological, structural, and compositional evolution of CoOOH during oxygen evolution reaction, ACS Catal. 13 (2023) 1400–1411.
[223] X. Lyu, Y. Jia, X. Mao, D.H. Li, G. Li, L.Z. Zhuang, X. Wang, D.J. Yang, Q. Wang, A. J. Du, X.D. Yao, Gradient-concentration design of stable core-shell nanostructure for acidic oxygen reduction electrocatalysis, Adv. Mater. 32 (2020) 2003493.
[224] X. Wang, Z. Zhang, Y.J. Ge, K. Shen, J.J. Qian, Few-layer Ag-coated ordered mesoporous pt nanocrystals for ethanol oxidation, Small Struct. 4 (2023) 2200390.
[225] S. Jiao, X. Fu, H. Huang, Descriptors for the evaluation of electrocatalytic reactions: d-band theory and beyond, Adv. Funct. Mater. 32 (2021), 2107651.
[226] Z.P. Shi, J. Li, Y.B. Wang, S.W. Liu, J.B. Zhu, J.H. Yang, X. Wang, J. Ni, Z. Jiang, L. J. Zhang, Y. Wang, C.P. Liu, W. Xing, J.J. Ge, Customized reaction route for ruthenium oxide towards stabilized water oxidation in high-performance PEM electrolyzers, Nat. Commun. 14 (2023) 843.